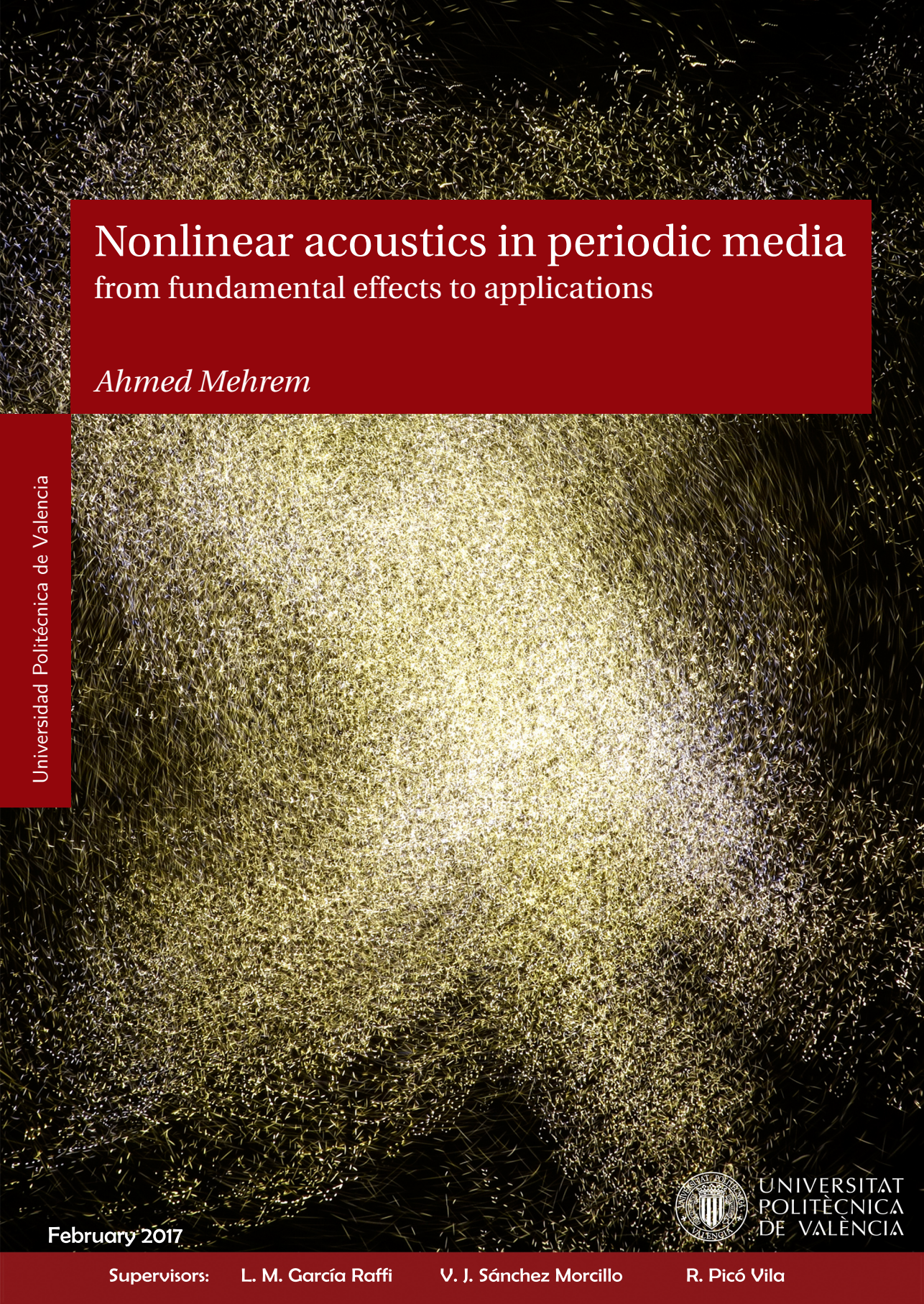

Nonlinear acoustics in periodic media

from fundamental effects to applications

Ahmed Mehrem

Universidad Politécnica de Valencia

February 2017

UNIVERSITAT POLITÈCNICA DE VALÈNCIA

Supervisors: L. M. García Raffi V. J. Sánchez Morcillo R. Picó Vila

NONLINEAR ACOUSTICS IN PERIODIC MEDIA

FROM FUNDAMENTAL EFFECTS TO APPLICATIONS

by

Ahmed Mehrem

Instituto de Investigación para la Gestión Integrada de zonas Costeras

A thesis submitted in partial fulfillment of the requirements of the degree of
Doctor of Philosophy
in Mathematics

Universidad Politécnica de Valencia
February 2017

Supervisors:

Luis M. García Raffi	*IUMPA - Universidad Politécnica de Valencia, Spain*
Víctor J. Sánchez Morcillo	*IGIC - Universidad Politécnica de Valencia, Spain*
Rubén Picó Vila	*IGIC - Universidad Politécnica de Valencia, Spain*

Dissertation Jury:

Francisco Camarena Femenia	Universidad Politécnica de Valencia
Faustino Palmero Acebedo	Universidad de Sevilla
Miguel Molerón Bermúdez	Eidgenössische Technische Hochschule Zürich

UNIVERSITAT POLITÈCNICA DE VALÈNCIA

"Truth is ever to be found in simplicity, and not in the multiplicity and confusion of things."

Isaac Newton
(1642-1726)

ACKNOWLEDGEMENTS

In my MSc and Ph.D., my supervisor **Víctor Sánchez-Morcillo** has always supported me. I am forever thankful to him for his incredible guidance. His constant enthusiasm and his perpetual energy in research extremely motivated me in my personal life before my studies. I thank you for giving me the opportunity to work with you.

In Ph.D., i was lucky to work with my professor **Lluis García-Raffi**. I have learned a lot from him not just academically but also personally. I owe him lots of gratitude for having shown me how to be an ideal scientist and a good supervisor.

To my professor **Rubén Picó-Vila**, thank you for your readiness to help, guidance and for your helpful discussions. I am particularly thankful to Noé Jiménez for helping me during the first few months in the laboratory and with Matlab. This thesis would not have been possible without their support, patience and endless guidance.

The main part of the thesis is based on a novel experiment *"chain of magnets"*. The professional idea and the creative design of the setup were accomplished by Víctor and Noé. The other part of the thesis is done as a collaboration with Jennifer Chaline, Serge Dos Santos and Ayache Bouakaz (Université François Rabelais, France) in *Microbubbles and nonlinear coupled oscillator rings*. I have enjoyed many useful and valuable discussions with Yasser Mustafa (South Valley University, Egypt) and El Mokhtar Hamham (Abdelmalek Essaadi University, Morocco) during their stay in Gandia.

This work was supported by Generalitat Valenciana (Santiago Grisolia program 2012/029) for the first 3 years and the last year by Spanish Ministry of Science and Innovation (FIS2011-29731-C02-02).

In the office *E-201*, I didn't take the road to my Ph.D. alone but I was accompanied by my friends; Luis Salmerón, Iván Herrero, Alejandro Cebrecos, Maria Saldaña, Patricia Ordóñez , Vicent Puig, Ivan Felis, Ester Soliveres, Xavi García,

and also in the last year Susana, Alvaro and Maria. I thank all for the great moments we had in the conferences and courses, and the delightful time we spent at lunchtime and coffee breaks.

After 5 years in Valencia, I've gained a new culture in a great city with a friendly people. I have met great friends, thanks to Juan B.Medina, Elisa and Sarah for a great time we had in Valencia. Thanks to my friends H. kasem, M. Awney, M. Ali, El nahal, A. Ghazal and O. Anas for being like brothers to me.

Finally, I would like to dedicate this thesis to my parents, my sisters, M. Ismail, M. Salah, my nephews (Zyad and Iyad) and my nieces (Hala and Anna) for their love, care, and for feeling so close despite being so far. During a time like this, i realize how much the family and friends mean to me.

Ahmed Mehrem
Gandia, January 2017

ABSTRACT

The natural dynamics are not ideal or linear. To understand their complex behavior, we needs to study the nonlinear dynamics in more simple models. This thesis is consist of two main setups. Both setups are simplified models for the behavior occurs in the complex systems. We studied in both systems the same nonlinear dynamics such as higher-harmonics, sub-harmonics, solitary waves,...etc.

In Chapter (2), the propagation of nonlinear waves in a lattice of repelling particles is studied theoretically and experimentally. A simple experimental setup is proposed, consisting in an array of coupled magnetic dipoles. By driving harmonically the lattice at one boundary, we excite propagating waves and demonstrate different regimes of mode conversion into higher harmonics, strongly in influenced by dispersion. The phenomenon of acoustic dilatation of the chain is also predicted and discussed. The results are compared with the theoretical predictions of α-FPU equation, describing a chain of masses connected by nonlinear quadratic springs. The results can be extrapolated to other systems described by this equation. We studied theoretically and experimentally the generation and propagation of kinks in the system. We excite pulses at one boundary of the system and demonstrate the existence of kinks, whose properties are in very good agreement with the theoretical predictions, that is the equation that approaches, under the conditions of our experiments, the one corresponding to full model describing a chain of masses connected by magnetic forces. The results can be extrapolated to other systems described by this equation. Also, In the case of a lattice of finite length, where standing waves are formed, we report the observation of subharmonics of the driving wave.

In chapter (3), we studied the propagation of intense acoustic waves in a multilayer crystal. The medium consists in a structured fluid, formed by a periodic array of fluid layers with alternating linear acoustic properties and quadratic nonlinearity coefficient. We presents the results for different mathematical models (Nonlinear Wave Equation, Westervelt Equation and Constitutive equations). We show that the interplay between strong dispersion and nonlinearity leads to new scenarios of wave propagation. The classical waveform distortion process typical of intense acoustic waves in homogeneous media can be strongly altered when nonlinearly generated harmonics lie inside or close to band gaps. This allows the possibility of engineer a medium in order to get a particular waveform. Examples of this include the design of media with effective (e.g. cubic) nonlin-

earities, or extremely linear media.

In chapter (4), the oscillatory behavior of a microbubble is investigated through an acousto-mechanical analogy based on a ring-shaped chain of coupled pendula. Observation of parametric vibration modes of the pendula ring excited at frequencies between 1 and 5 Hz is considered. Simulations have been carried out and show spatial mode, mixing and localization phenomena. The relevance of the analogy between a microbubble and the macroscopic acousto-mechanical setup is discussed and suggested as an alternative way to investigate the complexity of microbubble dynamics.

RESUMEN

La dinámica natural no es ideal ni lineal. Para entender su comportamiento complejo, necesitamos estudiar la dinámica no lineal en modelos más simples. Esta tesis consta de dos configuraciones principales. Ambas configuraciones son modelos simplificados de el comportamiento que se produce en los sistemas complejos. Estudiamos en ambos sistemas la misma dinámica no lineal como son la generación de armónicos superiores, los sub-armónicos, las ondas solitarias, etc.

En el Capítulo (2), se estudia, tanto teórica como experimentalmente, la propagación de ondas no lineales en sistemas periodicos de partículas acopladas mediante fuerzas repulsivas. Se propone una configuración experimental simple, que consiste en una matriz de dipolos magnéticos acoplados. Inyectando armónicamente la señal en un extremo, excitamos ondas de propagación y demostramos diferentes regímenes de conversión de modos en armónicos, fuertemente influenciados por la dispersión. También se predice y se discute el fenómeno de dilatación acústica de la cadena. Los resultados se comparan con las predicciones teóricas de la ecuación α-FPU, describiendo una cadena de masas conectadas por muelles cuadráticos no lineales. Los resultados pueden ser extrapolados a otros sistemas descritos por esta ecuación. Estudiamos también teórica y experimentalmente la generación y propagación de kinks. Excitamos pulsos en la frontera del sistema y demostramos la existencia de kinks cuyas propiedades están en muy buen acuerdo con las predicciones teóricas, es decir, con la ecuación que aproxima bajo las condiciones de nuestros experimentos la correspondiente al modelo completo que describe un cadena de masas conectadas por fuerzas magnéticas. Los resultados pueden ser extrapolados a otros sistemas descritos por esta ecuación. Además, en el caso de una red finita, donde se forman ondas estacionarias, describimos la observación de subarmónicos del armónico principal.

En el capítulo (3), estudiamos la propagación de ondas acústicas intensas en un cristal multicapa. El medio consiste en un fluido estructurado, formado por un conjunto periódico de capas fluidas con propiedades acústicas lineales alternas y coeficiente de no linealidad cuadrática. Presentamos los resultados de diferentes modelos matemáticos (ecuación de ondas no lineal, ecuación de Westervelt y ecuaciones constitutivas). Mostramos que la interacción entre la fuerte dispersión y la no linealidad conduce a nuevos escenarios de propagación

de ondas. El proceso de distorsión de la onda clásica, típico de las ondas acústicas intensas en medios homogéneos, puede ser alterado de forma importante cuando los armónicos generados no linealmente se encuentran dentro o cerca del gap. Esto permite la posibilidad de diseñar un medio con el fin de obtener una forma de onda en particular. Ejemplos de esto incluyen el diseño de medios con no linealidad efectiva (por ejemplo, cúbica) o medios extremadamente lineales.

En el capítulo (4), el comportamiento oscilatorio de una microburbuja se investiga a través de una analogía acusto-mecánica basada en una cadena en forma de anillo de péndulos acoplados. Se estudian los modos de vibración paramétrica del anillo pendular excitado a frecuencias entre 1 y 5 Hz. Se han llevado a cabo simulaciones que muestran la presencia de modos espaciales, mixtos y fenómenos de localización. Se discute la relevancia de la analogía entre una microburbuja y la configuración macroscópica acústico-mecánica y se sugiere como una vía alternativa para investigar la complejidad de la dinàmica de microburbujas.

RESUM

La dinàmica natural no és ideal ni tampoc lineal. Per entendre el seu comportament complex, es necessita estudiar la dinàmica no lineal dels models més simples. Aquesta tesi consisteix en l'estudi de dues configuracions principals, que són models simplificats del comportament que es produeix en els sistemes complexos. Estudiem en ambdós sistemes la mateixa dinàmica no lineal, com és la generació d'harmònics superiors, sub-harmònics, ones solitàries, etc.

En el capítol (2), estudiem, tant teòrica com experimentalment, la propagació de les ones no lineals en sistemes periòdics de partícules acoblades mitjançant forces repulsives. Es proposa una configuració experimental simple, que consisteixen en una matriu de dipols magnètics acoblats. En conduint harmònicament la xarxa en un límit, excitem la propagació de les ones i demostrem diferents règims de conversió de modes en harmònics més alts, força influenciada per la dispersió. El fenomen de la dilatació acústica de la cadena també es prediu i es discuteix. Els resultats es comparen amb les prediccions teòriques que descriu una cadena de masses conectades per molls quadràtics no lineals. Els resultats es poden extrapolar a altres sistemes descrits per aquesta equació. Hem estudiat teòrica i experimentalment la generació i propagació de Kinks. Excitem polsos a la frontera del sistema i demostrem l'existència d'Kinks, les propietats desl quals estan en molt bon acord amb les prediccions teòriques, és a dir, de l'equació que aproxima sota les condicions dels nostres experiments la corresponent al model complet que descriu un cadena de masses connectades per forces magnètiques. Els resultats es poden extrapolar a altres sistemes descrits per aquesta equació. A més, en el cas d'una xarxa finita, on es formen ones estacionàries, descrivim l'observació de subarmónicos de l'harmònic principal.

En el capítol (3), s'estudia la propagació d'ones acústiques intenses en un medi multicapa. El medi consisteix en un fluid estructurat, format per una matriu periòdica de capes de fluid amb l'alternança de propietats acústiques lineals i coeficient de no linealitat de segon grau. Es presenten els resultats per a diferents models matemàtics no lineals (equació d'ones no lineal, equació de Westervelt i les equacions constitutives). Es demostra que la interacció entre la forta dispersió i no linealitat condueix a nous escenaris de propagació de l'ona. El procés de distorsió en forma d'ona clàssica, típica de les ones acústiques intenses en medis homogenis, es pot alterar de manera significativa quan els harmònics generats de forma no lineal es troben dins o a prop del gap. Això obri la possibil-

itat de dissenyar un medi per tal d'obtenir una forma d'ona particular. Exemples d'això inclouen el disseny delsmedis amb una no linealitat efectiva (per exemple cúbica), o medis extremadament lineals.

En el capítol (4), el comportament oscilatori d'una micro-bombolla és investigat a través d' una analogia acústica-mecànica basada en una cadena en forma d'anell de pèndols acoblats. Es considera l'observació dels modes de vibració paramètriques de l'anell pendular excitat amb freqüències entre 1 i 5 Hz. S'han dut a terme simulacions que mostren la presència de moes espacilas, mixtes i fenòmens de localització. Es discuteix la relevància de l'analogia entre les microbambolles i la configuració macroscòpica acústica-mecànica i es suggereix una forma alternativa per a investigar la complexitat de la dinàmica de microbombolles.

CONTENTS

1

INTRODUCTION

1.1. NONLINEAR DYNAMICS

Although the first nonlinear phenomena were observed in the eighteenth century, the field of nonlinear acoustics has been developed strongly since the 60s. Before, the linear acoustic analysis largely met the needs of most physical phenomena. Moreover, nonlinear acoustics requires a mathematical framework that has been implemented relatively recently. An acoustic system is called linear if the output of a pure sinusoidal signal input is itself a pure sine wave with the same frequency. This characteristic is not retained in for a nonlinear system. The output signal can suffer different phenomena like distortion, a pseudo-periodic behavior, or chaotic among others. In 18^{th} century, acoustic propagation was connected to the theory of continuum physics. Starting with Leonard Euler in 1766, who derived the equation of motion of string in one dimension [1]. He also has derived the nonlinear wave equation in fluid (air) and predicted that the propagation velocity of a nonlinear wave changes through propattion [2, 3].

In 1860, Earnshaw has derived the law of propagation of plane progressive waves. In 1870, Macquorn Rankine [4] presented a significant study in fluid dynamics. He determined the relationship the laws of the elasticity and the heat of any substance (liquid or solid) and those of the wave-like propagation of finite longitudinal disturbance in that substance. In the period from 1887 to 1889, Rankine and Hugoniot [5] formulated conservation equations of mass, momentum, and energy connecting the flow field behind a shock with the flow field ahead of it. They express the discontinuity of varying amounts through a shock wave in a gas, this relation is called "Rankine-Hugoniot relations" [6].

In 1948, Johannes Burgers [7] derived the partial differential equation for the

acoustic wave propagating in a fluid medium. This equation is the main equation in nonlinear acoustics and depends on the acoustic pressure(p). Kuznetsov in 1971 [8] combined effects of nonlinearity, diffraction and absorption in directional sound beams. Kuznetsov's equation can be approximated to give Riemann's equation and Burgers' equation [9]. Khokhlov - Zabolotskaya - Kuznetsov (KZK) equation is used in acoustical problems as a mathematical model that describes the pulsed finite amplitude sound beam nonlinear propagation in the thermo-viscous medium. Westervelt [10] derived the nonlinear wave equation that accounts for nonlinearity up to the second order.

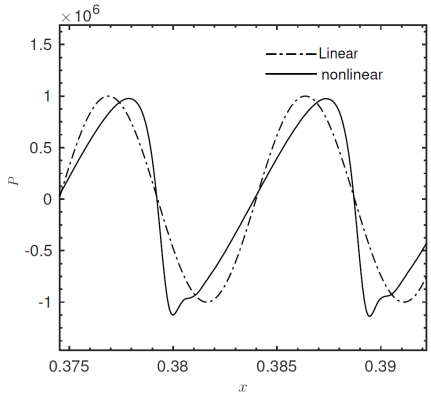

Figure 1.1: Linear and Nonlinear wave profile.

1.1.1. HIGHER HARMONIC GENERATION

Harmonic generation is a characterization of the nonlinearity of a material or/and a source. Harmonic components have frequencies that are multiple integers of the fundamental frequency. Thus, harmonic distortion is the degree to which a waveform deviates from its pure sinusoidal values as a result of the summation of all these harmonic elements. In Figure (1.1), the linear wave profile with a pure sinusoidal wave and the distorted wave are shown. The ideal sine wave does not have harmonic components. The spectrum of a distorted and non-distorted signal are shown in Fig(1.1) and Fig(1.2).

1.1.2. SOLITARY WAVES

In recent decades, the solitary wave theory has become a very active area of research due to its importance in many branches of mathematics and physics, such as nonlinear optics, acoustic, plasmas and fluid mechanics. The first observation

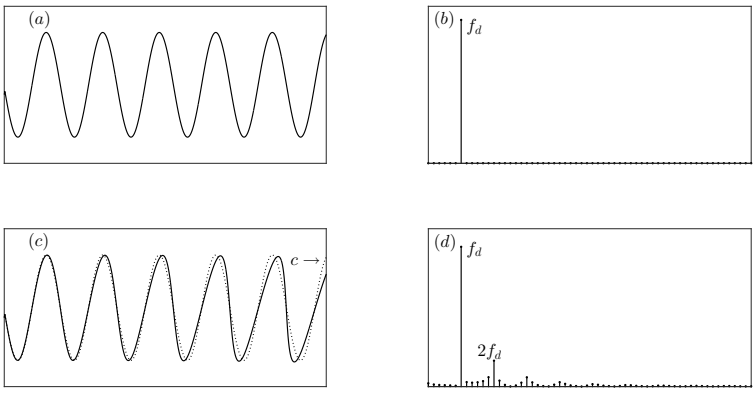

Figure 1.2: Nonlinearity effect on the wave. (a) the linear wave profile. (b) the spectrum of the linear wave. (c) the nonlinear wave profile (solid) compared with the linear wave (dots). (d) The spectrum of the nonlinear wave with the appearance of harmonics.

of a wave with characteristics of a soliton was made in 1834 by a Scottish naval engineer John Scott Russell [11].

There are different types of solitary waves, such as intrinsic localized modes, vortex solitons, q-breathers, topological soliton, and many others. In this work, we focus on a particular type of solitary wave named "kink". A kink is a one-dimensional topological soliton that appears as a solution of the wave equation. A kink represents a twist in the value of a solution and causes a transition from one value to another. As first pointed out by Bob Keolian [12] in 1992, his investigations of lattices have led to the discovery of domain walls and kinks. The kink can be found at frequency smaller than cut-off frequency.

Kink has been extensively studied during the recent years because of its relation with particle tracking physics. Some materials have the ability to track charged particle. Many studies focus on kink propagation in different media [11],[13] and [14]. Peyrard *et al.* [15] described and discussed subsonic kinks in a monoatomic chain when he showed the discreteness effects on non-topological kink soliton dynamics in nonlinear lattices. A.V. Savin *et al.* [16] studied moving topological solitons (kinks and antikinks) in the nonlinear Klein–Gordon chain by using the pseudo-spectral method. Pnevmatikos, Flytzanis and Remoissenet [17] studied propagation of kinks and solitons analytically and numerically in a nonlinear diatomic chain with cubic and quartic interaction potential. The book *"Waves called solitons: concepts and experiments"* by Remoissenet [11] describes a great many simple experimental realizations of nonlinear lattices in

which kinks, in particular,can be observed.

1.1.3. SUB-HARMONIC GENERATION

As stated before, when a nonlinear system is excited by a pure sinusoidal wave, new frequency components can appear under appropriate circumstances. Besides, the generation of higher harmonics and the static displacement mode with zero frequency, under some conditions new frequency components are nonlinearly generated, these components are called "*subharmonics*". These are the harmonics having frequencies lower than the driving frequency. In 1859, Melde [18] was the first to observe the generation of the subharmonics experimentally. His experiment consisted of a string with one end fixed to a tuning fork. When the fork set the string into longitudinal vibration at a particular frequency, he found that transverse vibrations were excited with a frequency nearly half of the driving frequency. In 1887, Rayleigh [19] reported that the generation of sub-harmonics is a result of the instabilities caused by the variation of the spring tension.

At higher sound levels, Dallos, Linnel [20] [21], and Dallos [22] observed fractional-harmonic pairs in the Peripheral Auditory System. Luukkala[23] [24] proposed a simple theory to explain the threshold and oscillation of sub-harmonic phonons.

Hutchins *et al.* [25] used a narrowband ultrasound source to generate solitary wave impulses in finite-length chains of spheres. In his model, both harmonics and sub-harmonics of the input frequency are generated. Also, he observed that sub-harmonics generation depends on the input amplitude.

1.2. OBJECT AND MOTIVATION

The main object of this thesis is to study the nonlinear dynamics in mechanical and acoustic systems presenting periodicity. This study is focused on three systems: a periodic discrete linear lattice, a multilayer crystal and a ring-shaped chain of coupled pendula.

The first system is a lattice of repelling particles. A simple experimental setup is proposed, consisting in an array of coupled magnetic dipoles. By driving harmonically the lattice at one boundary, we excite propagating waves and demonstrate different regimes of mode conversion into higher harmonics, strongly in influenced by dispersion. The proposed model for the system is compared with predictions of α-FPU equation, describing a chain of masses connected by nonlinear quadratic springs. The generation and propagation of kinks in the system is studied. By imposing an additional boundary conditions to the system, standing waves of the system with finite length is studied and subharmonic propagation is reported.

The second system is a multilayer crystal and we study the propagation of

intense acoustic waves through this dispersive media. The medium consists in a structured fluid, formed by a periodic array of fluid layers with alternating linear acoustic properties and quadratic nonlinearity coefficient. Predictions of different mathematical models of the system are compared and evaluated. We show that the interplay between strong dispersion and nonlinearity leads to new scenarios of wave propagation. The classical waveform distortion process typical of intense acoustic waves in homogeneous media is studied regarding how the nonlinearly generated harmonics lie or not inside or close to the band gaps.

The third model is a ring-shaped chain of coupled pendula, which is an acousto-mechanical analogy of the the oscillatory behavior of a microbubble Observation of parametric vibration modes of the pendula ring is considered. Simulations have been carried out and show spatial mode, mixing and localization phenomena. The relevance of the analogy between a microbubble and the macroscopic acousto-mechanical setup is discussed and suggested as an alternative way to investigate the complexity of microbubble dynamics.

2

NONLINEAR DISPERSIVE WAVES IN A REPULSIVE LATTICE

In this chapter, the propagation of nonlinear waves in a lattice of repelling particles is studied theoretically and experimentally. A simple experimental setup is proposed, consisting in an array of coupled magnetic dipoles. By driving harmonically the lattice at one boundary, we excite propagating waves and demonstrate different regimes of mode conversion into higher harmonics, strongly influenced by dispersion and discreteness. The phenomenon of acoustic dilatation of the chain is also predicted and discussed. The results are compared with the theoretical predictions of α-FPU equation, describing a chain of masses connected by nonlinear quadratic springs. In the case of a lattice of finite length, where standing waves are formed, we report the observation of subharmonics of the driving wave. Finally, we consider the case of impulsive excitations, demonstrating and characterizing the formation of localized travelling waves in the form of kinks. The results can be extrapolated to other systems described by this equation.

2.1. INTRODUCTION

Repulsive interactions among particles are known to form ordered states of matter. One example is Coulomb interaction, which is at the basis of the solid state physics [26]. In a crystal, atoms and ions are organized in ordered lattices by means of repulsive forces acting among them. Such non-contact forces provide also the coupling between neighbour atoms, what allows the propagation of perturbations in the form of phonons, or elementary excitations of the lattice. This picture is not restricted to the atomic scale. At a higher scale, the interaction of

charged particles other from atoms and ions has shown the formation of crystal lattices. A remarkable case are ionic crystals in a trap [27]. Such crystals, which are considered a particular form of condensed matter, are formed by charged particles (atomic ions) confined by external electromagnetic potentials (Paul or other traps), and interacting by means of the Coulomb repulsion. Crystallization requires low temperature that is achieved by laser cooling techniques. Different crystallization patterns have been observed by tuning the shape and strengths of the traps. Crystals of trapped ions have been subject of great attention as a possible configuration to perform quantum computation [28]. Crystallization of a gas of confined electrons, known as Wigner crystal, have been also predicted and observed [29, 30].

Waves in such crystals show strong dispersion at wavelengths comparable with the lattice periodicity. The linear (low amplitude) dispersion relation, and some nonlinear characteristics of wave propagation have been experimentally determined in an electrically charged, micrometer-sized dust particles immersed in the sheath of a parallel plate rf discharge in helium in a rf plasma [31], where the waves are excited by transferring the momentum from a laser to the first particle in the chain.

In other type of plasma crystals, linear wave mixing and harmonic generation of compressional waves has been theoretically [32] and experimentally [33] demonstrated. Also, nonlinear standing waves have been discussed in a two-dimensional system of charged particles [34]. Here the generation of second and third harmonics is predicted on the long-wavelength (non- or weakly dispersive) limit.

Some experiments with analogue models of repulsive lattices have been done using magnets as interacting particles, with the aim of demonstrating the generation and propagation of localized perturbations (discrete breathers and solitons). For example, in the seminal work [35] a chain of magnetic pendulums (very similar to the setup presented in this chapter) was used to simulate at the macroscopic level some natural layered silicate crystals, such as muscovite mica. More recently, in [13], the authors proposed another configuration of a chain of repelling magnets, for the study of solitary waves, similar to the highly discrete kinks studied theoretically for a model of Coulomb chain [36] extended to include realistic interatomic potentials.

Repulsive potentials are not restricted to those of electric or magnetic nature. A celebrated case is the granular chain of spherical particles interacting via Hertz potentials. Many studies have been done in this system, theoretical and experimental, on the propagation of the solitary waves. Recently, several nonlinear effects related to the propagation of intense harmonic waves in such granular lattices has been described in [37], with special attention to the dispersive

regime.

In this chapter, we present a theoretical and experimental study of the propagation of nonlinear dispersive waves in a repulsive lattice, by designing an array of coupled magnetic dipoles, and comparing the observations with the predictions from the α-FPU equation.

This equation is one of the most known and studied models in nonlinear physics and connects the results of our study with many other physical problems. Its physical and historical signifficance deserves a brief review.

The FPU problem has been at the origin of a discipline called nonlinear lattice dynamical systems theory, which has been an active area of research during the past 60 years, and is continuously growing in interest with applications to other recently emerged areas as nanotechnology, theoretical biology, and many others. It starts probably with one of the most simple and rich models solid state physics, the Frenkel-Kontorova (FK) model. In 1939, Frenkel *et al.* described the motion of a chain of interacting particles subjected to an external on-site periodic potential [38, 39]. This model is one of the most important models for discrete systems. It has received much attention because of its relevance to a wide variety of physical problems [40]. The first purpose of Frenkel and Kontorova was to model dislocations in epitaxial monolayers [41], but its surprising ability to describe many physically important phenomena, such as the dynamics of absorbed layers of atoms on crystal surfaces [42], or charge-density wave in two specific condensed matter systems [43, 44], opened the range of applications further than originally expected. Braun and Kivshar have studied intensively the nonlinear dynamics in the FK model, particularly kink propagation, which are topological excitations in chain of particles, and other features as kink diffusion and effects of disorder, and also for nonlinear localized modes or discrete breathers [45].

In 1955, a turning point in the study of discrete systems is traced, when the report of the experiment of Fermi, Pasta and Ulam (FPU) [46] appeared, after the death of Fermi in 1945. The study of the dynamics of nonlinear lattices has been greatly influenced by this pioneering work. The first numerical simulation, that is to say the first "virtual experience" made entirely on a computer, was completed in 1953. Its name recalls the role of physicist Enrico Fermi, the computer scientist John R. Pasta and mathematician Stanislaw Ulam. Two lines in the report recognized the important role of the programmer Mary Tsingou. Hence, many sicentists in the field propose today the namy of Fermi-Pasta-Ulam-Tsingou for this problem.

From the theoretical point of view, there were initially two lines that have been motivated by the FPU problem. The first line by Zabusky and Kruskal [47] in 1965, who numerically studied the interaction of solitons in a collisionless

plasma and the recurrence of initial states. These phenomena were observed in the numerical solutions of the Korteweg-deVries equation. The Kortweg de Vries equation (KdV) was describe the long wave solutions of the FPU [48]. A second line of research was initiated by Izrailev and Chirikov in 1966 [49]. They investigated the qualitative behavior of longitudinal oscillation of a nonlinear string with fixed ends. This study is based on the Kolmogorov Arnold Moser (KAM) theorem, or more generally on the application of canonical perturbation theory to the study of FPU [48]. The FPU problem has been extensively studied as a model for discrete system in the past few years [50–53].

The FPU problem has been demonstrated as an ideal framework for both theoretical and experimental studies. Specifically, first, the model was set up in the form of equations of motion. Then, numerical simulation or "numerical experiments" were performed to understand the effect of the nonlinear interactions. The history of the first twenty years of studies of the FPU problem can be found in the book of Weisser [54] or in the paper of Berman. [55].

In this chapter we study different problems of wave propagation in repulsive lattices, from theoretical and experimental point of view. The first part is devoted to the presentation of the theoretical model (array of repelling particles) and also of the experimental setup (array of coupled magnetic pendulum). A study of higher harmonic generation in the lattice is presented in this part. The weakly nonlinear limit is considered, where the model approaches to the α-FPU equation (with quadratic nonlinear term). In sec.(1.7), we presents the chain dilation. Sec.(1.8) considers the standing waves in the chain, when finite size effects are included. Effects as subharmonic generation or nonlinear frequency shift are reported in this part. Finally in Sec.(1.9), the third part presents a study of localized wave propagation, or kinks. Kinks in this system are characterized theoretically and experimentally, by measuring its propagation velocity and other characteristics. The effect of a substrate or on-site potential is also discussed in the same section.

2.2. THEORETICAL MODEL

2.2.1. EQUATION OF MOTION

We consider an infinite chain of identical particles with mass m aligned along the x-axis, interacting with their nearest neighbors via repulsive potentials, V_{int} (see Figure 2.1). In the absence of perturbations, every mass has a fixed equilibrium position, with the interparticle distance given by a. Since the forces are repulsive, note that for a finite chain this is only possible if there is an external potential V_{ext} that keeps the particles confined. This effect can be provided by a periodic on-

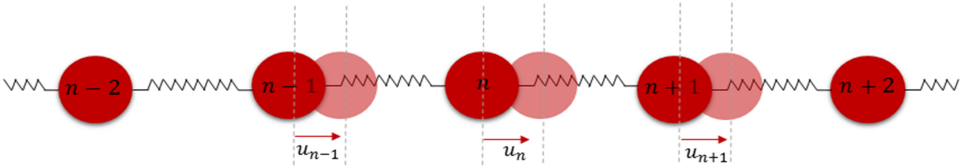

Figure 2.1: Scheme of the lattice.

site potential, or a force keeping the boundary particles at fixed positions. The equation of motion can be written as

$$M\ddot{u}_n = V'_{\text{int}}(u_{n+1} - u_n) - V'_{\text{int}}(u_n - u_{n-1}) + V'_{\text{ext}}, \tag{2.1}$$

where u_n stands for the displacement of the n-th particle measured with respect to its equilibrium position, M is the mass of the particle, V are the potentials and V' their derivatives with respect to the spatial coordinate, representing forces. For small displacements, the interaction force can be considered linear with respect to the distance between the particles, r, i.e., $V'(r) = \kappa r$ where κ is a constant, then Eq. (2.1) represents a system of coupled harmonic oscillators. For higher displacements, the linear approximation of the interaction force can not be assumed and nonlinearity must be considered. Chains of nonlinearly coupled oscillators have been extensively studied in the past for different types of anharmonic interaction potentials. Some relevant cases are the α-FPU lattice, where $V'(r) = \kappa_1 r + \kappa_2 r^2$ (quadratic interaction), the β-FPU lattice where $V'(r) = \kappa_1 r + \kappa_3 r^3$ (cubic interaction), the Toda lattice, with $V'(r) = \exp(-r) - 1$ or the granular lattice, with $V'(r) = \kappa r^{3/2}$. Here we consider the case of forces that decrease with an inverse power law of the distance, $V'(r) = \beta r^{-\alpha}$, typical of interatomic interactions, mediated by Coulomb repulsion between like charges. For such a potential, the equation of motion results in

$$M\ddot{u}_n = \frac{\beta}{(a - u_{n+1} + u_n)^\alpha} - \frac{\beta}{(a - u_n + u_{n-1})^\alpha} + V'_{\text{ext}}. \tag{2.2}$$

The exponent α can take different values depending on the particular system: $\alpha = 2$ for electrically charged particles (as e.g. in ion coulomb crystals [27] or dusty plasma crystals [33]), $\alpha = 4$ for distant magnetic dipoles [35], or any other non-integer power [13].

In general, Eq. (2.2) do not possess analytical solutions. Approximate analytical solutions can be obtained in the small amplitude limit, i.e., assuming that

the particle displacement $|u_{n\pm1} - u_n|$ is small compared to the lattice constant a. Then, the forces can be expanded in Taylor series and Eq.(2.2) can be reduced, neglecting cubic and higher order terms, to an equation in the form

$$\ddot{u}_n = \frac{1}{4}(u_{n-1} - 2u_n + u_{n+1}) - \frac{\varepsilon}{8}(u_{n-1} - 2u_n + u_{n+1})(u_{n-1} - u_{n+1}) + \Omega_0^2 u_n, \tag{2.3}$$

where dots indicate now derivative with respect to a dimensionless time $\tau = \omega_m t$, where $\omega_m = \sqrt{4\alpha\beta/Ma^{\alpha+1}}$ is the maximum frequency of propagating waves (upper cutoff frequency), $\Omega_0 = \omega_0/\omega_m$ and $\varepsilon = (1+\alpha)\frac{u_0}{a}$ is the nonlinearity coefficient. The displacement u_n is normalized to a typical reference value u_0, which we assume to be equal to the excitation amplitude. The external (e.g. on-site) potential, giving a restoring force V'_{ext} is in general nonlinear. However, for small displacements, as considered here, it may be represented by a term $V'_{\text{ext}} = ku_n$, where k is a constant that defines the frequency of oscillation of the particle in the external potential. The particular form of this term for the proposed experimental setup will be discussed later.

If the on-site potential term is neglected (no external forces acting on the chain), Eq. (2.3) reduces to the celebrated α-FPU equation. It has been considered as an approximate description of many different physical systems, and has played a central role in the study of solitons and chaos [56].

2.2.2. DISPERSION RELATION

Some important features of the propagation of waves in a lattice can be understood by analyzing its dispersion relation. For infinitesimal amplitude waves, it can be obtained analytically by neglecting the nonlinear terms in the equation of motion, and solving for a harmonic discrete solution in the form $u_n \sim \exp i(\Omega t - kna)$, where $\Omega = \omega/\omega_m$ is the normalized excitation frequency and k is the wave number. By replacing the solution in the linearized Eq. (2.3), we obtain the well known dispersion relation for a monoatomic lattice, which with the normalizations used it reads

$$\Omega = \sqrt{\sin^2\left(\frac{ka}{2}\right) + \Omega_0^2}. \tag{2.4}$$

There is an upper cutoff frequency at which the transition from propagative to evanescent solutions is produced and it is given in this normalization by $\Omega = 1$. The effect of the on-site potential is to create a low frequency bandgap in the dispersion relation, i. e., Ω_0 represents a –normalized– lower cut-off frequency.

In the absence of external confining potential, $\Omega_0 \to 0$ and the dispersion relation reduces to $\Omega = |\sin(ka/2)|$.

Although the dispersion relation has been derived assuming infinitesimal amplitude (linear) waves, it describes also the propagation of modes as the higher harmonics of a fundamental wave (FW), when these are generated by nonlinear processes, as described in the following sections.

2.2.3. ANALYTICAL SOLUTIONS

One known effect of the quadratic nonlinearity is the generation of second and higher harmonics of an input signal. This is the basic effect, for example, of nonlinear acoustic waves propagating in homogeneous, non-dispersive media [10, 57], where the amplitude of the harmonics depends on the nonlinearity of the medium, the excitation signal and the propagated distance (its amplitude u_0, frequency ω and its position n).

In a discrete lattice described by Eq. (2.3), the amplitude of the harmonics is also strongly dependent on dispersion. To study the process of harmonic generation, an analytical solution can be obtained by perturbative techniques, such as the successive approximations method. We follow this approach, by assuming that the nonlinear parameter ε is small (which implies displacements much smaller than the interparticle separation), and expressing the displacement as a power series in terms of ε, in the form $u_n = u_n^{(0)} + \varepsilon u_n^{(1)} + \varepsilon^2 u_n^{(2)} + \ldots$. After substituting the expansion into Eq. (2.3), and collecting terms at each order in ε, we obtain a hierarchy of linear equations that can be recursively solved. This has been done in Ref. [37] to study nonlinear waves in a granular chain, formed by spherical particles in contact interacting by Hertz potentials, and the result is readily extendible to chain of particles interacting by inverse power laws of arbitrary exponent, which results in a particular value of the nonlinearity coefficient. The equation of motion is always given by Eq. (2.3), the value of ε being dependent on the exponent α. In case of granular chain, it was shown that $\varepsilon = u_0/2a$, while fin this work of a chain with quasi-dipolar interaction,it is approximately 10 times higher.

Up to second order of accuracy in ε, the displacement field can be expressed as (the details of the derivation can be found in [37])

$$\begin{aligned} u_n =& \varepsilon\Omega^2 n + \\ & \frac{1}{2}\left[1 + \frac{1}{4} i\varepsilon^2 C_\Omega \sin\left(\frac{\Delta k}{2} n\right) e^{i\frac{\Delta k}{2} n}\right] e^{i\theta_n} + \\ & \frac{\varepsilon}{4}\cot\left(\frac{k}{2}\right)\sin\left(\frac{\Delta k}{2} n\right) e^{i\frac{\Delta k}{2} n} e^{2i\theta_n} + \text{c.c.}, \end{aligned} \tag{2.5}$$

where $\theta_n = \Omega t - kna$, n is the oscillator number corresponding to the discrete propagation coordinate, and

$$C_\Omega = 1 - \frac{\sin[k(2\Omega)/2]}{\sin[\Delta k(\Omega)/2]} \tag{2.6}$$

where $\Delta k = 2k(\Omega) - k(2\Omega)$ is the wave number mismatch between the forced, $2k(\Omega)$, and free, $k(2\Omega)$, contributions to the second harmonic (SH).

The solution given by Eq. (2.5) describes wave propagation in the system when the frequency of the SH belongs to the dispersion relation, which is the case for driving frequencies $\Omega < 1/2$. For higher driving frequencies, the SH frequency is outside the propagation band (evanescent mode) and the solution takes the form

$$\begin{aligned} u_n =& \varepsilon\Omega^2 n + \\ & \frac{1}{2}\left[1 + \frac{1}{8}\varepsilon^2 C_\Omega \left(1 - e^{-k''n} e^{ik'n}\right)\right] e^{i\theta_n} + \\ & \frac{\varepsilon}{8}\cot\left(\frac{k}{2}\right)\left(1 - e^{-k''n} e^{ik'n}\right) e^{2i\theta_n} + \text{c.c.}, \end{aligned} \tag{2.7}$$

where $k'' = 2\cosh^{-1}(2\Omega)$ and $k' = 2k(\Omega) - 1$ and the mismatch take now the form $\Delta k = k' + ik''$.

The previous analytical solutions (2.5-2.7) predict a number of distinctive features in the nonlinear dynamics of the system, depending on the frequency regime. In the case of the SH belonging to the propagation band, Eq. (2.5), dispersion causes a beating in the amplitudes of the different harmonics, since two components of the SH with different wavenumbers propagate asynchronously. FW and SH waves oscillate out of phase in space: the displacement in the FW is maximum where the SH vanishes, which occurs for magnets at positions satisfying the following condition:$n = 2\pi/\Delta k$. Energy is then transferred between the two waves as they propagate. The half distance of the spatial beating period corresponds to the coherence length l_c:

$$l_c = \frac{\pi}{\Delta k}, \tag{2.8}$$

and it physically corresponds to the position where free and forced waves are exactly out of phase.

When the SH frequency lies beyond the cut-off frequency, the free wave is evanescent. There still exists however a forced wave, driven by the first harmonic at any point in the chain. Due to this continuous forcing, the amplitude of the FW and the SH does not oscillate anymore, but it reaches a constant value after

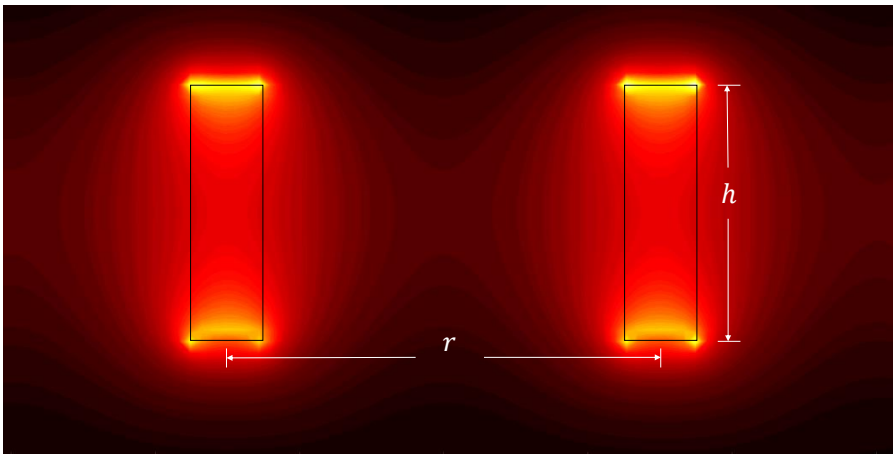

Figure 2.2: The scheme of magnetic filed.

a short transient of growth. Note that this implies propagation of the SH even in the forbidden region.

Finally, we note that the theory predicts the existence of a zero-frequency mode, $u_n = \varepsilon\Omega^2 n$, which represents an static deformation of the lattice. This effect will be studied in detail later.

2.3. THE LATTICE OF MAGNETIC DIPOLES

Consider two magnetic dipoles, with magnetic moments $\vec{m}_1$ and $\vec{m}_2$. The force between them is given by the exact relation [58]

$$\vec{F}_{1,2} = \frac{\mu_0}{4\pi}\vec{\nabla}\cdot\left[\frac{\vec{m}_1\cdot\vec{m}_2}{r^3} - 3\frac{(\vec{m}_1\cdot\vec{r})\,(\vec{m}_2\cdot\vec{r})}{r^5}\right], \tag{2.9}$$

where $\vec{r}$ is the vector joining the centres of the dipoles. This relation implies that, in general, the force depends on the angle between the dipoles. In the particular case when the dipole moments are equal in magnitude, parallel to each other, and perpendicular to $\vec{r}$ (dipoles in the same plane), the force takes the simpler form

$$\vec{F}_{1,2} = \frac{3\mu_0}{4\pi}\frac{m^2}{r^4}\hat{x}, \tag{2.10}$$

where $m = |\vec{m}_1| = |\vec{m}_2|$, and μ_0 is the permeability of the medium and $\hat{x}$ is an unitary vector in the direction of the axis that connect the centers of the mag-

nets. This is the force between two neighbour magnetic dipoles of the chain at equilibrium and $r = a$.

In the case of the perturbed chain of magnets with nearest neighbours interaction, the distance between centres $r(t)$ is a dynamic variable. Assumingsmall displacements of the magnets, i.e., the angles between the dipole moments are small, we can use Eq. (2.10) with $r(t) = a - u_n + u_{n+1}$ to describe the interaction between two neighbour oscillators

$$\vec{F}_{n,n+1} = \frac{3\mu_0 m^2}{4\pi} \frac{1}{(a - u_n + u_{n+1})^4}, \tag{2.11}$$

and comparing with the equation of motion of the chain, shown in Eq. (2.2), we identify the parameters:

$$\beta = (3/4\pi)\mu_0 m^2, \quad \alpha = 4. \tag{2.12}$$

This small angle Eq.(2.11) for the forces is a crude approximation and exact expressions can be found in Ref. [35]. However, since our aim is to obtain simple analytical expressions based on the FPU equation, Eq. (2.3), we will keep this degree of accuracy. The validity of this approximation to describe our setup will be tested in the next sections when the predictions are compared with the experimental results.

The above expressions for the forces between magnetic dipoles are valid for loop currents or magnets of negligible dimensions. Expressions for finite size magnets can be found in the literature [59] and are in general lengthy and cumbersome. Gilbert's model of magnetic field of magnets used here results in approximate but simple expressions for the forces [58]. For cylindrical magnets of length h with their magnetic moments parallel, and their axis perpendicular to the line joining the centres, the force between adjacent magnets is expressed as

$$\vec{F}_{1,2} = \frac{\mu_0 m^2}{2\pi h^2} \left(\frac{1}{r^2} - \frac{r}{\left(r^2 + h^2\right)^{3/2}} \right) \hat{x}, \tag{2.13}$$

where the magnetic moment is $m = \mathscr{M} h \pi R^2$, $\mathscr{M}$ is the magnetization and R the radius of a the cylindrical magnet.

In the limit $h \ll r$, Eq. (2.13) reduces to Eq. (2.10), i.e. magnets with small dimensions compared to their separation interact via dipolar forces, i.e., $\alpha = 4$. In the opposite limit $h \gg r$, parallel magnets close to each other, the interaction law approach to a Coulomb-type force, i.e., $\alpha = 2$. In general, the interaction law of magnets can be approached well by an inverse-law with any given exponent that ranges between monopole and dipole cases.

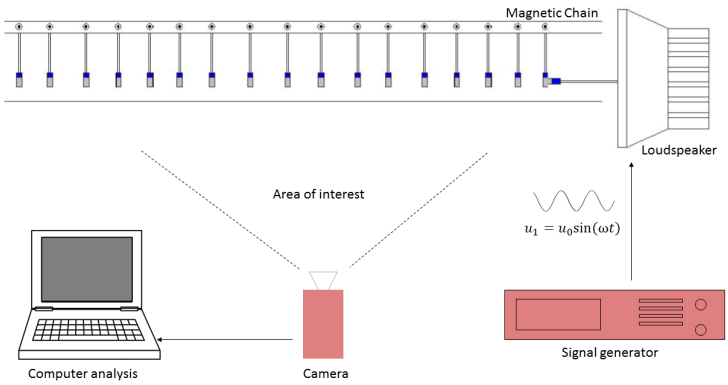

Figure 2.3: Schematic representation of the magnitic chain setup.

2.4. EXPERIMENTAL SETUP

A chain of coupled magnets has been built in order to test the theoretical predictions. The experimental setup is shown in Fig. 2.4. The chain consist of 53 identical cylindrical Neodymium magnets (Webcraft GmbH, DE, magnet type N45), with mass $M = 2$g, arranged in a one-dimensional periodic lattice. The radius and heigh of the magnets are $R = 2.5$ mm and $h = 14$ mm, respectively. The magnets are oriented with the closest poles being those of the same polarity, therefore the produced forces are repulsive. The value of the magnetization is $\mathscr{M} = 1.07\ 10^6$ A/m.

To achieve the necessary stability of the chain, the magnets are attached to a rigid bar which can rotate around a fixed T-shaped support, being each magnet actually a pendulum. The length of the vertical bars is $L = 100$ mm, and the distance between supports (and therefore the distance between magnets at equilibrium) is $a = 20$ mm. The support was specially designed to minimize the effects of friction by using additional ring magnets which keep the oscillators levitating on air, with just one contact point, as shown in the inset of Figs. (2.4) and (2.3).

The effect of the pendulums is to introduce an additional external force to the dynamics of the chain, as it corresponds to the term V'_{ext} in Eq. (2.2). If θ_n is the angle formed by a magnet with respect to its vertical equilibrium position, its restoring force due to gravity is $F_z = Mg\sin\theta_n$. For small angles θ_n, and using the notation of Eq. (2.2), the force per mass can be approximated as $V'_{\text{ext}} \simeq \omega_0^2 u_n$, with $\omega_0 = \sqrt{g/L}$.

All magnets oscillate freely except the outermost boundary magnets. The last

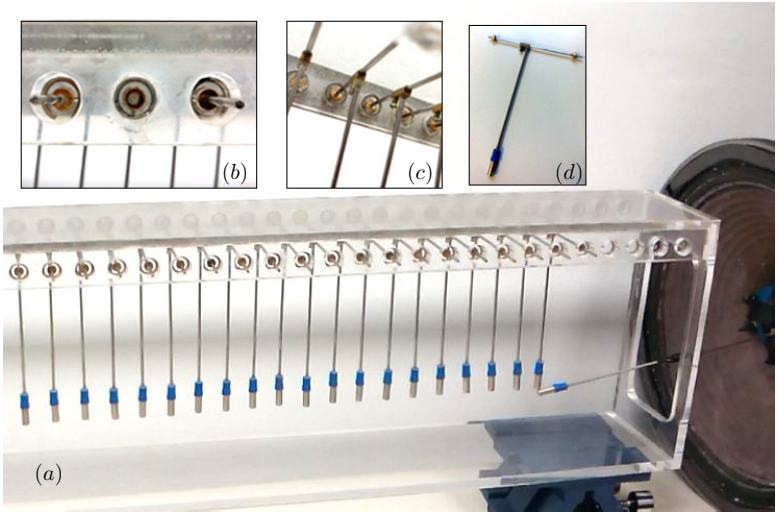

Figure 2.4: The experimental setup,(a) Details of the experimental lattice attached to the driving source, a loudspeaker. (b) and (c) shows that the pendulums that are "hanging" vertically by gravity. Friction is minimized by levitation, mediated the repulsion force between two discs magnets. (d) T-shaped pendulum. The distance between magnets is $a = 20$ mm.

magnet is fixed, and the first one is attached to the excitation system. The driving system consist of a electrodynamic loudspeaker (Fostex-L363) connected to an audio amplifier (Europower EPS2500) and excited by a arbitrary function generator (Tektronix AFG-2021). The first magnet is fixed to the loudspeaker's diaphragm and it is forced with a sinusoidal motion for different values of frequencies and amplitudes.

The motion of the chain is recorded by using a GoPro-Hero3 camera. The camera is placed at proper distance from the chain in order to track the motion of a certain number of magnets. In this work, 18 magnets have been recorded simultaneously. Then, each pendulum is optically tracked using image post-processing techniques. We considered the travelling wave regime, by ignoring the reflected wave by time window the recorded video. The duration of each record was about $3.5s$ and the camera resolution was set to $960p$ the frame rate of 100 frames per second, i.e., leading to a sampling frequency of 100 Hz of the measured displacement waveforms. Videos are analized with Matlab for obtaining the frequencies of movement of pendulums via the Fourier transform.

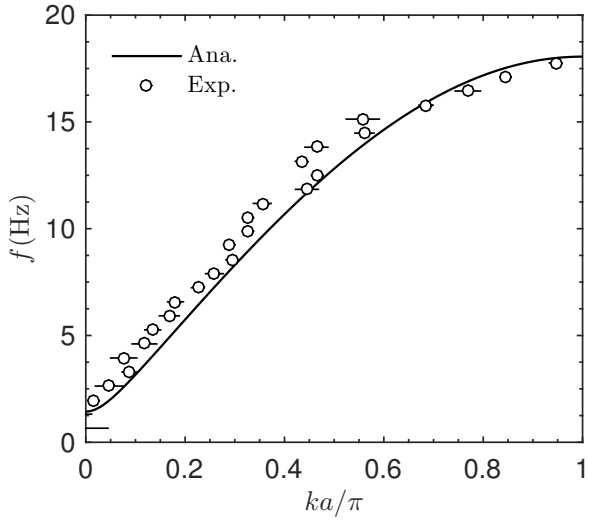

Figure 2.5: The dispersion relation of a mono-atomic chain obtained analytically by using Eq. (2.4) (continuous line) and by the experimental measurements (circles). Horizontal bars indicate the error of the normalized wavenumber.

2.5. DISPERSION RELATION

To obtain the dispersion relation experimentally, the first magnet was excited with short duration impulse with low amplitude excitation in order to assure that the chain is working in the linear regime. Then, the generated travelling pulse was recorded at two consecutive magnets and the phase difference between them was computed as

$$c_p(\omega) = \frac{\omega a}{\arg[H_2(\omega, n+1)/H_1(\omega, n)]}, \tag{2.14}$$

where $H(\omega, n)$ is the Fourier transform of the measured displacement of the n-th magnet. A set of 10 measurements of chain displacements were recorded in stationary regime to compute the mean value for each frequency. The frequency step was Δf and the small magnitude of the calculated errors indicates good repetitiveness of the measurements. Figure 2.5 shows the experimental results and linear dispersion relation of Eq. (2.4). The lower bandgap determines the minimum frequency for the waves to propagate, and it is $f_0 = 1.5$ Hz which agrees with the theoretical value $f_0 = (1/2\pi)\sqrt{g/L}$. The measured upper cutoff frequency is $f_m = 18.2$ Hz, which is in agreement with the theoretical prediction $f_m = (1/2\pi)\sqrt{4\alpha\beta/Ma^{\alpha+1}}$, which has been estimated by fitting Eq. (2.13) to an inverse power law with exponent $\alpha = 3.6$ (quasi-dipolar interaction). Both the

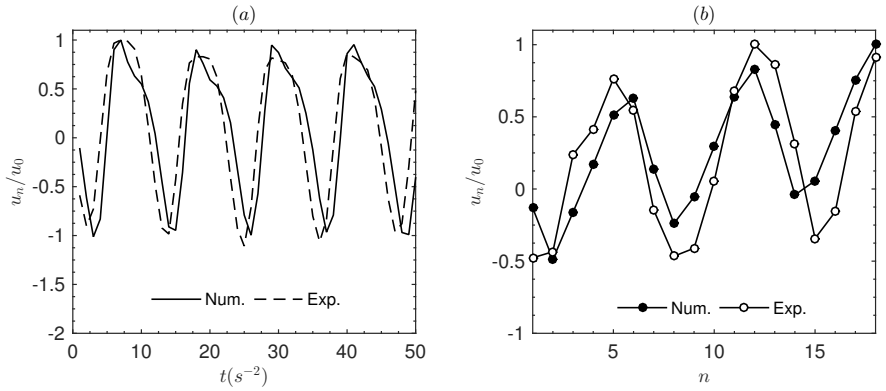

Figure 2.6: The waveform in space and time f_d = 8Hz. (a) The temporal waveform for 11^{th} pendulum. (b) Spatial waveform for 18 Pendulum.

upper and lower values of the dispersion relation obtained experimentally can slightly change with the amplitude of the input excitation u_0, which is in fact a signature of nonlinear dispersion. As the condition $u_0 << a$ is fullfield, the chain propagates waves in the linear regime and the dispersion relation can be obtained.

2.6. HIGHER HARMONIC GENERATION

By driving the first magnet with an sinusoidal motion, $u_1 = u_0 \sin\omega t$, harmonic waves are excited to propagate along the chain. The amplitude u_0 was fixed in all the measurements (u_0 = 3 mm). Fig.2.6 shown the effect of the nonlinearity on the spatial and temporal waveform. According to the dispersion relation shown in Fig. 2.5 the driving frequency , ω, can be chosen among to three different regimes regarding the propagation of the SH: (a) weakly dispersive, (b) strongly dispersive, and (c) evanescent. The first case (a) is obtained when the frequency of the FW lies in the lower part of the pass band and, the nonlinearly generated SH is also in the pass band, in the region of weak dispersion. Thus, the wave roughly propagates as if the chain was a continuous nondispersive medium. In this low frequency regime, all the firsts harmonics propagate with nearly the same velocity. The amplitude of the SH increases with distance while the first harmonic amplitude decreases due to the energy transfer from FW to the higher harmonics. This case is shown in Fig. 2.7(a), where the FW with frequency f = 5 Hz generates a SH with frequency $2f$ = 10 Hz in the weakly-dispersive part of the propagative band. We note that in this regime, third harmonic is also present, since it still belongs to the pass band.

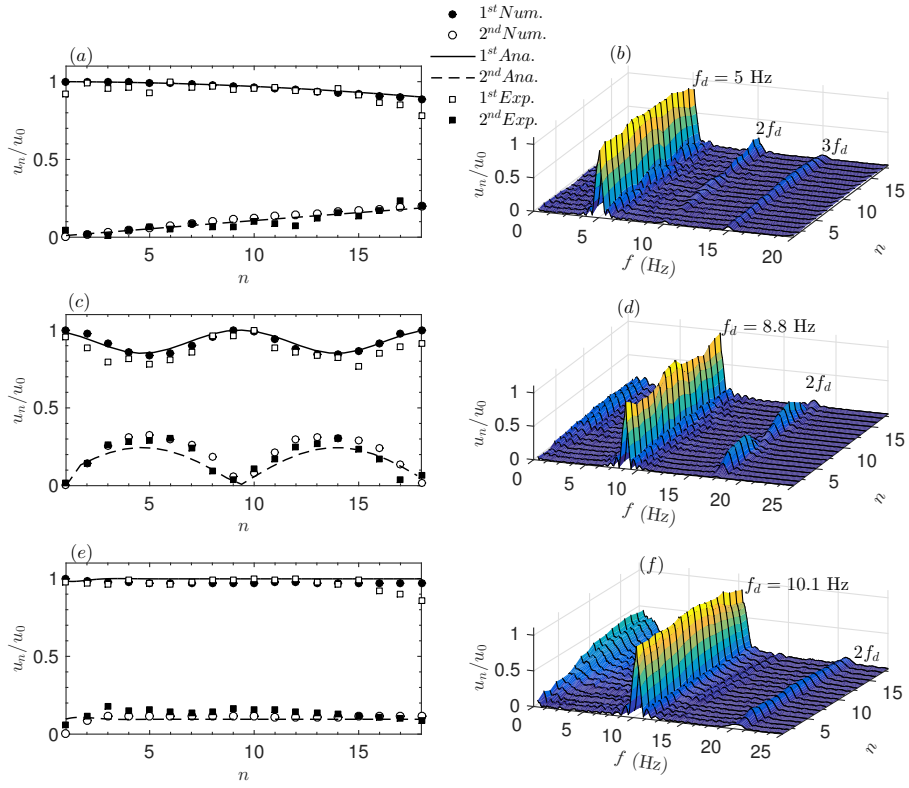

Figure 2.7: Three different regimes of harmonic generation, measured at different frequencies. Weakly dispersive regime (a), strongly dispersive regime (b), and evanescent regime (c) of the SH.

The case (b) of strongly dispersive SH is shown in Fig. 2.7(b), where the driving frequency approaches the half of the passband frequency. The SH lies in the highly dispersive part of the band, but still in a propagative region (slightly below the cutoff frequency f_m). As in the previous case, the amplitude of the SH increases with distance, but at a particular distance given by the coherence length, l_c, it decreases. Both, FW and SH present spatial oscillations or "beatings".

Figure 2.7(b) illustrates this case, for a FW with frequency $f = 8.8$ Hz and SH at $2f = 17.6$ Hz. The coherence length has been estimated to be $l_c = 4.5a$, which is in agreement with the theoretical given by Eq. (2.8).

Finally, the case (c) corresponds to the SH lying within the band-gap. In this case, the SH is evanescent and its amplitude do not change with distance. One would expect the absence of the SH field (since it is an evanescent wave) but it gets a finite amplitude. The SH is generated locally and it is "pumped" by the

FW. Its amplitude value is constant all along the chain and it depends on the amplitude of excitation signal and also on the properties of the medium (nonlinearity and the dispersion parameters). As shown in Fig. 2.7(c), the frequency of the excitation signal is $f = 10.1$ Hz and generates the SH in the upper band gap.

The experimental results shown in Fig. 2.7 are compared with the analytical predictions of the asymptotic theory (solid lines), and also with the numerical simulation of Eq. (2.3). The value of nonlinear coefficient, defined as $\varepsilon = (1+\alpha)u_0/a$, has been estimated using the previously calculated value of $\alpha = 3.6$, and setting the forcing amplitude to an average value $u_0 = 2.4$ mm, from which we obtained the value $\varepsilon = 0.55$. The figure shows that the analytical and numerical simulation results are in good agreement with the values obtained experimentally.

2.7. CHAIN DILATATION

Besides the harmonic generation, the FPU equation introduced the Sect. (2) also predicts the presence of a static (zero-frequency) mode. It physically represents an incremental shift of the average position of each oscillator, which in turn results in a dilatation or expansion of the chain. This term is accounted for by the first term in Eqs. (2.5). Since the average displacement grows linearly with distance, it can be interpreted as a constant strain produced by the acoustic wave along the lattice.

The phenomenon was originally reported for acoustic waves propagating in a solid described by a nonlinear wave equation[60], which is actually the continuous (long-wavelength) analogue of Eq. (2.3). The effect was described there as an acoustic-radiation-induced strain. The physical origin of the expansion of the discrete chain (and also in the continuous solid) is the anharmonicity of the interaction potential, and therefore is a generically nonlinear effect.

We remark that the phenomenon of acoustic expansion is analogous to the thermal expansion of solids, which also has its physical origin in the lattice anharmonicity. The link between these two effects and its relation with the acoustic nonlinear parameter has been pointed out in Ref. [61].

The same technique described above for the harmonics allowed to extract the evolution of the static displacement mode from the experiments. The results are shown in Fig. 2.8 for different excitation frequencies. It shows evidence of the existence of the static mode and its dependency with the excitation frequency. We can observe two regimes, and a transition between them at a particular distance (number of pendulum). In the region near the boundary (extending up to $n = 8$ in our experiment) the displacement grows linearly with distance, as pre-

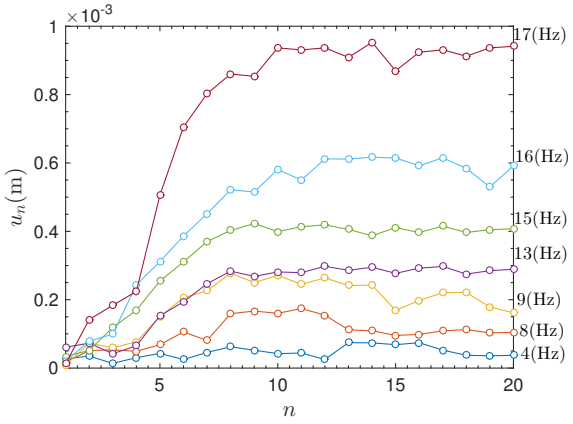

Figure 2.8: Relative amplitude of the static displacement mode, at each pendule n measured experimentally for different frequencies.

dicted by the theory. At that distance, the growth of the static displacement mode saturates, and the chain attains an unstrained state, with the oscillators moving around positions shifted with respect to their initial values. This behaviour is not predicted by the theory.

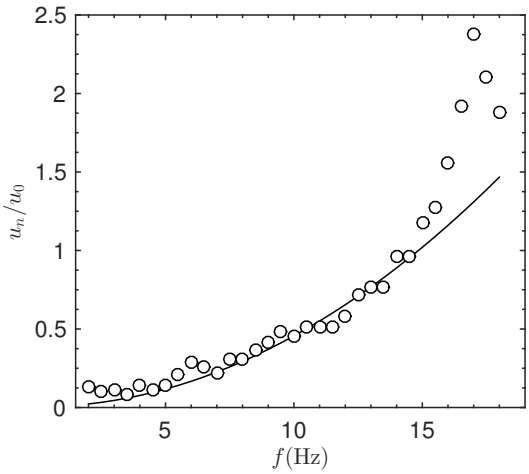

Figure 2.9: Dependence of the amplitude of static mode with the frequency, measured at the oscillator n=10. (Line) Analytically, (Circles) Experimentally.

The saturation effect can be understood if we recall that the theory was de-

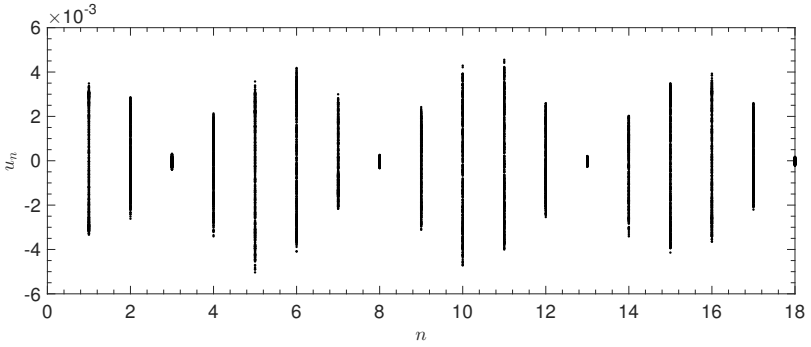

Figure 2.10: Experimental standing wave in a discrete system. Chain of 18 coupled oscillators, where u_n is the displacement of n^{th} oscillator, the driven frequency is f_d = 6.5 Hz and the excitation amplitude is u_0 = 3.4mm.

veloped assuming that there was not a prescribed equilibrium position for any oscillator in the chain, the chain was assumed semi-infinite, and the only force acting on the masses was the nearest neighbours interaction. However, in the experiment an additional force is present, due to gravity. This is equivalent to an on-site potential, whose effect is no more negligible at long distances: since the supports of the pendula are fixed, the maximum shift of a magnet with respect to the equilibrium position is also bounded.

Additionally, we observe that the existence of a low-frequency bandgap does not have a significant influence on the generated zero frequency mode. Figure 2.9 shows experimental (dots), numerical (crosses) and analytical (full line) results for the static displacement of a given magnet (n = 10), as a function of the driving frequency.

2.8. SUBHARMONIC GENERATION

When a nonlinear system is excited by a pure sinusoidal wave, new frequency components can appear under appropriate circumstances. Beside generation of higher harmonics and the static displacement mode with zero frequency, under some conditions new frequency components are nonlinearly generated, these components are called "*subharmonics*". These are the harmonics having frequencies lower than the driving frequency. In 1859, Melde [18] was the first to observe the generation of the subharmonics experimentally. His experiment consisted of a string with one end fixed to a tuning fork. When the fork set the string into longitudinal vibration at a particular frequency, he found that transverse vibrations were excited with a frequency nearly half of the driving frequency. In

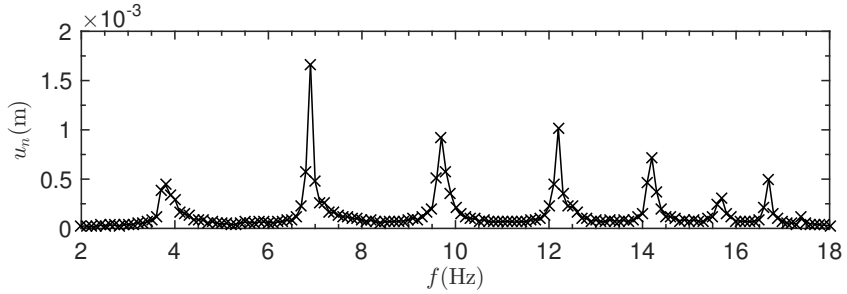

Figure 2.11: The experimental data for the resonance frequency in a finite chain with 10 pendulums, where u_m is the maximum amplitude of the 1^{st} harmonic. The chain has 8 modes at f_s = [3.8, 6.9, 9.8, 12.2, 14.2, 15.7, 16.7] Hz

1887, Rayleigh [19] reported that the generation of subharmonics is a result of the instabilities caused by the variation of the spring tension.

Korpel and Adler [62] in 1965 showed that above a certain energy-density threshold in an intense ultrasonic standing wave, subharmonics of the driving frequency were present. Bamberg *et al.* [63] studied the generation of subharmonics in an acoustic Fabry-Perot interferometer using two air-backed x-cut quartz transducers submerged in water, driving one around its 3 MHz resonance, and examining the frequency spectrum across the other with a spectrum analyzer. In Bamberg's model all subharmonics observed had frequencies that are integer harmonics of the fundamental cavity resonance.

In 1970, Adler [64] predicted the subharmonics in a liquid-filled ultrasonic cavity which are parametric excited ultrasonic waves. Adler investigated the wave propagating in finite medium, the driver transducer at one end and the other end a plane rigid reflector. His solution of Mathieu's equation predicts the experimentally observed doublets at about one-half, and at about three-halves, of the driver frequency. Also, he predicted the relation between the frequency separation of the doublet components to the cavity length and the vibration amplitude of the driver transducer.

Generally, one of the main parameters in the nonlinear dynamics is the excitation amplitude. There are at least five regions of excitation; *Linear regime:* at low amplitude, the spectrum only contain the component of the driven frequency. In *nonlinear regime*, as we increase the amplitude the system starts to generate higher harmonics (2^{nd}, 3^{rd}, 4^{th},..., etc). With further increase of the amplitude above a certain value (above nonlinear regime), subharmonics are generated. As we increasing the amplitude more the system becomes chaotic [65].

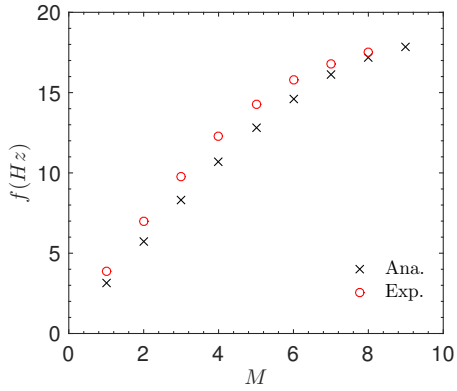

Figure 2.12: The dispersion relation $f \propto M$, where M number of modes. (Circles) The experimental results of a chain with 10 pendulums where the last one is fixed. (Cross) the analytic equation (2.15).

2.8.1. RESONANCE FREQUENCY

As we are dealing with standing waves, we can characterize the resonance frequency of the lattice. We excited the system with a harmonic signal with very low amplitude u_0 while the frequency was changed from $f = 2$ Hz to 18 Hz. Fig.(2.11) shows the experimental result of the resonance frequency in a chain with 10 pendulums where the last pendulum 10^{th} is fixed. The spectrum has 8 peaks at $f_s = [3.8, 6.9, 9.8, 12.2, 14.2, 15.7, 16.7]$ Hz. To obtain the relation between mode number and the frequency, we derived the dispersion relation in a finite discrete system as

$$\omega_M^2 = \omega_0^2 + \omega_c^2 \sin(\frac{\pi M}{2(N+1)})^2 \tag{2.15}$$

where N is the number of pendulums, M is the normal modes, ω_c is the cut-off frequency and ω_0 is the minimum frequency. We presented the Eq.(2.15) with the experimental results in Fig. (2.12), and it show a good agreement.

2.8.2. THE EFFECT OF THE EXCITATION AMPLITUDE

As we mentioned before, the main parameter in the nonlinear system is the excitation amplitude u_0. Fig.(2.13) shows the waveform and the spectrum for the 4^{th} pendulum in a chain consisting of 10 pendulums, the driving frequency $f_d = 9.8$ Hz and we changed the amplitude from $u_0 = 3$mm to $u_0 = 19$mm. Fig.(2.13,a,b) shows the waveform and the spectrum at very low amplitude which is in linear regime. As we increase the excitation amplitude to be in nonlinear regime, as in

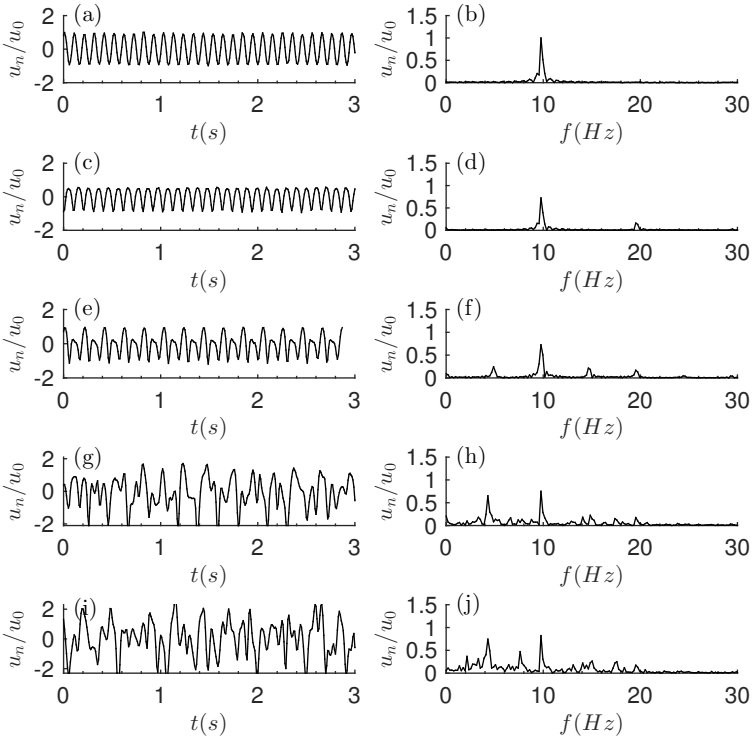

Figure 2.13: (a,c,e,g,i) Waveforms and (b,d,f,h,j) Frequency spectra of output signal for the 4^{th} pendulum in chain with 10 pendulum, where the input signal with a frequency at 9.8 Hz. (a,b) u_0 = 3 mm,(c,d) u_0 = 13 mm, (e,f) u_0 = 15 mm, (g,h) u_0 = 18 mm and (i,j) u_0 = 19 mm.

Fig.(2.13,c,d), the second harmonic is generated at $2f_d$ = 19.6 Hz. With further increase in the amplitude, subharmonics appear at $f_d/2$ = 4.8 Hz, a process that is also accompained by higher harmonics, as shown Fig.(2.13,e,f). With higher increase in the excitation amplitude, the wave become chaotic as Fig.(2.13,i.j) represents.

Figure (2.14) shows the relation between the excitation amplitude and harmonics amplitude (subharmonic and 1^{st} harmonic). With increasing the excitation amplitude leads to increasing the both harmonics (Subharmonc and 1^{st} harmonic) but from a certain amplitude the subharmonic amplitude jump to be higher than the 1^{st} harmonic.

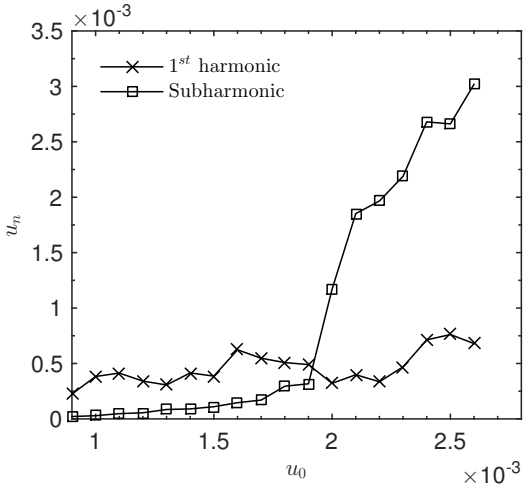

Figure 2.14: The amplitude of the first harmonic and subharmoncis versus the excitation amplitude, number of pendulums in the chain of 10 pendulums and a driving frequency f_d = 14Hz. The amplitude of the harmonics u_n has been normalized to the maximum amplitude of the first harmonic u_m.

2.8.3. MODULATIONAL INSTABILITY

In the theory of nonlinear waves, the modulation instability or "sideband instability" is a reinforcing effect by the nonlinearity and the distortion of a periodic wave which leads to appearance of side bands around the driving frequency. The phenomenon was first modelled in 1967 by Benjamin and Feir. They studied periodic surface gravity waves on deep water, and it's also called *Benjamin Feir instability* [66] [67] [68].

In a discrte system, Kivshar *et al.* studied analytically and numerically modulational instabilities in discrete nonlinear chains such as the Klein-Gordon equation [69]. Rapti *et al.* [70] examined the parametric and modulational instabilities arising in a discrete nonlinear Schrödinger equation. In Ref.[71], Zakharova and Ostrovsky discussed the early history of modulation instability with more detail.

In our model, we observed this kind of the waveform modulation. Fig.(2.15) shows the observation of the wave modulation for different amplitudes and the spectrum components. In a chain with 11 pendulums, we inject the signal with a frequency 10 Hz. As the figure shows, the effect of modulation instability is the result of interaction between a strong carrier harmonic wave at a frequency ω, and small sidebands $\omega \pm \Delta\omega$.

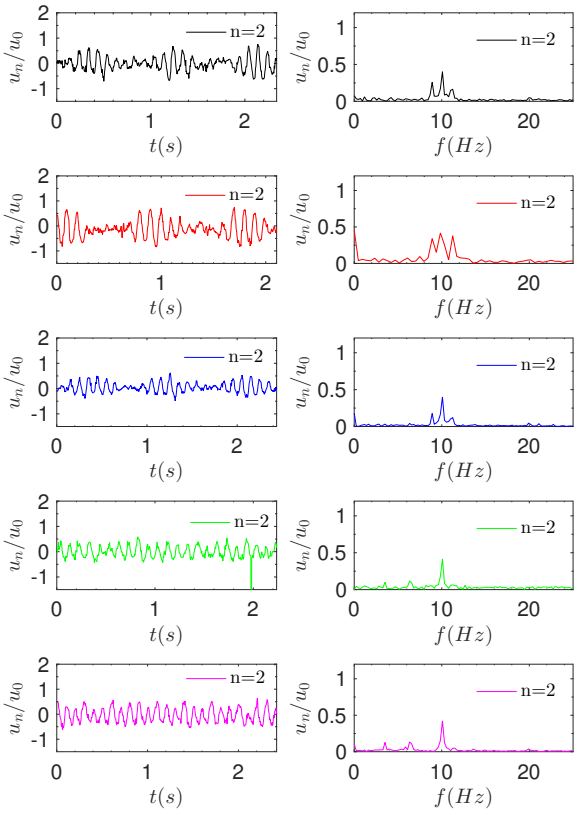

Figure 2.15: Subharmonics generation After Parametric Instability ; the driven frequency 10 Hz, the number of pendulums 11. (Black) u_0 = .9mm, (Red) u_0 = 1mm, (Blue) u_0 = 1.1mm mm,(Green) u_0 = 1.2mm, (Magenta) u_0 = 1.3mm.

2.9. SOLITARY WAVES AND KINKS

In recent decades, the solitary wave theory has become a very active area of research due to its importance in many branches of mathematics and physics, such as nonlinear optics, acoustic, plasmas and fluid mechanics. The first observation of a wave with characteristics of a soliton was made in 1834 by a Scottish naval engineer John Scott Russell [11], see figure (2.16). He observed a hump of water several feet high gather at the front of the boat traveling intact for a long distance in the canal at a high speed without any damping or distortion. To get a proper

explanation in this time was very difficult, for linear dynamic theory, in a dispersive medium like water, the wave should be dispersive but this wave propagates without distortion over long distances.

This was the beginning of a whole new field of study which scientists over the years have contributed. One of the first mathematical equations describing solitary waves was formulated in 1895 [72]. Generally, a soliton is an exact solution to a special family of equations to nonlinear partial differential [73, 74]. A soliton is a special form wave can propagate without distortion over long distances. This is however merely the particular property of that wave. In fact, another feature is that the soliton retains their shapes and speeds after a collision with other adjacent solitons, it has been intensively studied [75–77]. Solitons can propagate in a variety of environments and are used in many applications. In some mediums, they can carry an electric charge. When these charged solitons traveling through some polymer chains [78–80]. This property may one day be used in applications such as artificial muscles [81].

Figure 2.16: Soliton on the Scott Russell Aqueduct on the Union Canal near Heriot-Watt University, 12 July 1995. Photo from Nature v. 376, 3 Aug 1995.

The solitary waves are also used in optical telecommunications where they can transfer large amounts of information over long distances without errors in signal [82]. They also find other applications namely in photonic optical fibers, fiber lasers, molecular systems, cosmology and condensed matter physics [83]. Thus, a huge amount of research has been conducted over the past four decades to make more progress in understanding the solitary waves phenomenon. In addition, most of the physical phenomena of fluid dynamics, plasma physics,

wave propagation in shallow water, and many other models are controlled within the range of validity by equations to a nonlinear partial differential .

Today, there are a number of equations known to have soliton solutions, the most famous of them is the Korteweg-de Vries (KdV). Korteweg and de Vries have developed a nonlinear partial differential equation (KdV) to model wave propagation in shallow water [84]. They published a theory that describes the shallow water waves which reproduced Russell's observations in its essential characteristics [85]. The work of Russell was a motivation for some mathematicians like Norman Zabusky and Martin Kruskal. In 1965, they published their numerical solutions of the KdV equation [86]. They were the first persons to call the wave "soliton". Kruskal derived as a continuum description of oscillations of one-dimensional waves propagating on the Fermi–Pasta–Ulam (FPU) lattice with a cubic nonlinear term [87]. In 1967, Morikazu Toda became the first to discover a soliton in a discrete, integrable system [88]. In 1965, Gary Deem, Zabusky, and Kruskal produced films that showed interacting solitary waves in an FPU lattice, the KdV equation, and a modified KdV equation [89].

Figure 2.17: Radiation tracks in Mica.

There are different types of solitary waves, such as intrinsic localized modes, vortex solitons, q-breathers, topological soliton, and many others. In this work, we will concentrate on a particular type of solitary wave named "kink". A kink is a one-dimensional topological soliton that appears as a solution of the wave equation. a kink represents a twist in the value of a solution and causes a transition from one value to another. As first pointed out by Bob Keolian [12] in 1992, his investigations of lattices have led to the discovery of domain walls and kink. The kink can be found at frequency ω_d smaller than cut-off frequency ω_c. A kink is a type of soliton distinct from the pulse-shaped solitons of the KdV and NLS

equations.

kink has been extensively studied during the recent years because of its relation with particle tracking physics. Some materials have the ability to track charged particle. In figure (2.17) an example for radiation tracks in Mica. This tracking is caused by vibration of particles in the medium. Most studies have been content to these vibration and solitary waves propagation. Many studies have been done about kink propagation in different medium [11],[13] and [14]. Peyrard *et al.* [15] described and discussed subsonic kinks in a monoatomic chain when he showed the discreteness effects on non-topological kink soliton dynamics in nonlinear lattices. A.V. Savin *et al.* [16] studied moving topological solitons (kinks and antikinks) in the nonlinear Klein–Gordon chain by using the pseudo-spectral method. Pnevmatikos, Flytzanis and Remoissenet [17] studied propagation of Kink and Soliton analytically and numerically in a nonlinear diatomic chain with cubic and quartic interaction potential. The book *"Waves called solitons: concepts and experiments"* by Remoissenet [11] describes a great many simple experimental realizations of nonlinear lattices in which kinks, in particular,can be observed.

The objective of this section aims essentially a theoretical and experimental study of kink propagation in a discrete system as the "chain of magnets" presented in the previous section. We considered the wave propagating in a medium with properties within the weakly nonlinear and weakly dispersive systems. We are particularly interested in studying the relation between excitation amplitude and speed of kinks. The effect of an additional substrate chain is also studied.

2.9.1. APPROXIMATE ANALYTICAL SOLUTION

Since we are working only on the moved magnet, Let us define a new variable. The relative displacement or strain $v_n = u_n - u_{n-1}$. so we can convert the equation of motion (2.1) to a new form

$$\ddot{v_n} = \frac{2}{(1+v_n)^2} - \frac{1}{(1+v_{n+1})^2} + \frac{1}{(1+v_{n-1})^2} \tag{2.16}$$

we assume the fixed particles at the ends of the chain. Numerically, Kink can produce by *half* sin wave perturbation. For that, to describe kink profile traveling to the write, the following *ansatz* was introduced by Kosevich [14]

$$v_n = -\frac{u_0}{2}(1+\cos(k(n-1)-\omega t) \qquad \text{if} \qquad -\pi < \frac{2\pi}{3}n - \omega t < \pi \tag{2.17}$$

and $v_n = 0$ otherwise. Also, we can introduce it in the term of displacement u_n

$$u_n = \frac{u_0}{2}(1+\cos(kn-\omega t))) \tag{2.18}$$

Equation (2.17) represents a solution where $k = 2\pi/3$ so called the "*magic wavenumber*", which means in term of relative displacement v_n there only three particles in motion in the displacement wave.

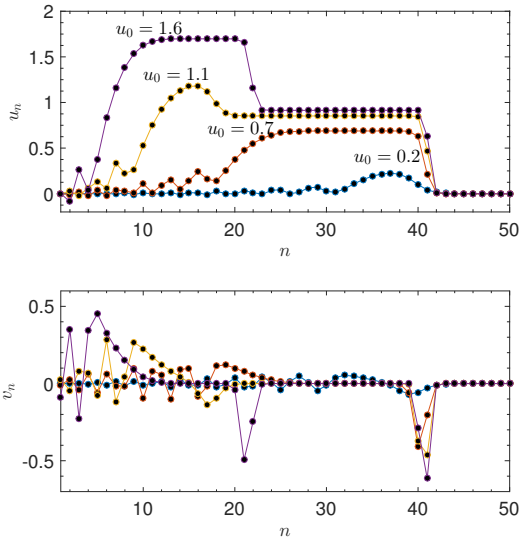

Figure 2.18: Kink profile in two different coordinates, displacement u_n and strain $v_n = u_n - u_{n-1}$. (Up) Kink profile for different amplitude $u_0 = [0.2, 0.7, 1.1, 1.6]$. At high amplitude, we observe a sequence of kinks with different amplitude. (Down) The strain profile corresponding to the kinks amplitudes $u_0 = [0.2, 0.7, 1.1, 1.6]$.

2.9.2. NUMERICAL SIMULATION

Numerically, kink propagation has been studied before in different models. Kosevich *et. al* [90] studied the propagation of the kink in FPU equation with a cubic nonlinearity, Archilla *et. al* [36] presented a theoretical study for a kink in the mica mineral which is governed by coulomb potential equation and Braun [91] studied kink propagation in the Frenkel-Kontorova model. The Eq. (2.1) has been solved numerically by using Finite Difference method (FDM). To excite the kink, we oscillate the first pendulum of the chain in the following signal (Kosevich [90])

$$u_1 = u_0 \sin(\omega_0(t_0 - t)) \quad \text{if} \quad 0 < t < t_0 \tag{2.19}$$

$$\text{and} \quad u_1 = 0 \quad \text{if} \quad t > t_0 \tag{2.20}$$

where we considered a fixed end $u_N = 0$ and after the excitation signal u_1 will fixed. Fig.(2.18) shows the numerical simulation in two coordinates, Fig.(2.18,Up) represent the kink displacement profile in different excitation amplitude ($u_0 = [0.2, 0.7, 1.1, 1.6]$). Fig.(2.18,Down) represent the strain profile. With increasing the amplitude of perturbation, kink velocity increases as the theoretical Eq.(2.22) predicted. Starting from a certain amplitude, higher amplitudes, we can excite more than one kink, as we can see in Fig.(2.18) for amplitudes $u_0 = [1.1, 1.6]$.

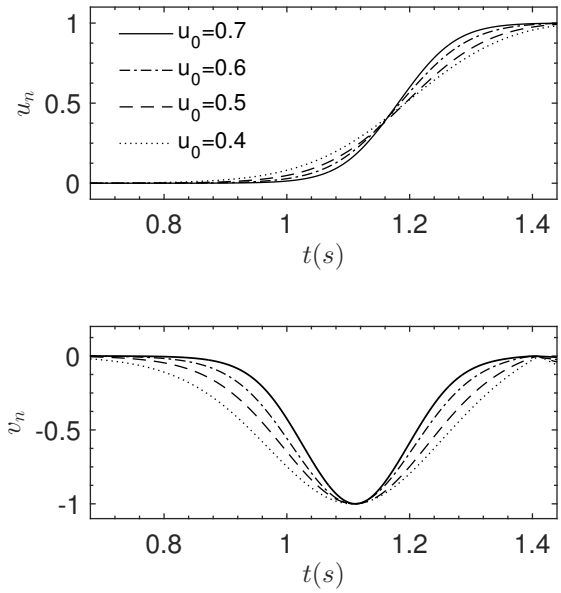

Figure 2.19: Numerical simulation for Kink profile in time domain, Eq.(2.2). (Up) The displacement u_n with different amplitudes, the results has been normalized to the excitation amplitude u_n/u_0 to observe the change. (Down) The strain $v_n = u_n - u_{n-1}$. As the amplitude u_0 increases, the shape of the strain become more triangle.

Fig.(2.19) shows the temporal evolution of kink profile u_n and the strain v_n in different amplitudes $u_0 = [0.4, 0.5, 0.6, 0.7]$. As the figure shows, with increasing the excitation amplitude, the width of the strain wave become more narrow. This behavior has been studied before theoretically by Friesecke [92] and experimentally by Moleron et al.[13].

2.9.3. KINKS WITHOUT SUBSTRATE POTENTIAL

Consider no external forces acting on the chain. We inject *half* sinusoidal wave perturbation to the first pendulum, starting and ended at the equilibrium position. In Fig.(2.20) shows the kink profile in space which presents the comparison between the experiment results and the numerical simulation for the Eq.(2.2) where $k = 0.45\pi$, with the corresponding analytic solution derived from Eq.(2.18) and Eq.(2.17), displacement and strain respectively. The experimental data has a good agreement with the numerical simulation and the analytic solution.

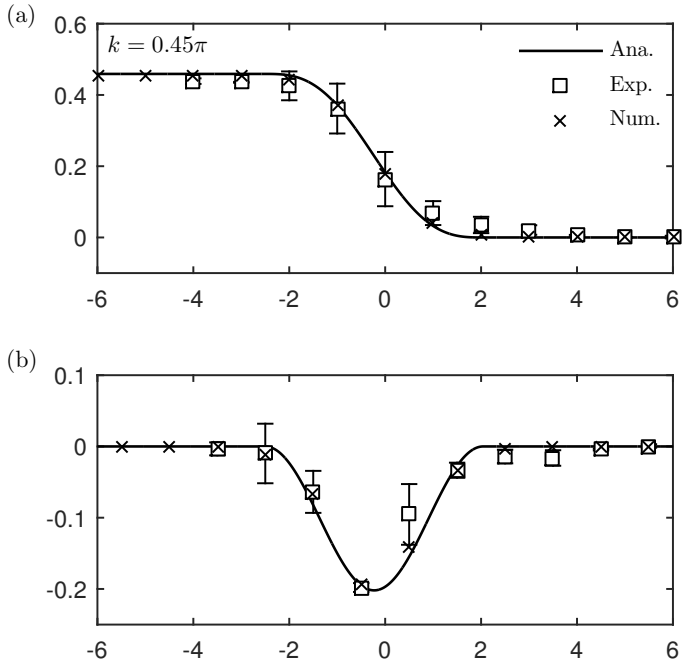

Figure 2.20: (Up) Kink profile in *space* u_n,Chain with $N = 53$ magnets, tracked pendulum from 23^{th} to 33^{th} and $k = 0.45\pi$. (Up-solid) Analytic solution derived from Eq. (2.18),(Up-dots) Numerical simulation Eq.(2.2) and (Up-circls) The experiment results. (Down) The relative displacement $v_n = u_n - u_{n-1}$. ((Down-solid) Analytic solution Eq. (2.17),(Down-dots) Numerical simulation Eq.(2.2). (Down-circls) The experimental data. Note, The experimental time axis was shifted so the wave time fit with the numerical simulation and analytic solution.

2.9.4. KINK VELOCITY

Calculating kink velocity has been studied before by Archilla *et. al* [93]. They used the Rotating Wave Approximation (RWA) to obtain the relation between the kink velocity V and the excitation amplitude u_0. Substituating the *ansatz* Eq.(2.17)

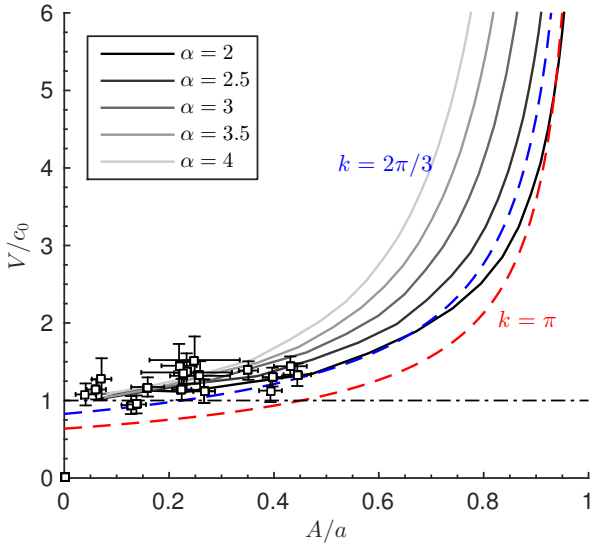

Figure 2.21: Kink velocity V versus excitation amplitude u_0, (Line, Dashes) Analytic solution Eq. (2.22) where $k = [p; 2p = 3]$ and (Circles) Experimental data with calculating confidence intervals. We tracked 25th, 26th and 27th pendulum.

into Eq.(2.16) and using the rotating wave approximation as proposed in [94] for the second harmonic and neglecting the higher harmonics. We obtain the frequency ω as a function in amplitude u_0.

$$\omega = \frac{1}{(1-u_0)^{3/4}}\omega_c \sin(\frac{k}{2}) \tag{2.21}$$

from Eq. (2.21) we can calculate kink velocity V

$$V = \frac{\omega}{k} = \frac{1}{(1-u_0)^{3/4}}\frac{2c_0}{k}\sin(\frac{k}{2}) \tag{2.22}$$

Fig.(2.21) shows kink velocity V versus excitation amplitude u_0. We studied experimentally the relation between kink velocity V and excitation amplitude u_0. The experimental results have been compared with the analytic solution in Eq.(2.22) where $k = 2\pi/3$ and $k = 2\pi/3$.

2.9.5. KINKS WITH SUBSTRATE POTENTIAL

Before studying the kink in the case including substrate potential (on-site, as shown in fig. 2.22) we have to study the new dispersion relation. After adding the

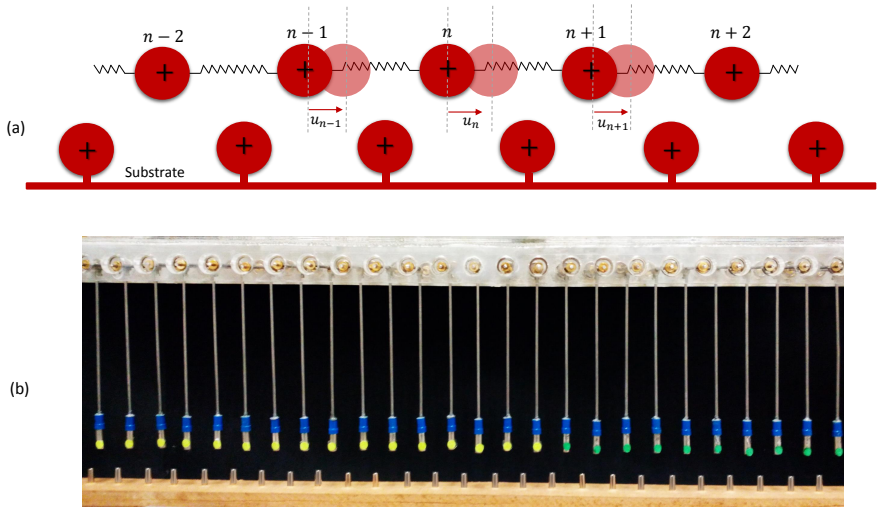

Figure 2.22: (a) The scheme of chain with added substrate. The force between chain magnets and substrate magnets is repulsion force. (b) The experimental setup, chain magnates *Supermagnete* S-05-14-N and substrate magnets *Supermagnete* S-04-13-N.

substrate, some parameters will change such as interaction force between magnets, minimum frequency ω_0, cut-off frequency ω_c,...etc. In the previous section we calculated the dispersion relation in case of absence of the substrate. After adding the substrate, the minimum propagative frequency will increase from 1.5 Hz to 6.5 Hz and the cut-off frequency increase from 18 Hz to 19.1 Hz, as shown in Fig(2.23), the results have been obtained experimentally and compared with the analytically solution.

Fig.(2.24) shows the experiment results for the kink in the existence of extra potential with two different amplitudes. After injecting the excitation signal, the opposite force of the substrate makes the pendulum to turn back to the equilibrium position very rapidly. Fig.(2.24,a,b) represents the displacement for two different amplitude $u_n = [22,24]$mm and Fig.(2.24, c,d) represents the relative displacement v_n which corresponding to the $u_n = [0.5,1]$.

2.10. CONCLUSION

The propagation of waves in a lattice of nonlinear repelling forces between particles has been studied theoretically and experimentally. In the limit of small am-

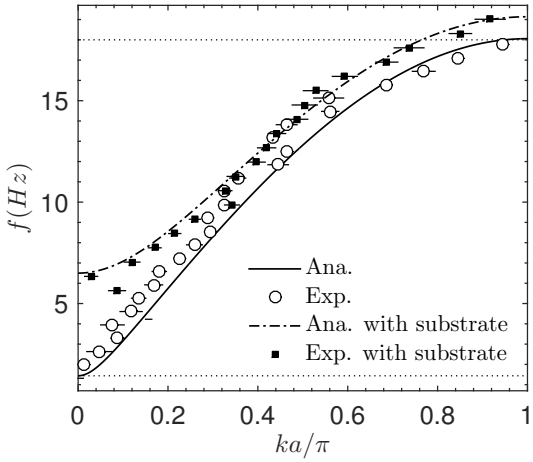

Figure 2.23: Dispersion relation in case of the setup with/without substrate. (line-Dashed) Analytically presented by Eq. $\omega^2 = \omega_0^2 + \omega_c \sin^2(kd/2)$. The experimental data with error bars (Circles) in case of without substrate (Squares)in case of with substrate.

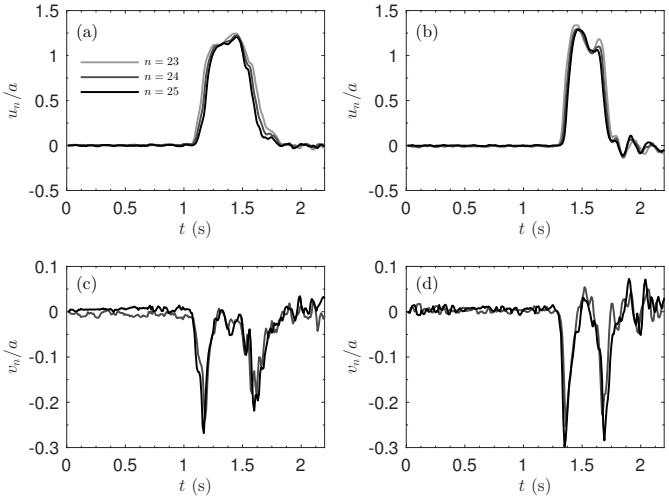

Figure 2.24: Experimental results with substrate for two amplitudes A = [22mm;24mm]. (a) The temporal kink profiles for particles n = [23;24;25], (b) corresponding strain.

plitudes, where the system can be described by a FPU equation with quadratic nonlinearity, analytical solutions can be obtained by using the successive ap-

proximations method. Explicit expressions for the amplitude of the FW and the SH, as well as the static (dilatation) mode are presented.

An experiment consisting in a lattice of coupled magnetic dipoles sinusoidally driven at one boundary was designed to check the theoretical predictions. In spite of the simplifying assumptions made in the theoretical analysis, the observations agree quite well with the model. These results indicate that the lattice of magnetic dipoles is well described by an α-FPU equation, which opens the possibility of extending the results to other systems which are described by the same generic equation. Additionally, the experimental setup can be used to explore other effects of nonlinear discrete systems that have been predicted in the literature. The proposed system can be also viewed as a toy model of a microscopic crystal of interacting charged particles (atoms or ions) at a macroscopic scale. Despite the limited applicability of this simple lattice to describe real crystals, the approach possess however some advantages, as the possibility of varying parameters that are normally fixed, as the strength of the interaction and on-site potentials, or exploring strongly nonlinear regimes which are hardly achievable at atomic scales.

Beside the propagation of higher harmonics in chain of magnets, we observed the propagation of subharmonics. Appropriate initial amplitude can let for subharmonic to be excited. Subharmonics are the harmonics which having frequencies less than the driven frequency. These components can appear in singlet, doublets or more. With a suitable excitation amplitude, the system generates the both higher harmonics and sub-harmonics of the input frequency. The promising experimental results are considered as starting point to complete the study beside the theoretical work. Additionally, we observed experimentally the phenomena of the parametric instability "Benjamin Feir Instability" in a discrete system.

Finally, we studied the propagation of kink analytically, numerically and experimentally. The analytic solution of the kink profile has been driven from FPU equation. The numerical simulation is performed from magnetic force interaction equation. We introduced experimentally the relation between kink velocity and excitation amplitude. The effect of add an additional substrate in the dispersion relation has been studied. we have also shown the propagation of kink in substrate setup. The agreement in the dispersion relation between analytic solution and experimental results is so good that it motivates us to study supersonic kink.

3

NONLINEAR PROPAGATION IN PHONONIC SUPERLATTICES

In this chapter, the propagation of intense acoustic waves in a one-dimensional phononic crystal is studied. The medium consists in a structured fluid, formed by a periodic array of fluid layers with alternating linear acoustic properties and quadratic nonlinearity coefficient. The spacing between layers is of the order of the wavelength, therefore Bragg effects such as band-gaps appear. We show that the interplay between strong dispersion and nonlinearity leads to new scenarios of wave propagation. The classical waveform distortion process typical of intense acoustic waves in homogeneous media can be strongly altered when nonlinearly generated harmonics lie inside or close to band gaps. This allows the possibility of engineer a medium in order to get a particular waveform. Examples of this include the design of media with effective (e.g. cubic) nonlinearities, or extremely linear media (where distortion can be cancelled). The presented ideas open a way towards the control of acoustic wave propagation in nonlinear regime.

3.1. INTRODUCTION

One of the most celebrated effects of wave propagation in periodic media is the appearance of forbidden propagation regions in the energy spectrum of electrons, or band-gaps. Most of the physics of semiconductors, and therefore many electronic devices, are somehow based on this concept [26]. In the late 80's, these ideas where extended by Yablonovich and John [95] to light waves (electromagnetic waves in general) propagating in materials where the optical properties like the index of refraction were distributed periodically. These materials were

named, by analogy with ordered atoms in crystalline matter, as photonic crystals. The typical scale of the periodicity is given by the wavelength. Actually, not only light but any wave propagating in a periodic medium may experience the same effects, and acoustic waves are not an exception. Sound wave propagation in periodic media has become very popular in the last 20 years in acoustics, after the introduction of the concept of sonic crystals [96]. Exploiting the analogies with other type of waves many interesting effects, as the mentioned forbidden propagation bands (band-gaps), but also focalization, self-collimation, negative refraction, and many others have been proposed. We consider here the simplest case plane waves propagating in a 1D structure, formed by a periodic alternation of layers with different properties. Depending on the context, such a structure has been named a multilayer, a superlattice (particularly in the context of semiconductors) or a 1D phononic crystal (this include more exotic structures, as the granular crystal or lattice [97]). The huge majority of the studies considered so far have assumed a low-amplitude (linear) regime, neglecting the nonlinear response of the medium. Intense wave propagation in nonlinear periodic media, and in particular the case of sound waves, is almost unexplored. In this chapter we present different examples of new phenomena related to sound wave propagation in 1D periodic media, where each of the layer has a nonlinear quadratic elastic response. Nonlinear acoustical effects in such structure have been studied only in a few works. In [98] the harmonic generation process is described in a fluid/fluid multilayered structure (water/glycerine), based in a nonlinear wave equation. Also, acoustic solitons in solid layered nonlinear media have been presented in [99]. More recently, the complementary action of nonlinearity and periodicity has been considered in [100], where an asymmetric propagation device (acoustic diode) was proposed. There, the nonlinearity and the periodicity act at different locations and its effect is considered separately. The effects discussed in this chapter are the result of the interplay between nonlinearity and periodicity. Here we describe how the geometrical and acoustic parameters of the structure can be used to control the harmonic distortion processes in a multilayer. The conditions required to selectively act on the nonlinearly generated spectrum, and therefore manipulate the waveform in the desired way, are obtained and discussed.

The theory presented here has been developed for fluid-fluid (scalar) structures, however the main conclusions are extendable to fluid-solid or to solid-solid multilayers, if particular conditions are given. Also, the main conclusions of this paper are independent on the regime of the waves (audible, ultrasound,...), and therefore on the size or scale of the structure.

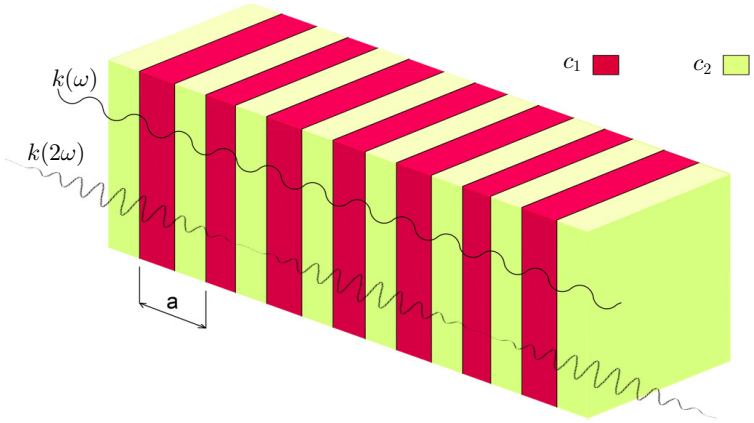

Figure 3.1: Layered acoustic system with two different layers and second harmonic generation scheme. Here the lattice period is $a = a_1 + a_2$.

3.2. MODELS

3.2.1. THE MEDIUM AND ITS DISPERSION RELATION

We consider a periodic medium made of an arrangement of homogeneous fluid layers of thickness a_1 and a_2 with different material properties. For the sake of simplicity only longitudinal waves under normal incidence are considered.

The propagation of small amplitude waves in an infinite periodic system is completely described by its dispersion relation, often known as band structure, that for 1D systems as in Fig. 3.1 can be expressed analytically as in [101]. In the next lines, we deduce the band structure for the system proposed here. It is assumed that the wave propagation direction is along x. The linear wave propagation is described in both media, 1 and 2

$$\frac{\partial^2 u}{\partial t^2} = c_1^2 \frac{\partial^2 u}{\partial x^2}, \qquad -a_1/2 < x < a_1/2 \tag{3.1}$$

$$\frac{\partial^2 u}{\partial t^2} = c_2^2 \frac{\partial^2 u}{\partial x^2}, \qquad -(a - a_1/2) < x < -a_1/2 \tag{3.2}$$

we assume harmonic solutions, so that $u(x,t) \approx e^{-i\omega t}$ and we can express both equations 3.1 and 3.2 as

$$u(x) = De^{ik_1 x} + Ee^{-ik_1 x}, \qquad -a_1/2 < x < a_1/2 \tag{3.3}$$

and

$$u(x) = Fe^{ik_2 x} + He^{-ik_2 x}, \qquad -(a - a_1/2) < x < -a_1/2 \tag{3.4}$$

where $a = a_1 + a_2$ is the lattice period, and $k_i = \omega/c_i$ is the local wavenumber. where $k_1 = \omega/c_1$ and $k_2 = \omega/c_2$ are the . We take the origin of each medium at $x = -a_1/2$. Then, the continuity conditions for the two interfaces that form a cell unit are:

$$u(-a_1/2 - 0) = u(-a_1/2 + 0) \tag{3.5}$$

$$\frac{\partial u(-a_1/2 - 0)}{\partial x} = \frac{\partial u(-a_1/2 + 0)}{\partial x} \tag{3.6}$$

at the first condition $x = -a_1/2$, Substituting the both solutions in the Eq.(3.1 and 3.2) we get

$$De^{-ik_1 a_1/2} + Ee^{ik_1 a_1/2} = Fe^{-ik_1 a_1/2} + He^{ik_1 a_1/2} \tag{3.7}$$

and

$$k_1 c_1 (De^{-ik_1 a_1/2} - Ee^{ik_1 a_1/2}) = k_2 c_2 (Fe^{-ik_1 a_1/2} - He^{ik_1 a_1/2}) \tag{3.8}$$

The second condition to apply is $x = a_1/2$.The conditions of continuity of acoustic field at $x = a_1/2$ is:

$$u(a_1/2 - 0) = u(a_1/2 + 0) \tag{3.9}$$

$$\frac{\partial u(a_1/2 - 0)}{\partial x} = \frac{\partial u(a_1/2 + 0)}{\partial x} \tag{3.10}$$

we get

$$De^{ik_1 a_1/2} + Ee^{-ik_1 a_1/2} = e^{ik(a_1+a_2)} (Fe^{-ik_1(a-a_1/2)} + He^{ik_1(a-a_1/2)}) \tag{3.11}$$

and

$$k_1 c_1 (De^{ik_1 a_1/2} - Ee^{-ik_1 a_1/2}) = k_2 c_2 (Fe^{-ik_1(a_2-a_1/2)} - He^{ik_1(a_2-a_1/2)}) \tag{3.12}$$

the condition inside the region $-a_1/2 < x < a_1/2$ can satisfy Bloch theory

$$u(x+a_1+a_2) = e^{ikx}u(x) \tag{3.13}$$

where k is the block wave number. So at $-a_1/2 < x < a_1/2$

$$u(x) = e^{ik(a_1+a_2)}(Fe^{ik_2x} + He^{-ik_2x}) \tag{3.14}$$

With all the last equation we can get the solution for all coefficients D, E,F and H

$$\triangle = \begin{bmatrix} e^{-ik_1a_1/2} & e^{ik_1a_1/2} & -e^{-ik_2a_1/2} & -e^{ik_2a_1/2} \\ k_1c_1e^{-ik_1a_1/2} & -k_1c_1e^{ik_1a_1/2} & -k_2c_2e^{-ik_2a_1/2} & -k_2c_2e^{ik_2a_1/2} \\ e^{ik_1a_1/2} & e^{-ik_1a_1/2} & -e^{i(k(a_1+a_2)-k_2(a-a_1/2))} & -e^{i(k(a_1+a_2)+k_B(a_2-a_1/2))} \\ k_1c_1e^{ik_1a_1/2} & -k_1c_1e^{-ik_1a_1/2} & -k_2c_2e^{i(k(a_1+a_2)-k_2(a-a_1/2))} & k_2c_2e^{i(k_1(a_1+a_2)+k_2(a-a_1/2))} \end{bmatrix}$$

where all the matrix equal to Zero $\triangle = 0$. The dispersion relation will be in the form

$$\cos(ka) = \cos(k_1a_1)\cos(k_2(a_2)) - \frac{1}{2}(\frac{k_1}{k_2} - \frac{k_2}{k_1})\sin(k_1a_1)\sin(k_2(a_2)) \tag{3.15}$$

also known as the Rytov formula, where k is the Bloch wave-number, $a = a_1 + a_2$ is the lattice period, and $k_i = \omega/c_i$ is the local wavenumber, with c_i the sound speed in the i layer.

$$\cos(ka) = \cos(\frac{\omega}{c_1}a_1)\cos(\frac{\omega}{c_2}a_2) - \frac{1}{2}(\frac{c_2}{c_1} - \frac{c_1}{c_2})\sin(\frac{\omega}{c_1}a_1)\sin(\frac{\omega}{c_2}a_2) \tag{3.16}$$

An example of dispersion relation plot is shown in Fig. 3.2 for $a = 2.2mm$ and $a_2 = 2mm$ and for different sound speed ratios c_1/c_2. Increasing the impedance ratio between layers increases the reflected intensity in the trans-layer propagation, while the transmitted energy of the multiple internal reflections diminishes. As can be seen, due to these scattering processes band-gaps are progressively opened around the wavenumber $k = n\pi/a$ with $n = 1, 2, ...$ Thus, the bandwidth of these band-gaps also increases when the impedance ratio grows.

On the other hand, its imaginary part increases in amplitude with c_1/c_2, leading to shorter evanescent propagation inside the band-gap for high sound speed contrast layers, while remains zero (no attenuation) in the propagation band. We recall that the system is conservative: the physical interpretation of the complex wavenumber is not energy absorption, but back-reflection of the incident wave. Thus, at band-gap frequencies the waves penetrate only a short distance into the medium with a forward evanescent mode, and if the medium is perfectly periodic and lossless the energy is back-reflected (it behaves as a mirror).

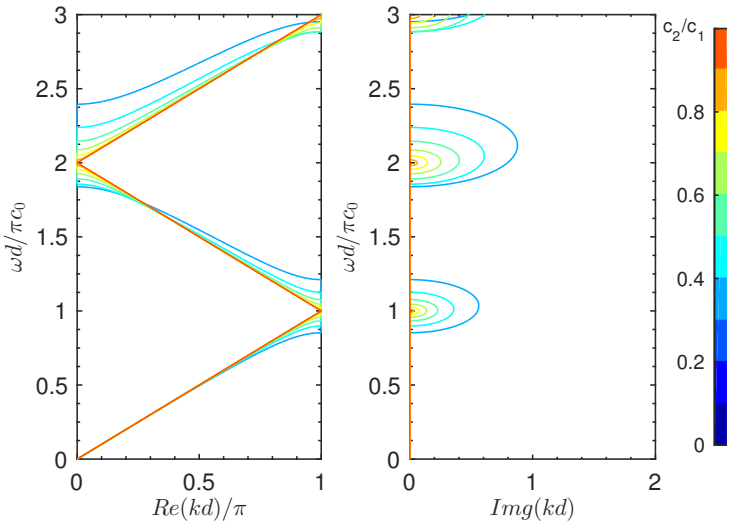

Figure 3.2: The dispersion relation for different vale of c_2/c_1, where $a = 2.2mm$ and $a_2 = 2mm$.

3.2.2. NONLINEAR CONSTITUTIVE MODEL

The nonlinear propagation of sound in the acoustic inhomogeneous media, and in particular in multi-layered media can be described by several models, with different levels of accuracy. Here, we use the equations of continuum mechanics for ideal fluids with space dependent parameters. These are the continuity equation for mass conservation [102]:

$$\frac{\partial \rho}{\partial t} + \nabla \cdot (\rho \mathbf{v}) = 0\,. \tag{3.17}$$

and the equation of motion that follows from conservation of momentum

$$\rho \frac{D\mathbf{v}}{Dt} + \nabla p = 0\,, \tag{3.18}$$

where ρ is the total density, $\mathbf{v}$ is the particle velocity vector over a Eulerian reference frame, p is the acoustic pressure, t is the time and D is the material derivative operator.

For non homogeneous media, the ambient properties of the fluid in the absence of sound are space dependent, so the total density becomes $\rho(t,\mathbf{x}) = \rho'(t,\mathbf{x}) + \rho_0(\mathbf{x})$, where $\rho_0(\mathbf{x})$ is the spatially dependent ambient density and $\rho'(t,\mathbf{x})$ is the perturbation of the density or acoustic density, that is space and time dependent. Then, using the material derivative, Eq. (3.18) becomes

$$\rho_0 \frac{\partial \mathbf{v}}{\partial t} + \nabla p = -\rho' \frac{\partial \mathbf{v}}{\partial t} - (\rho' + \rho_0)(\mathbf{v} \cdot \nabla)\mathbf{v}, \tag{3.19}$$

In this equation, the first two terms in the left-hand-side account for linear acoustic propagation, where the terms in the right-hand-side introduce nonlinearity in the Eulerian reference frame through momentum advection processes.

On the other hand, we can expand Eq. (3.17) for nonhomogeneous media as

$$\frac{\partial \rho'}{\partial t} + \rho_0 \nabla \cdot \mathbf{v} + \mathbf{v} \cdot \nabla \rho_0 = -\rho' \nabla \cdot \mathbf{v} - \mathbf{v} \cdot \nabla \rho'. \tag{3.20}$$

Here, the first two terms on the left-hand-side account for linear acoustic propagation, the third, also linear, accounts for the magnitude of the changes in the ambient layer properties. Note this term is space dependent but only changes at the interface between adjacent layers. For density matched layers, $\rho_i = \rho_{i-1}$, this terms vanishes. The terms on the right-hand-side are nonlinear and accounts for mass advection.

Finally, a fluid thermodynamic state equation $p = p(\rho, s)$ is needed to close the system, with s the entropy. During the propagation the pressure changes within the medium causing the energy transfer from the fundamental harmonics (ω) to the rest of harmonicas (2ω, 3ω, 4ω,....). This attenuation increases with excitation frequency (ω). The level of the nonlinearity it can be measure by the parameter B/A. The nonlinear parameter is important because it determines distortion of a finite amplitude wave propagating in the fluid. The values of A and B are the coefficients of the first and second order terms of the Taylor series expansion of the equation of state

$$P = P(\rho, s) \tag{3.21}$$

where s is the constant entropy, p is the pressure, ρ is the density and v particle velocity, then:

$$p = P - P0 = (\frac{\partial p}{\partial \rho})_{s,0}(\rho - \rho_0) + \frac{1}{2!}(\frac{\partial^2 p}{\partial \rho^2})_{s,0}(\rho - \rho_0)^2 + ... \tag{3.22}$$

This equation can be rewritten more succinctly as:

$$p = P - P0 = A\frac{\rho'}{\rho_0} + \frac{B}{2!}(\frac{\rho'}{\rho_0})^2 + \frac{C}{3!}(\frac{\rho'}{\rho_0})^3 + ... \tag{3.23}$$

where $\rho' = \rho - \rho_0$ is the density change and

$$A = \rho_0(\frac{\partial p}{\partial \rho}) = \rho_0 c_0^2 \tag{3.24}$$

$$B = \rho_0^2 \left(\frac{\partial^2 p}{\partial \rho^2}\right) \tag{3.25}$$

Thus leading to the nonlinear parameter B / A

$$\frac{B}{A} = \frac{\rho_0}{c_0^2} \left(\frac{\partial^2 p}{\partial \rho^2}\right)_{s,0} \tag{3.26}$$

For medium non-linearities, also called the second order nonlinear parameter B/A [103], is medium specific and is widely used to describe the continuous distortion course of a finite-amplitude acoustic wave as it travels through the medium. The acoustic nonlinear parameter B/A is the ratio of the quadratic terms and linear terms in the Taylor series expansion of the state equation relating pressure variations in density variations. B/A is describing the response of a medium stresses of an acoustic wave. This ratio characterizes the variation of the speed of sound of the medium induced by a change in pressure in a fluid.

Common materials have an inherently non-linear behavior due to structural inhomogeneities in the microscopic or nanoscopic level [104], as irregularities in the crystal lattice, the debonding at the scale of grains of the material or dislocations [105]. These diffuse defects within the material are small to the wavelength and therefore usually have a negligible effect on the propagation of acoustic waves. However, there are some materials where this volume intrinsic nonlinearity can not be neglected. This is primarily geological or granular material [106] and biological materials [107] [108].

From Eqs. (3.22-3.26) The local nonlinear medium response relating density and pressure variations, retaining up to second order terms, can be written as

$$p = c_0^2 \rho' + \frac{B}{2A} \frac{c_0^2}{\rho_0} \rho'^2, \tag{3.27}$$

where $B/A(\mathbf{x})$ is the quadratic nonlinear parameter and $c_0(\mathbf{x})$ is the sound speed, that can be also spatially dependent.

The is now a system of equations, in which quadratic nonlinearity appears in the equation of motion (3.19) and in the continuity equation (3.20), in the momentum and mass advection terms respectively, and also in the equation of state, Eq. (3.27), relating pressure and density acoustic perturbations. We note that here we only take into account nonlinear processes through the layer's bulk. The nonlinear effects at the boundary between adjacent sheets are neglected. These nonlinear boundary effects include cavitation processes, that in the case of fluids with very different compressibility can be very important. In the case of solid layers, other local nonlinear effects relative to boundaries, e.g. clapping

phenomena between surfaces, can lead to nonlinearities that are orders of magnitude in importance compared to the *bulk* cumulative nonlinearities.

3.2.3. WESTERVELT EQUATION

For moderate amplitudes, the system of Eqs. (3.19-3.27) can be simplified. For that aim, we use a perturbative method with same ordering scheme as in [109], where $\mathcal{O}(\epsilon)$, $\mathcal{O}(\epsilon)^2$ and $\mathcal{O}(\epsilon)^3$ represents the terms of generic smallness parameter ε. The derivation of a second-order nonlinear wave equation requires the substitution of the linearized acoustic approximations (first order) into second order terms of Eq. (3.19, 3.20). This substitution procedure will give third order errors, so the final nonlinear wave equation will be a second order approximation of the full constitutive relations.

These equations can be combined to form a single nonlinear wave equation valid for nonhomogeneous media up to second order approximation

$$\nabla^2 p - \frac{1}{c_i^2}\frac{\partial^2 p}{\partial t^2} - \frac{1}{\rho_0}\nabla\rho_0\nabla p = -\frac{\beta}{\rho_0 c_0^4}\frac{\partial^2 p^2}{\partial t^2} - (\nabla^2 + \frac{1}{c_0^2}\frac{\partial^2}{\partial t^2})\mathscr{L} + \mathcal{O}(\epsilon)^3 . \tag{3.28}$$

where we introduced the coefficient of nonlinearity $\beta = 1 + \frac{B}{2A}$ that accounts for material and mass advection quadratic nonlinearities. It is worth noting here that the second-order Lagrangian density vanish for plane progressive waves due to the first order relation $p = uc_0\rho_0$ that leads to $\mathscr{L} = 0$. In this case, Eq. (3.28) simplifies to the well-known Westervelt equation for inhomogeneous media

$$\nabla^2 p - \frac{1}{c_0^2}\frac{\partial^2 p}{\partial t^2} - \frac{1}{\rho_0}\nabla\rho_0\nabla p = -\frac{\beta}{\rho_0 c_0^4}\frac{\partial^2 p^2}{\partial t^2} + \mathcal{O}(\epsilon)^3 . \tag{3.29}$$

In general, the Lagrangian density term can be discarded based on the distinction of cumulative and local nonlinear effects. In this way, for progressive quasi-plane wave propagation in homogeneous media the nonlinear local effects become insignificant in comparison to the nonlinear cumulative effects, where in most practicals situations, beyond a distance of only few wavelengths away from the source local nonlinear effects can be neglected. However, local nonlinear effects can become significant in other complex situations including standing-wave fields and finite amplitude acoustic waveguides. Concerning the layered media, in this work we solve numerically the full constitutive relations, and the effect of the Lagrangian term is shown to be negligible under the conditions of our study. The term accounting for the inhomogeneities is not taken into account as the equation is solved numerically in both media:

$$\nabla^2 p - \frac{1}{c_0^2}\frac{\partial^2 p}{\partial t^2} = -\frac{\beta}{\rho_0 c_0^4}\frac{\partial^2 p^2}{\partial t^2} \tag{3.30}$$

NUMERICAL SIMULATION

Westervelt equation (3.30) is solved numerically using Finite Difference Method (FDM) in One-dimensional [110]. The grid is a little bit simple because it depend on 1D direction x. One vector in space, and one vector in time. The grid has space step Δx in meter and time steps Δt in second. p_i^n denotes the variation of the acoustic pressure at time step (n) and space steps (i). This is scheme has been used before in [111] and [112]. The scheme of finite difference method as follows, in time

$$\frac{\partial p}{\partial t} \approx \frac{p_i^n - p_i^{n-1}}{\Delta t} \tag{3.31}$$

$$\frac{\partial^2 p}{\partial t^2} \approx \frac{p_i^{n+1} - 2p_i^n + p_i^{n-1}}{\Delta t^2} \tag{3.32}$$

the same discretization in space

$$\frac{\partial p}{\partial x} \approx \frac{p_i^n - p_{i-1}^n}{\Delta x} \tag{3.33}$$

$$\frac{\partial^2 p}{\partial x^2} \approx \frac{-p_{i+2}^n + 16p_{i+1}^n - 30p_i^n + 16p_{i-1}^n - p_{i-2}^n}{12\Delta x^2} \tag{3.34}$$

and the term $\frac{\partial^2 p^2}{\partial t^2}$ is calculated by making use of the chain rule and product rule:

$$\frac{\partial^2 p^2}{\partial t^2} = 2((\frac{\partial p}{\partial t})^2 + p(\frac{\partial^2 p}{\partial t^2})) \tag{3.35}$$

so

$$\frac{\partial^2 p^2}{\partial t^2} = 2((\frac{p_i^n - p_i^{n-1}}{\Delta t})^2 + p(\frac{p_i^{n+1} - 2p_i^n + p_i^{n-1}}{\Delta t^2})) \tag{3.36}$$

By substituting Eqs. (3.32), (3.34) and (3.36) in the original Eq. (3.30) using a second-order accurate finite difference scheme for the remaining temporal derivative then gives

$$p_i^{n+1} = 2p_i^n + p_i^{n-1} + \frac{c_0^2 \Delta t^2}{12\Delta x^2}(-p_{i+2}^n + 16p_{i+1}^n - 30p_i^n + 16p_{i-1}^n - p_{i-2}^n) + \frac{\beta \Delta t^2}{\rho c_0^2}\frac{\partial^2 p^2}{\partial t^2} \tag{3.37}$$

Take into account the medium parameters c_0 and β depend on i. In case of homogeneous medium, all of these parameters are equal along x-direction. In our case, in heterogeneous medium, multilayer structure, these parameters are taken a periodic form along the space as shown in Fig.(3.3)

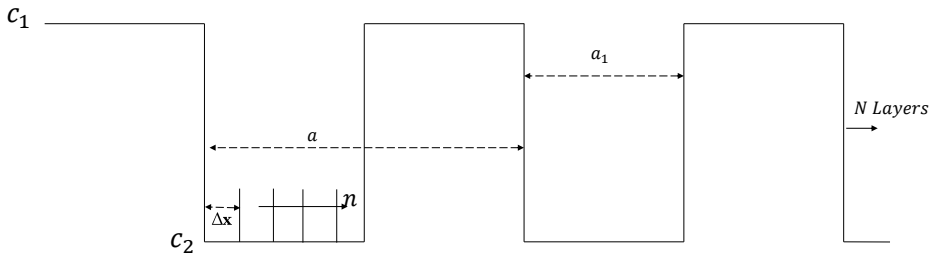

Figure 3.3: The periodic scheme of the medium parameters, Speed of sound in medium A is c_1 and speed of sound in medium B is c_2. The discrtization in space Δx at x direction for N Layer and Lattice constant a.

3.2.4. NONLINEAR WAVE EQUATION

The one dimensional version of wave equation was first derived in 1747 by d'Alembert [113] for the case of vibrating string. He recognized its possible applicability to sound in air. Euler in 1750 and Lagrange in 1759 [114] both treated the case of discrete masses connected by linear spring. This model used in early theories of sound propagation. The general form of the waves equation regards a function $u(x,t)$ at the position x and time t. It is a hyperbolic partial differential equation whose general expression is

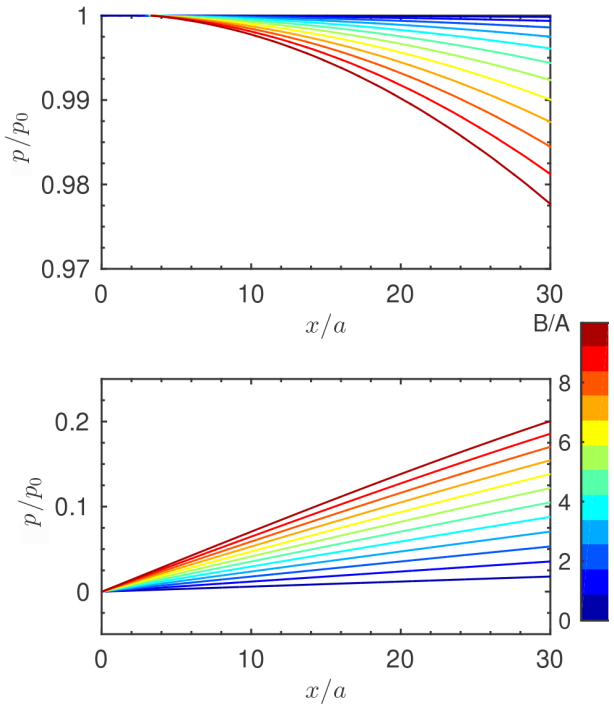

Figure 3.4: Numerical simulation of Westervelt equation (3.30) with different value of the nonlinear parameter B/A; where the amplitude $p_0 = 1MPa$ and $f_d = 1MHz$. (Upper) The first harmonic (Down) The second harmonic.

$$\frac{\partial^2 u}{\partial x^2} - \frac{1}{c_0}\frac{\partial^2 u}{\partial t^2} = \beta \frac{\partial u}{\partial x}\frac{\partial^2 u}{\partial x^2} \tag{3.38}$$

where u represents the displacement, c_0 is sound speed and $\beta = 1 + B/2A$ is the nonlinear coefficient. Fig. (3.5) and Fig. (3.5) shown the numerical simulation for nonlinear wave equation (3.38) and Westerwelt equation (3.30), respectively, for different value of nonlinear parameter B/A.

3.3. HARMONIC GENERATION IN LAYERED MEDIA

We will study the response of the layered system for plane-harmonic wave excitation. Then, as sketched in Fig. 3.1, the source is placed at one boundary of the layered system, and the acoustic relevant magnitudes are calculated along space and time. As the wave propagates, cumulative nonlinear effects generate

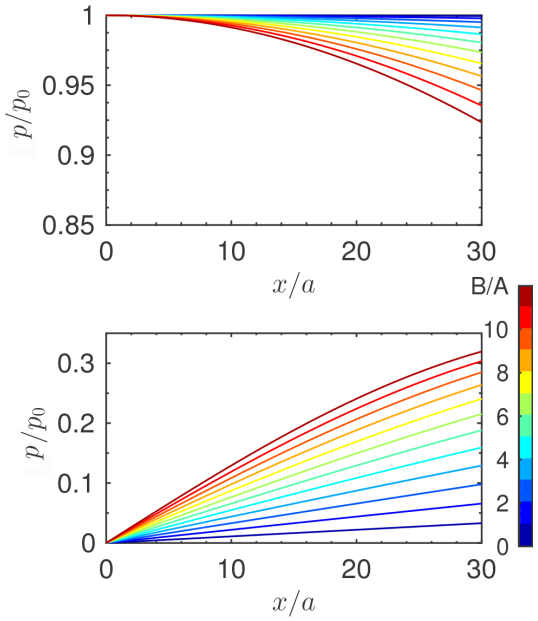

Figure 3.5: Numerical simulation of Nonlinear wave equation (3.38) with different value of the nonlinear parameter B/A; where the frequency $f_d = 0.5MHz$. (Upper) The first harmonic (Down) The second harmonic.

harmonics of the fundamental frequency, ω_0, and due to the multiple scattering processes into the layers, local nonlinear effects also distorts the wave. However, the high dispersion of the layered system have a strong impact on the nonlinear harmonic generation. Dispersion modify the resonance conditions between fundamental and second harmonic wave, and also for other nonlinearly generated higher frequencies. In this way, nonlinear energy transfer efficiency from one component to another is modified in a wide variety of configurations, leading to the possibility of engineering and controlling the nonlinear wave processes by tuning the dispersion relation.

Depending on the frequency of the input wave, different scenarios can be observed, as reported in the following subsections.

3.3.1. NONDISPERSIVE (FUBINI) REGIME

We start studying the propagation in the layered system for harmonic excitation in the very low frequency regime, where we assume that $ka \ll 1$ holds. As the Rytov's Eq. (3.16) predicts, in the very low frequency regime the slope of the $\omega(k)$

curve is nearly constant. The dispersion of all the spectral components is negligible, and they all propagate at nearly the same velocity and are correspondingly phase-matched. Thus, in the absence of dispersion and attenuation process, the system of Eqs. (3.17-3.18) and (3.27) can be reduced for a harmonic-plane wave to a Burger's evolution equation expressed in traveling coordinates with effective parameters, namely $\tilde{c_0}$, $\tilde{\rho_0}$ and $\tilde{\beta}$. An analytic solution of this equation in terms of the nth-harmonics of the fundamental wave of frequency ω and initial amplitude p_0 is known as the Fubini solution,

$$p(\sigma,\tau) = p_0 \sum_{n=1}^{\infty} \frac{2}{n\sigma} J_n(n\sigma)\sin(n\omega\tau), \tag{3.39}$$

where J_n is the Bessel function of order n, and $\sigma = x/x_s$ is the propagation coordinate, normalized to the shock formation distance, $x_s = 1/\tilde{\beta}\tilde{\varepsilon}k$, with the effective match number $\tilde{\varepsilon} = u/\tilde{c_0}$ and the effective wavenumber $k = \omega/\tilde{c_0}$, that can be also found from Eq. (3.16). This celebrated solution is valid for $\sigma < 1$ (pre-shock region).

Simulations were carried out using a full-wave constitutive relations solver. Thus, we shall define the normalized reference frequency as $\Omega_0 = \pi\tilde{c_0}/a$ (located in the first band-gap). The source frequency was set to $\omega = 0.1\Omega_0$.

3.3.2. DISPERSIVE REGIME

For frequencies above the (idealized) homogeneous-Fubini regime, finite (weak and strong) dispersion effects are observed. The dispersive effects of the layered system deeply affects harmonic generation processes.

As intense waves propagate through a quadratic nonlinear medium, their frequency components interact with each other and new frequencies arise at combination frequencies, including higher harmonics. The cumulative energy transfer from the interacting waves to the harmonics is dependent on the resonance conditions $\omega_1 \pm \omega_2 = \omega_3$, $\mathbf{k}_1 \pm \mathbf{k}_2 = \mathbf{k}_3$. Note these conditions express the laws of conservation of energy ($\hbar\omega$) and momentum ($\hbar\mathbf{k}$) in the quantum description for the disintegration and merging of quanta [102]. These conditions can be satisfied in a variety of situations. The most simple case is observed in nondispersive media and for collinear waves $k_i = \omega_i/c_0$. In this situation the resonance conditions are fulfilled all over the spectra and a large number of harmonics interacts synchronously: when there exist in the system a *free* wave with velocity $\omega_3/|\mathbf{k}_3|$ that matches the excited (*forced*) wave $\omega_1 \pm \omega_2/|\mathbf{k}_1 \pm \mathbf{k}_2|$, the *free* wave is excited in a resonant way. The resonant interaction leads therefore to synchronous (phase matched), cumulative energy transfer from the initial wave to the secondary wave fields.

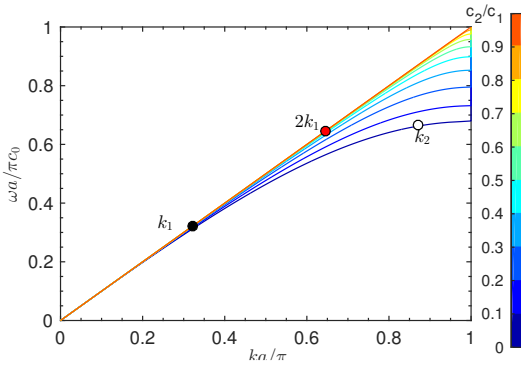

Figure 3.6: Scheme of the phase miss-matching situation. The fundamental wave vector k_1 at frequency ω generates a *forced* wave $2k_1$ at frequency 2ω. The *free* wave that the system allows to propagate is k_2, located in the dispersion relation curve. Due to dispersion, $k_2 \neq 2k_1$, thus there exist a phase mismatch, Δk_2 between both waves and the generation is therefore asynchronous.

In the case of an initial monochromatic wave, the main wave generates its second harmonic. The resonant conditions in this situation read $2\omega_1 = \omega_2$, $2\mathbf{k}_1 = \mathbf{k}_2$, that holds true for nondispersive collinear waves, leading to the simple relation $2\mathbf{k}(\omega_1) = \mathbf{k}(2\omega_1)$. However, in the case of dispersive media this condition is, in general, not fulfilled and the *forced* and *free* waves interact asynchronously. Figure 3.6 shows such situation for a layered media with a fundamental wave in the first dispersion band.

In order to study asynchronous second harmonic generation processes, we recall here for the lossless second-order wave equation Eq. (3.29), for one-dimensional propagation. This equation does not include dispersion by itself, dispersion arises from the solution of the linearized wave equation with the layered media boundary conditions, where the eigenvalue problem leads to the Rytov's dispersion relation Eq. (3.16).

In the following, we apply a perturbation method to obtain an approximate solution for the second harmonic field. We expand the pressure field as sum of contributions of different orders, i.e. $p = p^{(1)} + \varepsilon p^{(2)} + \cdots$, where ε is the smallness perturbation parameter, which we identify with the acoustic Match number. Thus, $p^{(1)}$ is the first order (linear) solution of the problem and $p^{(2)}$ its the second order contribution. By substituting the expansion in the second order wave Eq. (3.29), assuming constant density[1] and neglecting $\mathcal{O}\epsilon^3$ terms we get a coupled set of equations that can be solved recursively. The solution of the first

[1] We neglect the ambient density variations for the sake of simplicity. Dispersion arise also for sound speed variations, that are assumed to be implicit in the boundary conditions.

order equation corresponds to a monochromatic plane wave of frequency ω

$$p^{(1)} = p_0 \sin(\omega t - k_1 x) \tag{3.40}$$

where $k_1 = k(\omega)$ is the wave vector associated with the primary frequency ω, and p_0 is the excitation pressure amplitude. Substitution of the first order solution into the equation obtained at the next order in the expansion, leads to an inhomogeneous equation for the second harmonic field:

$$\frac{\partial^2 p^{(2)}}{\partial x^2} - \frac{1}{c_0^2}\frac{\partial^2 p^{(2)}}{\partial t^2} = -\frac{4\beta\omega^2 p_0^2}{\rho_0 c_0^4}\sin(2\omega t - 2k_1 x). \tag{3.41}$$

The general solution of the this equation is the sum of the solution of the homogeneous equation ($p_0 = 0$), and the particular solution of the inhomogeneous equation ($p_0 \neq 0$). Therefore the field for the second harmonic can be expressed as $p^{(2)} = p_h^{(2)} + p_f^{(2)}$, where the corresponding waves for this two solutions are the *free*, and *forced* waves respectively. Such homogeneous and particular solutions are:

$$p_h^{(2)} = p_h^{(2)}\Big|_{x=0} \sin(2\omega_1 t - k_2 x), \tag{3.42}$$

$$p_f^{(2)} = \frac{A}{(k_2 + 2k_1)(k_2 - 2k_1)} \sin(2\omega_1 t - 2k_1 x), \tag{3.43}$$

where $k_2 = k(2\omega_1)$ is the wavenumber of the *free* wave at second harmonic frequency, and the constant $A = -4\beta\omega_1^2 p_0^2/\rho_0 c_0^4$. It is worth noting here that as long $2k_1 \neq k_2$, the *forced* and *free* waves in dispersive media have different phase speed, i. e. the *forced* and *free* waves are phase mismatched as can be seen in the argument of the sin function in Eq. (3.42-3.43). Imposing the boundary condition, that the second harmonic must be absent at $x = 0$, the second harmonic field can be expressed as

$$p^{(2)} = \frac{A}{k_2 \Delta k}\sin(\frac{\Delta k}{2}x)\cos(2\omega_1 t - k_2' x), \tag{3.44}$$

where the effective wave number is $k_2' = (k_2 + 2k_1)/2 \approx k_2$ and the detuning parameter that describes the asynchronous second harmonic generation is defined as

$$\Delta k = k_2 - 2k_1 = k(2\omega) - 2k(\omega). \tag{3.45}$$

Equation (3.44) describes the well-known effect in second harmonic generation in dispersive media, that is the beatings in space of the second harmonic

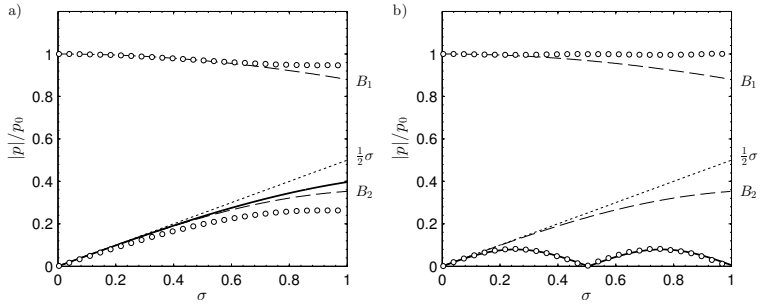

Figure 3.7: Second harmonic evolution for $x_c/x_s = (1, 1/4$ and $1/8)$ obtained using Eq. (3.44) (continuous line), numerically (white circles), nondispersive linear law of growth (dotted line) and Bessel-Fubini nondispersive solution (dashed).

field when the resonant conditions are not fulfilled. Thus, as Δk increases, the beating spatial period and also its maximum amplitude decreases. The position of the maximum of the beating, also called the coherence length, can be related to the second-harmonic phase-mismatching frequency as

$$x_c = \frac{\pi}{|\Delta k|} = \frac{\pi}{|k(2\omega) - 2k(\omega)|}. \tag{3.46}$$

This length corresponds to the half of the spatial period of the beating, where the maximum of the field is located. It can be expressed also for other higher harmonics simply as $x_c(n) = \pi/|\Delta k_n| = \pi/|k(n\omega) - nk(\omega)|$.

In the limiting case of $\Delta k \to 0$, the second harmonic field is generated synchronously and accumulates with distance, so a linear growth is predicted. In this case, phase matching conditions are fulfilled and the *free* wave is excited synchronous to the *forced wave*. Note here that in the derivation of Eq. (3.44) only second order processes are taken into account and therefore, only second harmonic is predicted. This leads to overestimate the second harmonic field: as long no energy is transferred to third harmonic, second harmonic predicted by Eq. (3.44) in the absence of dispersion grows indefinitely. The validity of this model can be explored expanding the Bessel functions of Fubini series near the source. A simple comparison between the full Fubini solution and linear second harmonic growth gives a reasonable approximation for distances $\sigma < 0.5$ or for second harmonic field values of $p(2\omega) < p_0/4$.

Figure 3.7 shows three different simulations in the dispersive regime of the layered media where the wave amplitude and frequency has been selected to match $x_c/x_s = 1, 1/4$ and $1/8$. The higher beating spatial period waves corresponds to lower frequencies. The analytical solution for the second harmonic matches the full-wave numerical solution. However, differences can be observed

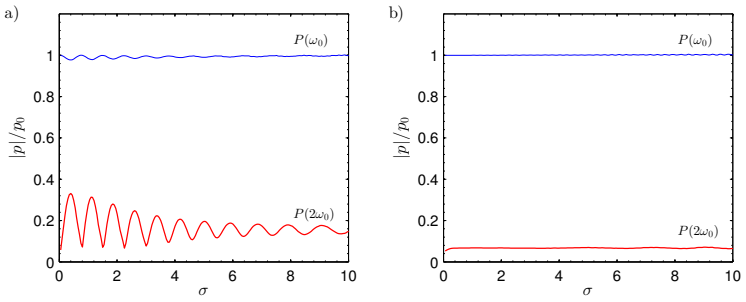

Figure 3.8: Evolution of the second harmonic field propagating in bang-gap for second harmonic frequencies (a) just above band-gap $2\omega_0 = 0.84\Omega_0$, (b) in the middle of the bandgap $2\omega_0 = \Omega_0$. All results for a layered medium with $\alpha = 1/2$ and $c_1/c_2 = 1/2$. (c) Detuning of the second harmonic (continuous line) and imaginary part (dotted line) in function of the normalized frequency.

in the second harmonic amplitude estimation for $x_c/x_s = 1$ (Fig. 3.7 (a). This overestimation by the analytical solution can be related to the absence of energy transfer to higher harmonics, that is not considered by the perturbation solution but is included in the simulation and also in the Bessel-Fubini solution. Therefore, this model is specially suitable in situations where the third harmonic does not grow cumulative with distance. In the lossless layered media, this situations include frequencies that leads to very high-third harmonic detuning and also when the third harmonic falls in band gap.

3.3.3. SECOND HARMONIC IN BAND GAP

Waves with frequencies falling into the band-gap of the dispersion relation are evanescent due the non negligible imaginary part of its complex wave number. Thus, its amplitude decays exponentially with distance. If the nonlinearly generated second harmonic falls into a band-gap, its amplitude does not decay but reaches a constant value [98]. Figure 3.8 shows this case for two different frequencies. The constant amplitude value of the second harmonic wave depends on the imaginary part of the wave vector.

This effect can be understood in terms of the *free* and *forced* waves. If the second harmonic is evanescent (as follows from the dispersion relation), the wave will not accumulate with distance. The fundamental wave is “pumping" energy to the second harmonic field at every point in space. Thus, the second harmonic field is generated locally and remains trapped inside the layered media. It reaches a constant level that depends on three main factors. In first place, the "pumping” rate, characterized by the fundamental wave amplitude and medium nonlinearity, or more strictly the ratio between the layer thickness and the shock distance a/x_s. Secondly, it also strongly depends on the magnitude of the imag-

inary part of the complex wave number, i.e. the ratio between its characteristic exponential decay length and the shock distance in a layer. The characteristic decay length of the evanescent propagation is always shorter when the second harmonic is in the middle of the band-gap, leading to a weaker second harmonic field in this frequency region, as seen in Fig. 3.8. Finally, it depends also on the detuning of real part of the wave number, where for the first band-gap is minimum at the center. The first factor can be isolated and studied separately. However, the two last factors are linked through the specific dispersion relation of the medium.

Figure 3.8(c) shows the detuning of the second harmonic and the imaginary part as a function of the frequency for a medium with $\alpha = 1/2$ and $c_1/c_2 = 1/2$, showing that at the middle of the band-gap these two factors have opposite effects: detuning is null (phase matching) when evanescent decay is nearly maximized, and viceversa. However, the magnitude of the effects can be very different. As the rate of the second harmonic generation (see the initial slope in Fig. 3.7) is independent on the detuning, and the evanescence implies that the wave decays after few layers, there not exist a practical compensation of the effects at the center of the band-gap. However, the situation is different for frequencies around the limits of the band-gap, where the coherence length is of the order of the exponential decay characteristic length. Thus, for frequencies just above bad-gap and for amplitudes with shock distance comparable to the evanescent characteristic decay length, the beatings can be also observed, as shown in Fig. 3.8 (a). Then, if frequency is increased the characteristic decay length becomes shorter than the shock wave distance and beatings cannot be observed, leading to to the characteristic constant second harmonic field shown in Fig. 3.8.

3.3.4. FUNDAMENTAL HARMONIC IN BAND GAP

When the fundamental frequency of the wave lies within the band-gap, small amplitude waves propagate evanescently. Essentially, the same applies to finite amplitude harmonic waves. In general, if the shock distance is large compared to the characteristic decay length of the evanescent wave, the nonlinear effects have no chance to accumulate and harmonic amplitude is negligible. Since the characteristic exponential decay is about few lattice sites, this means that the initial amplitude necessary to achieve nonlinear effects in this configuration is much higher than those in the preceding sections. Figure 3.9 shows the evolution of the first and second harmonic waves for a fundamental frequency at the Bragg frequency, $2\omega_0 = 1\Omega_0$, and with a frequency just above but into the band-gap, $\omega_0 = 0.87\Omega_0$ for a layered media of $\alpha = 1/2$ and $c_1/c_2 = 1/2$. In the first case,

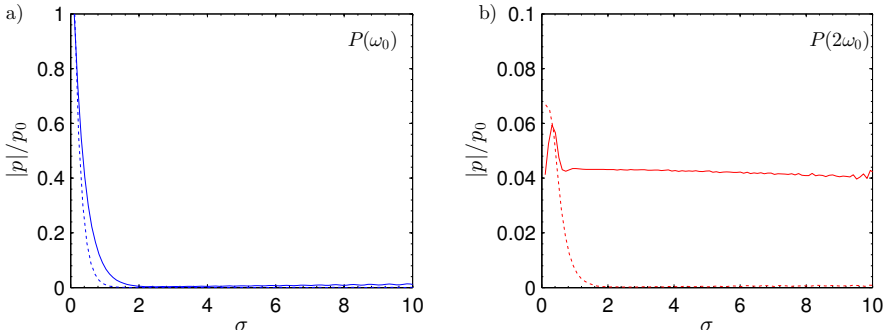

Figure 3.9: (a) Evolution of the fundamental harmonic wave field with its fundamental frequency falling just above into band-gap, $\omega_0 = 0.87\Omega_0$, (continuous line), and in the middle of the bad-gap, $2\omega_0 = 1\Omega_0$ (dotted line). (b) Corresponding second harmonic field, where for $\omega_0 = 1\Omega_0$ (dotted line) second harmonic frequency falls in the 2nd band band-gap while for $\omega_0 = 0.87\Omega_0$, (continuous line) lies into a propagating band.

the imaginary part of the wave vector is remarkable high and the waves decay fast after few lattice units. Due to this fast decay, the second harmonic interacts only over a short distance with the first, and its amplitude is very limited. After a few lattice units, the fundamental wave can be treated as a small-amplitude evanescent-wave. The second harmonic, that also falls in bandgap (but in the second band gap) also decays exponentially.

On the other hand, if the fundamental frequency is set just above the band-gap, where the imaginary part of the wave-vector is smaller, the amplitude of the fundamental wave decays more slowly, penetrating deeper into the material. The interaction region with the second harmonic is larger, and nonlinear effects result in a more efficient generation of the second harmonic. Furthermore, as long the different (higher order) bandgaps in the layered media can have different bandwidth, in this configuration at $\omega_0 = 0.87\Omega_0$ second harmonic does not fall inside a bandgap. Therefore, the generated second harmonic wave at the beginning of the lattice propagates through the medium essentially without amplitude change. Due to the evanescence of the fundamental wave, there is only *forced* wave at the beginning of the medium. Therefore, although in this configuration waves are phase mismatched, beatings are not present: only the *free* wave propagates through the medium.

3.4. NONLINEAR ACOUSTIC FIELD MANAGEMENT

3.4.1. TUNING NONLINEARITY WITH DISPERSION

In the preceding sections we have explored the fundamental behavior of nonlinear waves generated inside the layered media. But also, medium parameters can be designed to provide specific conditions. The material parameters can be tuned to get coherence at one frequency of interest, e.g. at one of the harmonics of the fundamental wave, or to get detuning or evanescent propagation at other specific harmonics. Using these mechanisms the layered medium can be used to provide a balance of the harmonic amplitudes, or to obtain specific nonlinear waveforms, providing a control of the nonlinear process inside the medium.

In the design of a system for this purpose, the coherence length is a useful control parameter. For this aim, the analytic Eq. (3.16) is used, which is shown to provide an excellent framework to tune the layered parameters to obtain the desired balance between detuning, evanescent propagation, synchronous generation and, at the same time, it allows to find those conditions for a specific phase/group speed. Figure 3.11(a,b) shows an example of a dispersion relation, the coherence length for the second and third harmonic. The resulting harmonic amplitudes when phase matching of all harmonics is achieved is shown in Figure 3.10. This happens for a set of frequencies $\omega_0 = (0, 1.75, 2.333, ...)/\Omega$. On the other hand, there also exist frequencies at which there exist coherence for the second but a non-negligible detuning is observed for the third. The opposite effect can be also obtained, where coherence is achieved for the third harmonic but second harmonic presents strong dispersion. Finally, other interesting regions are those where second harmonic component is almost phase matched and for the same frequency third harmonic falls into a band-gap.

In the following subsections, we propose and analyze different configura-

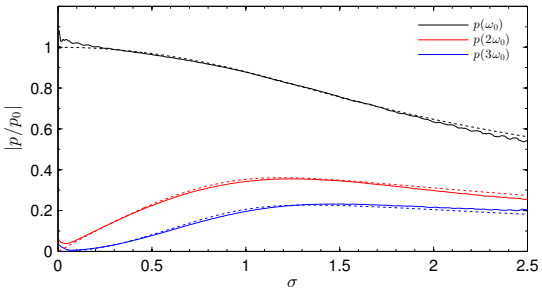

Figure 3.10: Harmonic distribution for the frequency $\omega_0 = 1.75/\Omega$. Coherence is recovered for at least the lowest spectral components. Blackstock solution (dotted lines).

tions of the layered medium with specific balance between detuning, evanescent propagation and synchronous generation.

3.4.2. ENHANCED SECOND HARMONIC GENERATION

One can expect that second harmonic generation is maximized in homogeneous nondispersive media. However, in nondispersive media coherence is achieved not only at second harmonic frequency, but also in the higher spectral components. As a result, energy is transferred from second harmonic field to higher spectral components and therefore second harmonic field does not grow indefinitely. Moreover, shock waves are formed and nonlinear absorption reduces wave intensity for $\sigma > \pi/2$ even in lossless media [109].

The dispersion of the layered system can be used to modify this situation by including phase mismatches that alter the higher harmonic cascade processes, while maintaining coherence for the second harmonic. Figure 3.10 shows an example of a dispersion relation where for $\omega_0 = 1.668\Omega_0$ it can be observed that there exist a reasonable coherence for the second harmonic ($x_c/a \approx 1000$), while the third harmonic falls in a band-gap. Figure 3.11 shows the harmonic distribution in this situation. Here, energy is transferred to second harmonic field that grows almost linearly for $\sigma < 2$. On the other hand, the energy transferred from second to third harmonic is not cumulative and its amplitude does not grow with distance. Third harmonic experiment evanescent propagation due to the imaginary part of the complex wave-vector at this frequency. A constant field, as studied in Sec. 3.3.3, is obtained for the third harmonic.

The total amount of the second harmonic amplitude in nondispersive media is $p_2|_{\max} \approx 0.36 p_0$, while in the example of Fig. 3.11 a maximum second harmonic amplitude of $p_2|_{\max} \approx 0.75 p_0$ is predicted. As can be shown the decreasing of the first harmonic follows the analytic nondispersive Blackstock solution for $\sigma \lessapprox 3$. Thus, in this regime all the energy of the first harmonic is being transferred to the second harmonic field. However, due to finite detuning of the second harmonic a long spatial beating is produced, with normalized period 8σ, and energy is returned back to the first harmonic component.

It is worth noting here that at distance $\sigma \approx 3$ sawtooth profile is observed in the nondispersive media. In contrast, only second and first harmonic have remarkable amplitude into the layered media. Waveforms are shown in Fig. 3.11(d-g). Near the source, where the amplitude of higher harmonics in not relevant the nondispersive waveform (in red dotted) is well approximated by the fundamental and its second harmonic of the layered medium. However, due to the evanescent propagation of the third harmonic for longer distances the nonlinear solution of the layered medium is mainly composed by the fundamental and

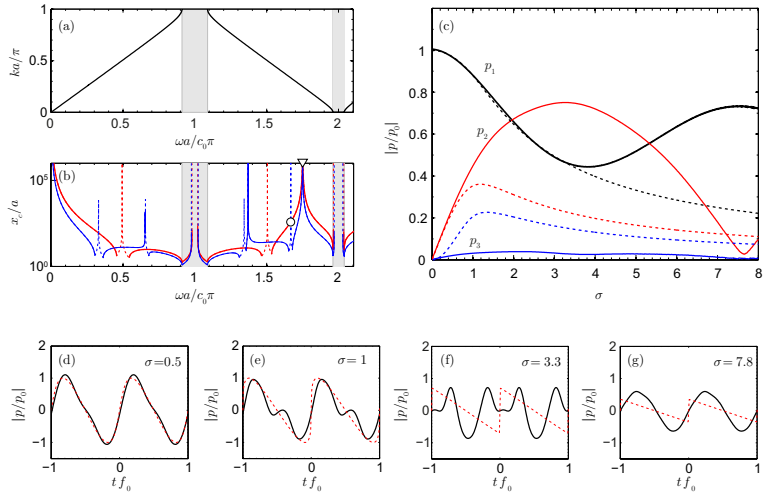

Figure 3.11: (a) Dispersion relation for a layered media of $c_1/c_2 = 1.33$ and $\alpha = 1/2$. (b) Coherence length for second (red) and third (blue) harmonics as a function of the fundamental frequency. Phase matched frequencies are those with $x_c \to \infty$, while asynchronous generation is predicted for $x_c \to 0$. Frequencies at which the fundamental frequency is in band-gap are are marked in gray regions, while band-gap regions for second and third harmonic are marked in dashed lines.(c) Harmonic distribution for $\omega_0 = 1.668\Omega_0$ where a coherence is achieved for second harmonic while the frequency of the third harmonic falls into the bad-gap. (d-g) (continuous lines) Waveforms at different distances for $\omega_0 = 1.668\Omega_0$. At $\sigma = 3.3$ second harmonic generation field is maximize and can be seen the period doubling in the waveform. Then, at $\sigma = 7.8$ due to second harmonic detuning nearly sinusoidal wave is recovered. Analytic Fubini-Blackstock solution for the harmonics (red dotted lines) are plotted for comparison.

its second harmonic. The maximum second harmonic in this configuration is observed at $\sigma = 3.3$, as it can be appreciated in the waveforms of Fig. 3.11 the period doubling. Moreover, due to finite detuning of the second harmonic the process is not cumulative for all distances and at $\sigma = 7.8$ the energy is restored in the first harmonic again and a sinusoidal wave is obtained. Note that not all the energy is restored to the first harmonic in Fig. 3.11 at $\sigma = 7.8$, leading to a sinusoidal wave of different amplitude as can be observed in Fig. 3.11. The energy loss is mainly due to the artificial (numerical) viscosity necessary to nonlinear convergence[109]. For these simulations the total distance is 1200 lattice sites and therefore the effects of attenuation are not negligible. However, the main nonlinear effects related to strong lattice dispersion still appreciated. An analogous effect has been also studied [102] where instead of dispersion, selective absorption at specific frequencies is used to modify and enhance harmonic generation.

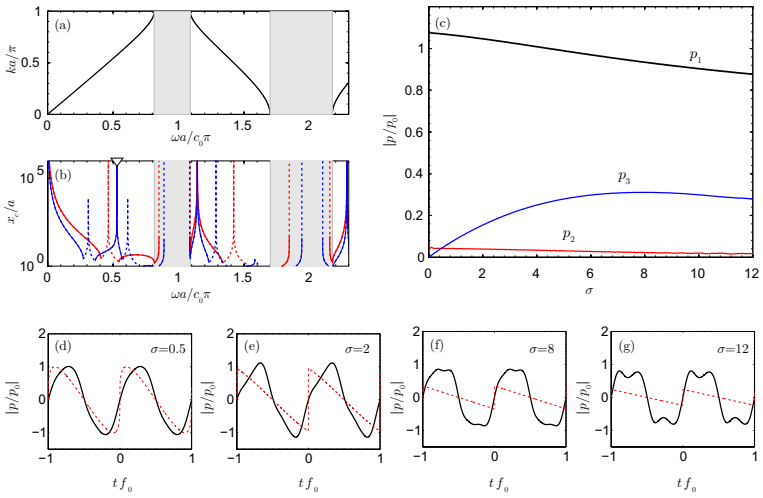

Figure 3.12: (a) Dispersion relation for a layered media of $c_1/c_2 = 1/3$ and $\alpha = 0.3$. (b) Coherence lengths for second (red) and third (blue) harmonics, (c) Harmonic distribution for $\omega_0 = 0.529/\Omega$ where a coherence is achieved for second harmonic while the frequency of the third harmonic falls into the bad-gap. Bottom: (continuous lines) Waveforms at different distances for $\omega_0 = 0.529/\Omega$. At $\sigma = 3.3$ second harmonic generation field is maximize and can be seen the period doubling in the waveform. Then, at $\sigma = 7.8$ due to second harmonic detuning nearly sinusoidal wave is recovered. Analytic Fubini-Blackstock solution for the harmonics (red dotted lines) are plotted for comparison.

3.4.3. ENHANCED THIRD HARMONIC GENERATION

In the first band ($\omega < \Omega_0$), coherence is always lower for the third harmonic than for the second. However, in the superior bands the layered medium parameters can be tuned to obtain higher coherence for the third than for the second harmonic. Essentially we follow same ideas on the preceding section but for the third harmonic. In this case, the lattice is designed forcing the second harmonic to fall in bandgap. A the same time, perfect coherence can be found for the third harmonic at $\omega = 1.4\Omega_0$. This situation is illustrated on Fig. 3.12 around $\omega = 1.4\Omega_0$. In this case, the dispersion relation was obtained for a layered medium with parameters $\alpha = 0.3$ and $c_2/c_1 = 1/3$.

In this situation, as Fig.3.12 shows, the second harmonic wave attains a constant value of about $0.04p_0$. As discussed in Sec.3.3.3, this constant field does not grow with distance and is related to the evanescent solution of the *free* wave and the local nonlinear "pumping". On the other hand, due to the coherence of the third harmonic, all the energy transferred form second to third is accumulated with distance. Therefore, near the source the rate of energy transfer from second to third harmonic is constant. Thus, third harmonic start to grow almost linearly

with distance, opposite to quadratically in homogeneous media.

Numerical simulations also show fourth and fifth harmonics grow (not shown in Fig. 3.12), but only fifth harmonic harmonic reach a remarkable amplitude, growing near the source almost quadratically with distance. Therefore, the entire system behaves as an artificially cubic-like nonlinear medium formed by quadratic nonlinear layers.

The corresponding waveforms measured at $\sigma = (0.5, 2, 8, 12)$ are shown in Fig. 3.12(d-g). For $\sigma = 0.5$ and 2, it can be observed how the wave steepens with the characteristic shape of cubic nonlinearity. No shock waves are formed as long as strong dispersion is present for high frequency harmonics. It is worth noting here a remarkable fact: it steepens in the positive time axis direction (to the right in the figure), opposite than the quadratic nonlinearity plotted in red dotted as a reference. This effect, i.e. the steepening on the opposite side of the propagation direction, is characteristic of materials with negative parameter of nonlinearity. Therefore, the effective nonlinear behavior observed by the simulations in this conditions can be described as negative-cubic-like nonlinearity.

3.5. CONCLUSIONS

The interplay of dispersion and nonlinearity in multilayered periodic media, such as one-dimensional phononic crystals or superlattices is shown to have a strong impact on the acoustic waves propagating through the structure. Nonlinearly generated harmonics propagating at different velocities are phase-mismatched, modifying the transfer of energy between the different harmonics, and therefore the waveform itself. Shock formation, typical of nonlinear homogeneous media, is in this way avoided. We propose a model and some particular solutions to study this problem, and report examples of configurations that result in an effective control of the spectrum of nonlinear acoustic waves by tuning the dispersion relation of the medium. Selective enhancement of second or third harmonic is demonstrated, leading in some cases to situations where the structure behaves with an effective nonlinearity different from that of its constitutive elements.

4

THE CHAIN OF COUPLED PENDULA AS AN ANALOGUE OF GAS MICROBUBBLES

Microbubbles, either in the form of free gas bubbles surrounded by a fluid or encapsulated bubbles used currently as contrast agents for medical echography, exhibit complex dynamics under specific acoustic excitations. Nonetheless, considering their micron size and the complexity of their interaction phenomenon with ultrasound waves, expensive and complex experiments and/or simulations are required for their analysis. The behavior of a microbubble along its equator can be linked to a system of coupled oscillators. In this chapter, the oscillatory behavior of a microbubble is investigated through an acousto-mechanical analogy based on a ring-shaped chain of coupled pendula. Observation of parametric vibration modes of the pendula ring excited at frequencies between 1 and 5 Hz is considered. Simulations have been carried out and show spatial mode, mixing and localization phenomena. The relevance of the analogy between a microbubble and the macroscopic acousto-mechanical setup is discussed and suggested as an alternative way to investigate the complexity of microbubble dynamics.

4.1. INTRODUCTION

When subjected to an external acoustic field, bubbles can undergo complex radial oscillations. This oscillatory behavior has been an important and continuously developing research subject since the beginning of the twentieth century. The investigation of bubble dynamics started with the work of Lord Rayleigh

[115], who was mandated by the Royal Navy to explain the origin of damages on submarine propellers. Rayleigh focused on the oscillatory behavior of cavitation bubbles suspended in a fluid. He showed that the overpressure generated by the oscillations and the collapse of bubbles could explain the damages caused on propellers. In the 30's, Minnaert was interested in the origin of the sound of running water [116]. He supposed that bubbles oscillating periodically in water were at the origin of rivers whispering. After these seminal works, many studies on bubble oscillations have been carried out in different research fields.

In addition to the radial motion, bubbles can show non-spherical oscillations or vibration modes. These vibration modes, characterized by an index n, were first analyzed theoretically at the interface between immiscible and incompressible fluids with spherical symmetries [117]. Later, Neppiras [118] analyzed the acoustic response from gas bubbles suspended in a fluid and subjected to sound fields. Eller and Crum [119], and Prosperetti *et al.* [120] focused on the instability of the motion and the nonlinear dynamics of a bubble within a sound field. In the 90's, the discovery of single bubble sonoluminescence (SBSL) by Gaitan and Crum [121], led to additional studies on nonlinear oscillations of bubbles [122–124]. Finally, with the use of ultrasound contrast agents [125], the understanding of bubble dynamics have found a renewed interest in the field of ultrasound imaging and targeted drug delivery [126, 127]. Therefore, the problem of vibration modes in bubbles is still under investigation.

In this study, the interaction between ultrasound and a microbubble, and especially the appearance of vibration modes, are studied using a macroscopic analog system [128, 129]. The mechanisms underlying its nonlinear behavior are sought to improve our understanding of the microbubble dynamics. The study of a single microbubble is a difficult task, particularly because of the interaction with other microbubbles or microstreaming that sweep away the bubble. Moreover the smallness and the complexity of the phenomena involved, require complex modeling and expensive experiments. In this work, we propose the use of a macroscopic mechanical analog as an alternative way to investigate microbubble dynamics.

The study of analog models in the field of physics is a tool that allows recreating in the laboratory phenomena that are difficult to observe directly. Concerning microbubbles, some of its dynamic features (vibration modes, subharmonic oscillations, chaos) can be captured by a system of coupled oscillators. Here, the oscillatory behavior of a microbubble and its vibration modes are investigated through the use of a macroscopic analogy consisting of a chain of coupled pendula, parametrically excited by a vertical force. Based on a discrete nonlinear model of coupled pendula and its continuous limit describing low frequency excitations, vibration modes are investigated theoretically and experimentally.

This approach is used here to set up a formal basis for the acousto-mechanical analogy of a gas microbubble.

The structure of this chapter is as follows: The recent advances on ultrasound contrast agents and the mathematical formulations of a gas microbubble in an ultrasound field are presented in section 2. The acousto-mechanical analog system, the parametrically driven chain of coupled pendula, in introduced in Section 3. The description of the experimental setup and the obtained experimental result are presented in section 4. Finally, the conclusions of the study are presented in section 5.

4.2. MICROBUBBLE DYNAMICS

In this section we review and discuss the motivation and interest of our study, based on the current important applications of the use of encapsulated microbubbles in the field on medical imaging and therapy. A derivation of the basic model of gas microbubbles oscillating in the presence of an untrasound field, the Rayleigh-Plesset equation, is reviewed, in order to stablish later a connection with the discrete mechanical analogue proposed in our study. The basic nonlinear features, existence of non-spherical vibration modes of microbubbles, is discussed.

4.2.1. MOTIVATION: ULTRASOUND CONTRAST AGENTS (UCAS)

Image formation and processing is an important tool used in different areas such as astronomy, geology, physical, biological, and even used in human sciences, for example, in archeology or art history. However, one of the most important applications is in the field of medicine, where one can get multiple benefits concerning health and human welfare. Contrast agents have taken much interest in recent years. The greatest successes have been achieved in contrast agents consisting of microbubbles, as those described before. These ultrasound contrast agents not only interact with image processing, but form a part of it. Because of the great potential for improvements in diagnosis using ultrasound with application of contrast media based on microbubbles, it is very important to know and improve the techniques, and to simplify the complex behavior of these new contrast agents.

A contrast agent substance consists of microbubbles which are injected into the bloodstream intravenously at the time of patient ultrasound examination. The microbubbles are highly reflective to ultrasound. It is possible, for example, to detect a tumor metastasis whose contrast enhancement (temporal evolution of the contrast agent concentration in the blood) is faster than that of healthy biological tissue surrounding the tumor, as shown in Figure 4.1.

The development of contrast agents applied to ultrasound diagnostic exam-

ination has been slow and sporadic. In recent times there have been great advances in the production of contrast media with different characteristics and study techniques. Today the contrast agents are widely used. Hence the importance of knowledge of its usage, with its advantages and disadvantages, to thereby obtain better results in their application.

The beginnings of the Ultrasound Contrast Agents, or UCAs, are reported in the publication of Gramiak and Shah in 1968 [130], who considered a rabbit aorta and obtained a better contrast due to the air bubbles generated by cavitation. To know how the complexity of UCAs is going on, currently commercially available UCAs are microparticles with 3 μm to 10 μm diameter of air or other gas [131, 132], these systems are called genericcally microbubbles [133]. Despite the progress that has represented the introduction of the microbubbles for ultrasound diagnosis it is still not possible the efficient detection of tumors; This limitation is related in part to the current size of commercially available UCAs. It has been suggested that miniaturization of these systems could improve the ability to detect tumors in a variety of organs such as liver, kidney, pancreas, ... etc [134]. Moreover, having relatively large particles greatly increases the possibility of adverse effects such as thrombolysis and cell lysis, etc. [135].

Up to now, very few studies have been published about development of UCAs at the nanoscale, which is more complex than microscale. Wheatley et al. (2004)[136] achieved centrifugally separate populations of nanometric size in about 450 nm to 690 nm of a suspension of microbubbles obtained by sonication of a solution of Tween ® 80 and Span ® 60 in the presence of octafluoropropane. However, the main disadvantage of these "nanobubbles" is its low stability. Additionally, a recent paper by the same authors (Wheatley et al.) extended information about these systems, but could not solve the stability problem.

Fox and Herzfield [137] showed how an encapsulating shell increases the resonance frequency of the free gas microbubble. Later, de Jong and Hoff [138] carried out some experiments and measured this increased resonance frequency when studying acoustic attenuation from the contrast agent Albunex ®.

Hoff and Sontum [139] investigated an experimental contrast agent from Nycomed ®, using a linear model based on the bulk properties of the particles. Haran [140] incorporated these studies into a model for the transmission and scatter of ultrasound pulses in tissue. A more well-founded, nonlinear theoretical model for shell-encapsulated bubbles was presented by Church in 1995. Frinking and de Jong [141] have presented a phenomenological model describing the contrast agent Quantison®. All these studies show that the shell increases the mechanical stiffness of the contrast agent particles, and that shell viscosity increases sound absorption.

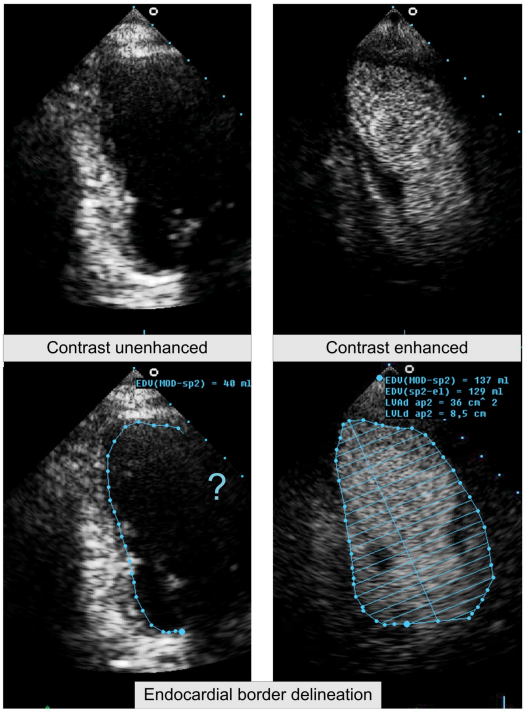

Figure 4.1: Heart left ventricle recorded from apical position. Bottom images show that contrast enhancement using an ultrasound contrast agent improves the detection of the heart wall border, which is useful to study the wall motion and the ejection fraction of the heart. Images by courtesy of Dr. F.J. ten Cate of the Erasmus MC, Rotterdam, the Netherlands.

4.2.2. THE FREE GAS BUBBLE: RAYLEIGH-PLESSET EQUATION

In this section, we present the process which leads to obtain Rayleigh-Plesset equation, the basic model of a ultrasound-driven gas bubble [115]. This equation describes the nonlinear radial pulsation of a bubble. It determines the dynamic response if the bubble in an incompressible fluid. At $t = 0$, the radius of the bubble is given by its equilibrium value R_0. The static pressure of the environment P_0 is assumed constant. At $t > 0$, a a time-varying pressure $P_{ac}(t)$ is added to the static pressure and the total pressure P_1 is

$$P_1 = P_0 + P_{ac}(t). \tag{4.1}$$

Due to the geometry of the bubble, it is convenient to use spherical coordi-

nates, taking the center of the bubble as the origin. In the presence of the pressure field $P_{ac}(t)$, it is assumed that the bubble begins to oscillate radially. By assuming the spherical symmetry of the bubble, we can write that the velocity of the bubble surface is

$$\vec{v} = v(r,t)\vec{e}_r = 0 \tag{4.2}$$

We begin the derivation with the fundamental equations of fluid mechanics: the continuity equation

$$\partial_t \rho + \vec{\nabla}\cdot(\rho\vec{v}) \tag{4.3}$$

and the Euler equation, in the form

$$\rho\frac{d\vec{v}}{dt} = \rho(\partial_t\vec{v} + (\vec{v}\cdot\vec{\nabla})\vec{v}) = \vec{F}. \tag{4.4}$$

We consider that the only forces present are due to the pressure and we can write the second Newton's law as

$$\vec{F} = -\vec{\nabla}P, \tag{4.5}$$

where

$$P = P_L(r) + P_\infty(t) \tag{4.6}$$

being $P_L(r)$ the pressure of the liquid at a point a distance r from the center of the bubble. By considering that the fluid is incompresible, Eq. (4.3) becomes

$$\vec{\nabla}\cdot\vec{v} = 0, \tag{4.7}$$

and

$$v(r,t) = \dot{r} = \frac{R^2}{r^2}\dot{R}, \tag{4.8}$$

for $r \geqslant R$. we introduce the potential for the velocity ϕ as $\vec{v} = \vec{\nabla}\phi$, and from Eq. (4.8) we obtain

$$\phi = \frac{R^2}{r^2}\dot{R} \tag{4.9}$$

where $\phi(r\to\infty) = 0$. We also assume that the fluid is irrotational, which implies that

$$(v\cdot\vec{\nabla})\vec{v} = \vec{\nabla}(\frac{1}{2}v^2). \tag{4.10}$$

By replacing $\vec{v}$ by its expression in terms of the velocity potential and introducing Eq. (4.10) in the Euler equation (4.4), we get the Bernoulli equation

$$\dot{\phi} + \frac{1}{2}(\vec{\nabla}\phi)^2 = -\frac{P_L(r)}{\rho} + \frac{P_\infty(t)}{\rho} \tag{4.11}$$

Replacing ϕ by its expression given by equation (4.9) and by standing at $r = R$, we finally obtain the equation of Rayleigh-Plesset [117]

$$\ddot{R}R + \frac{3}{2}\dot{R}^2 = \frac{1}{\rho}(P_L(r) - P_\infty(t)). \tag{4.12}$$

If the surface tension is neglected, the pressure in liquid at R is equal to the gas pressure at R (i.e. $P_L(R) = P_G(R)$). We assume that the gas has a polytropic behavior which means that the pressure at R can be written as

$$P_G(R) = P_{G,0}(\frac{R_0}{R})^{3\kappa} \tag{4.13}$$

where R_0 the radius at equilibrium and κ the polytropic exponent. $\kappa = 1$ applied to isothermal gas behavior. Instead, if the gas has an adiabatic behavior, $\kappa = \gamma$.

$P_{G,0} = P_0$ at $t = 0$, where P_0 is the hydrostatic pressure. Replacing in equation (4.12), the equation of Rayleigh-Plesset becomes

$$\ddot{R}R + \frac{3}{2}\dot{R}^2 = \frac{1}{\rho}\left(P_0(\frac{R_0}{R})^{3\kappa} - P_0 - P_{ac}(t)\right). \tag{4.14}$$

Note that by perturbing the radius of the bubble by placing $R(t) = R_0 + r(t)$ where $r(t) << R_0$ and substituting into Eq. (4.14), where R_0 is the equilibrium radius of the bubble, the equation of motion of a linear harmonic oscillator is obtained

$$\ddot{x} + \frac{3\kappa P_0}{\rho R_0^2}x = 0, \tag{4.15}$$

or

$$\ddot{x} + \omega_0^2 x = 0, \tag{4.16}$$

where the natural frequency is given by

$$\omega_0^2 = \frac{3\kappa P_0}{\rho R_0^2}. \tag{4.17}$$

Subsequently, Rayleigh-Plesset equation (4.14) was completed by additional terms. In 1950 Noltingk and Neppiras took into account the surface tension σ of the bubble [142]. The equation (4.14) then becomes

$$\ddot{R}R + \frac{3}{2}\dot{R}^2 = \frac{1}{\rho}((P_0 + \frac{2\sigma}{R_0})(\frac{R_0}{R})^{3\kappa} - \frac{2\sigma}{R} - P_0 - P_{ac}(t)). \tag{4.18}$$

Later in 1952, Poritzky added a viscosity term of the surrounding fluid μ [143]

$$\ddot{R}R + \frac{3}{2}\dot{R}^2 = \frac{1}{\rho}\left((P_0 + \frac{2\sigma}{R_0})(\frac{R_0}{R})^{3\kappa} - \frac{2\sigma}{R} - \frac{4\mu\dot{R}}{R} - P_0 - P_{ac}(t)\right). \tag{4.19}$$

where ρ is the density of the surrounding fluid, P_g is the gas pressure inside the bubble that can be written as

$$P_g = \left(P_0 + \frac{2\sigma}{R_0}\right)\left(\frac{R_0}{R}\right)^{3\kappa} \tag{4.20}$$

We recall that $P_{ac}(t)$ is the acoustic pressure, σ the surface tension of the bubble, μ the dynamic viscosity and κ the polytropic exponent. Some generalizations of this model have been proposed [139, 144–146]. As shown in Fig.4.2 the numerical simulations based on the Rayleigh-Plesset equation with a bubble radius $R_0 = 1\mu m$, predict the linear and nonlinear dynamic behavior of the bubble with only the change in the excitation amplitude. At low amplitude the system is nearly linear, and with increasing the amplitude the system behaves as nonlinear system. The first harmonic start to decrease with increasing the rest of harmonics.

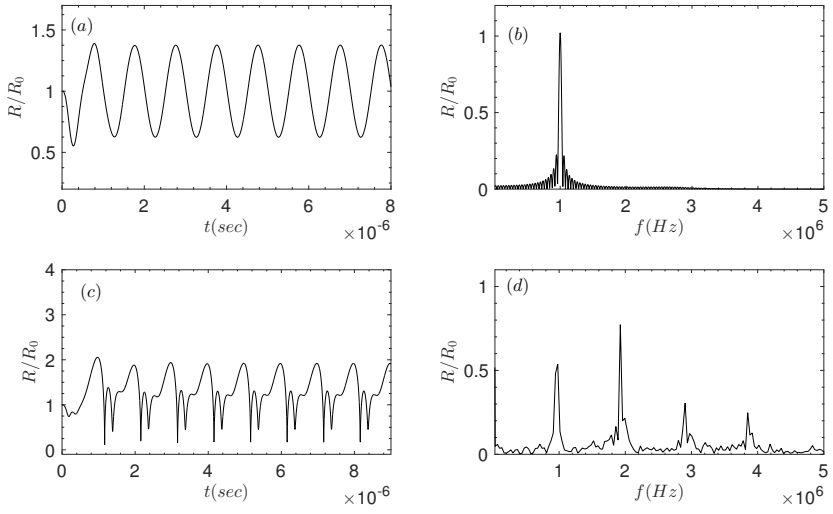

Figure 4.2: Numerical simulation of Eq. (4.14). (a) Linear behavior of the Rayleigh-Plesset Equation, resulting from the removal of the nonlinear part. The radius of the bubble as a function of time is shown, for an initial radius $R_0 = 1\mu m$. It is observed that the bubble oscillates symmetrically. (b) Signal spectrum of the time-dependent radius. The bubble oscillates at a frequency equal to the excitation frequency $f_e = 1$ MHz. (c) Nonlinear behavior, again the radius of the bubble as a function of time is shown. Here, $f_e = 1MHz$ and $P_{ac} = 100$ kPa (c) Signal spectrum of the nonlinear case, where harmonic generation is observed.

4.2.3. NONLINEAR BEHAVIOR OF MICROBUBBLE

In response to an ultrasound excitation, the bubbles can vibrate, in addition to the fundamental component f_d, into other higher frequencies (f_d, $2f_d$, $3f_d$ and $4f_d$, ...). Often, subharmonics of the excitation ($f_d/2$, $f_d/3$...) are also observed. For a fixed-size microbubbles, the generation of these harmonics essentially depends on the excitation amplitude P_{ac}, the driving frequency f_d and the shape of the excitation signal. The different harmonic components generated by a bubble are illustrated in Fig.4.3. The presented figures are obtained from the simulated response of Rayleigh-Plesset Eq.(4.16) with a bubble radius $R_0 = 3\mu$ m and other parameters typical of a free gas bubble. The excitation signal frequency f_d is 1 MHz and the pressure is changing from low to high with a change in the harmonic amplitudes.

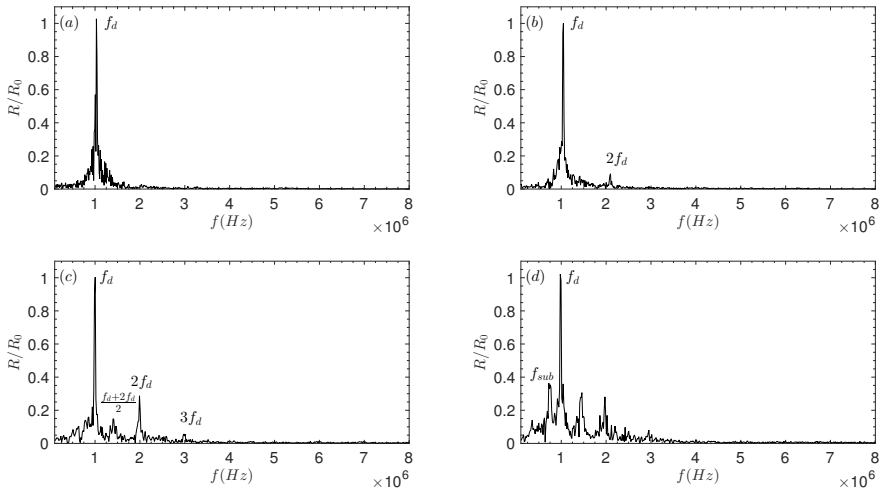

Figure 4.3: Nonlinear behavior of microbubble of Eq.(4.14). (a) Linear simulation show the first harmonic and there is exist of the rest of harmonics at Frequancy $f_d = 1MHz$, the Amplitude $P_{ac} = 3KP$ and the radius $R_0 = 3\mu m$. (b) The spectrum with the same parameters but with increasing acoustic Pressure $P_{ac} = 16KP$. the figure shows the second harmonic at $2f_d = 2MHz$. (c) By increasing the amplitude again to $P_{ac} = .13MP$ the thisd harmonic show up at $3f_d = 3MHz$ and also some harmonic appears between first and second harmonic at $\frac{f_d+2f_d}{2}$. (d) With increasing the acoustic pressure to $P_{ac} = .16MP$, the Sub-harmonics start to appear, at the same time the amplitude of the rest of harmonics increase.

4.2.4. VIBRATION MODES OF A MICROBUBBLE

In addition to radial oscillations, the microbubbles may present vibration modes when subjected to specific ultrasonic excitation. Surface oscillations mode of bubble (in millimeter-size and micrometer size) have been studied before in many works. One of the seminal articles written by Plesset in 1954 discussed the stability or instability of the interface between two immiscible incompressible fluids in radial motion [147]. Marston and Goosby studied the shape oscillation and fission of drops of an oil in water [148]. Lundgren and Mansour studied nonlinear oscillations and other motions of large axially symmetric liquid drops in zero gravity [149]. Basaran focused on nonlinear oscillations of a viscous liquid drop [150]. He analysed large amplitude axisymmetric oscillations of a viscous liquid drop by by solving the free boundary problem comprised of the Navier–Stokes system and appropriate interfacial conditions at the drop–ambient fluid interface.

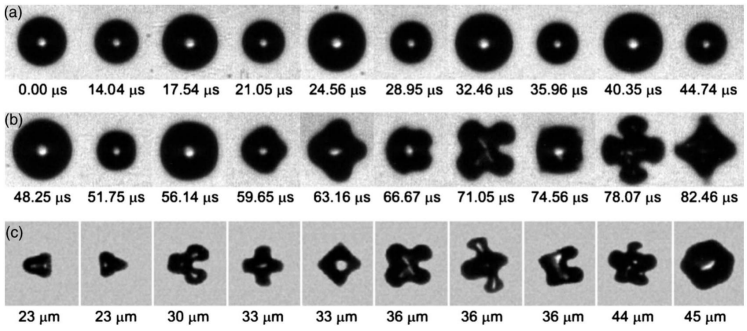

Figure 4.4: Versluis et al [151]. Growth of a surface mode vibration for a bubble with a radius of $36\mu m$ as captured with the Brandaris high-speed camera. First, the bubble oscillates in a purely volumetric radial mode(a), then after 5 cycles of ultrasound (b) the bubble becomes shape-unstable and a surface mode $n = 4$ is formed. (c) A selection of surface modes observed for various bubble radii.

The microbubble shape oscillations under the action of ultrasound has been also studied [151]. There, they focused an ultrasound beam with frequency 130 KHz on a single air bubble with radius ranging 10 to 45μm and detected the motion by a high speed camera with a rate of 25 million frames per second. They observed the oscillation modes from $n = 2$ to $n = 6$ of micron-sized single air bubbles.

Figure 4.4 shows a selection of a high-speed recording displaying the dynam-

ics of a 36μ m radius bubbles driven at an acoustic pressure of 120kPa. The first frame in Fig.4.4,a show the bubble at rest. the next nine frames show how the bubble oscillates radially in a spherical volumetric mode. In Fig.4.4,b the bubble develops a surface mode vibration with $n = 4$. Finally, in Fig.4.4,c a different vibration mode were observed.

4.2.5. MODELLING OF NONSPHERICAL OSCILLATIONS OF MICROBUBBLES

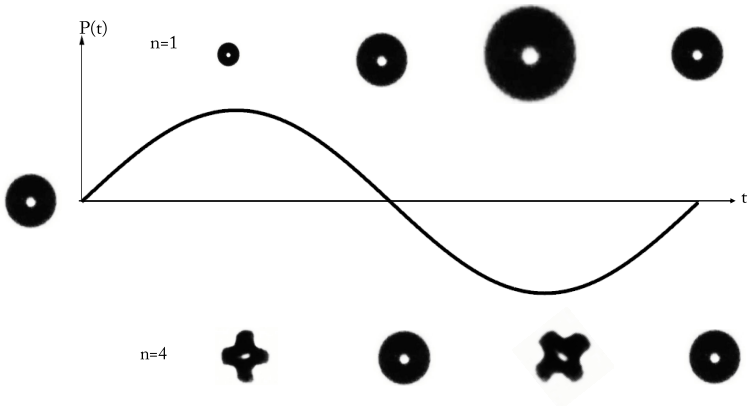

Figure 4.5: A bubble oscillating volumetrically within an acoustic field. For positive and negative pressures, compression and expansion phases are observed respectively. Several modes are shown: the radial mode $n = 0$ and the non-spherical mode $n = 4$.

In the presence of an acoustic field, microbubbles can be forced to oscillate in different ways. The most common oscillation mode is the radial mode Fig. 4.5 with the index $n = 0$, and where the bubble compresses and expands radially, maintaining its spherical shape. The basic model describing the radial dynamics of a bubble is the Rayleigh-Plesset equation for the time dependent radius R, derived in the previous section and written here agis for convenience

$$\rho\left(R\ddot{R}+\frac{3}{2}\dot{R}^2\right)=P_g-P_0-P_A(t)-\frac{2\sigma}{R}-4\mu\frac{\dot{R}}{R}, \tag{4.21}$$

with ρ the density of the surrounding fluid, $P_g=\left(P_0+\frac{2\sigma}{R_0}\right)\left(\frac{R_0}{R}\right)^{3\gamma}$, the gas pressure inside the bubble, P_0 is the hydrostatic pressure, R_0 is the equilibrium radius of the bubble, $P_A(t)$ the acoustic pressure, σ the surface tension of the bubble, μ the dynamic viscosity and γ the polytropic exponent in the case of adiabatic

behaviour. Some generalizations of this model have been proposed [139, 144–146]. The resonance frequency of the radial mode of the bubble, the so called Minnaert frequency, can be obtained from linearization of Eq. (4.21) and is given by

$$f = \frac{1}{2\pi R_0}\left(\frac{3\gamma P_0}{\rho}\right)^{1/2}. \tag{4.22}$$

Under typical conditions, the relation fR_0 is a magnitude of order 1. In particular, for a bubble in water at standard pressure (P_0=100 kPa, ρ=1000 kg/m^3, $\gamma = 1.4$), this equation gives the condition $fR_0 \approx 3$ m/s.

Microbubbles can also undergo non-spherical oscillations (see Fig. 4.6, left column) through instabilities at the gas/fluid interface. In this case, the radius becomes a space-dependent function,

$$R(t) \rightarrow R(\theta,\varphi,t) = R(t) + \xi(\theta,\varphi,t), \tag{4.23}$$

where $R(t)$ describes the evolution of the radial mode and $\xi(\theta,\varphi,t)$ a perturbation depending on the spherical coordinates θ and φ. As Fig.4.6 (left) shows, microbubbles can develop different surface patterns that depend on the excitation parameters (amplitude and frequency of the ultrasound wave) and the bubble radius. The radial oscillation corresponds to the mode $n = 0$; the mode $n = 1$ corresponds to the displacement of the center of mass. Non-spherical surface modes are those modes with $n \geq 2$.

To describe non-spherical modes in bubbles, a common analytical approach is to expand the perturbation of the radial mode, $\xi(\theta,\varphi,t)$, on the basis of spherical harmonics [117]

$$\xi(\theta,\varphi,t) = \sum_{n,m} a_n(t)\, Y_n^m(\theta,\varphi), \tag{4.24}$$

where $a_n(t)$ is the time-dependent amplitude of the surface mode of index n, and $Y_n^m(\theta,\varphi)$ is the spherical harmonic defined as

$$Y_n^m(\theta,\varphi) = \frac{(-1)^m}{\sqrt{4\pi}}\sqrt{\frac{(n-m)!}{(n+m)!}}\sqrt{2n+1}P_n^m(\cos\theta)e^{im\varphi}, \tag{4.25}$$

where P_n^m are Legendre polynomials. Although $Y_n^m(\theta,\varphi)$ defines a large set of possible surface modal oscillations, experiments [151] show that the observed modes present symmetry along the axis of the incident ultrasound beam, corresponding to $m = 0$, also known as zonal harmonics. Then, spherical harmonics $Y_n^0(\theta,\phi)$ are proportional to Legendre polynomials $P_n(\cos\theta)$. The evolution

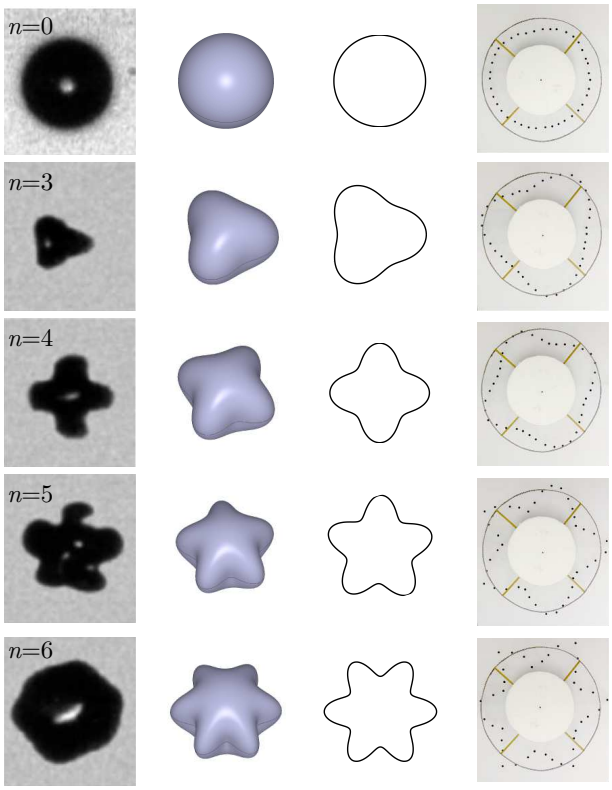

Figure 4.6: Representation of microbubble surface modes with index n the mode's order. The left pictures are experimental results from [151], and show a selection of surfaces modes observed for different microbubble radius between 36-45 μm. The two columns in the center are 3D analytical solutions from Eq. (4.25), and its equatorial cross-section. The right column shows the corresponding vibration modes experimentally observed with the acousto-mechanical system, as described later in section 4

equation for the amplitude of each mode can be found by matching velocity potentials and pressures at both sides of the interface, and linearizing for small amplitudes [117],

$$\ddot{a}_n + \left(\frac{3\dot{R}}{R} + \frac{2(n+2)(2n+1)}{\rho R^2}\mu\right)\dot{a}_n + \left(\frac{(n+1)(n+2)\sigma}{\rho R^3} + \frac{2(n+2)\mu\dot{R}}{\rho R^3} - \frac{\ddot{R}}{R}\right)(n-1)a_n = 0, \tag{4.26}$$

where, μ is the viscosity and σ the surface tension. Defining $b(t) = a(t)R^{3/2}$, the

equation can be simplified as [152]

$$\ddot{b}_n + \left(\frac{(n-1)(n+1)(n+2)\sigma}{\rho R^3} - \frac{3\dot{R}^2}{4R^2} - \frac{(2n+1)\ddot{R}}{2R} \right) b_n = 0. \tag{4.27}$$

Within this approach, each mode n obeys to the equation of a harmonic oscillator, with time dependent coefficients. The resonance frequencies of the surface modes readily follow from Eq. (4.27) by considering the static condition $R = R_0$, and $\dot{R} = \ddot{R} = 0$.

$$\omega_n = \sqrt{\frac{(n-1)(n+1)(n+2)\sigma}{\rho R_0^3}}, \tag{4.28}$$

which is the Lamb expression for surface modes for a free gas bubble.

The acoustic pressure term $P_A(t)$ in Eq. (4.21) is usually a harmonic function with angular frequency ω_e, i.e. $P_A(t) = p_A \cos(\omega_e t)$. For sufficiently small amplitudes p_A, the bubble response will be also harmonic at the same frequency, i.e.

$$R(t) = R_0 + R_\varepsilon \cos(\omega_e t), \tag{4.29}$$

with $R_\varepsilon \ll R_0$. Substituting Eq.(4.29) into Eq.(4.27) and linearizing, a Mathieu equation for each surface mode is obtained [152]

$$\ddot{b}_n + \left(\omega_n^2 + \left(\frac{(2n+1)\omega_e^2}{2} - 3\omega_n^2 \right) \frac{R_\varepsilon}{R_0} \cos(\omega_e t) \right) b_n = 0. \tag{4.30}$$

The Mathieu equation is a special case of a linear second-order homogeneous differential equation with time dependent coefficients, and appears in many applications in physics and engineering, specially in the description of parametrically driven systems [153], as the systems considered in this work.

4.3. THE PARAMETRICALLY DRIVEN CHAIN OF COUPLED PENDULA

In this section the model equations for the macroscopic analog of the microbubble are formulated. First, we consider the exact problem of the discrete lattice of coupled masses, that corresponds to our experimental system. Later, the continuum limit of this model is used to establish the analogy with gas microbubble, by deriving an equation isomorphic to Eq. (4.30).

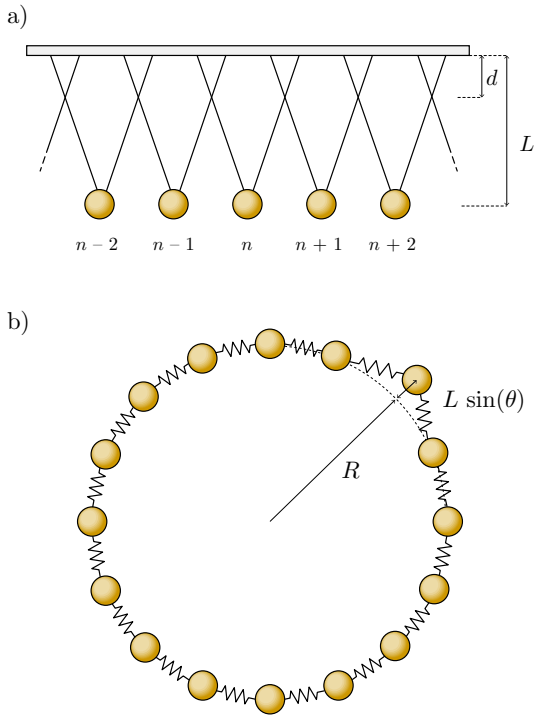

Figure 4.7: Schematic representation of the chain of pendula coupled by V-shaped strings and knots, hanging from a rigid support. (a) Lateral view of a section of the chain, (b) top view of the whole chain in a circular arrangement. Deviation of one mass with respect to its equilibrium position, and its coordinates are shown for illustration.

4.3.1. THE DISCRETE LATTICE

The equation of motion of a pendulum of length L is given by

$$\ddot{\Theta} + \omega_0^2 \sin\Theta = 0, \tag{4.31}$$

where $\Theta(t)$ is the angle with respect to the vertical, and $\omega_0 = \sqrt{g/L}$, g being the acceleration due to gravity. When a set of oscillators are coupled to their nearest neighbors, they form a lattice or chain, supporting waves. Consider that the lattice is subjected to a parametric forcing with displacement amplitude h_e and angular frequency ω_e, then its motion is described by

$$\ddot{\Theta}_i + (\omega_0^2 + \eta\cos\omega_e t)\sin\Theta_i - c^2(\Theta_{i+1} - 2\Theta_i + \Theta_{i-1}) = 0, \tag{4.32}$$

where Θ_i is the angle of the i-th pendulum, $\eta = 4\omega_e^2 h_e/L$ is the forcing parameter, and c is a constant denoting the strength of the coupling, equivalent to the

speed of sound for the waves for the lattice waves. Lattice models like Eq. (4.32) have been extensively studied, in the context of Frenkel-Kontorova chain [154]. Most of the work is theoretical, and focused on the formation of localized states (breathers, solitons and kinks). There are few experimental works [155–157], where different parametric driving mechanisms and coupling have been implemented. In Ref. [155], coupling is achieved by strings and knots, while in Ref. [157] torsional springs are used. In all the cases, a linear arrangement of pendula was considered. Boundary conditions typical of this configuration are either fixed or free ends. For the sake of simplicity, in the forthcoming analytical treatment we have ignored dissipation, which is small but finite in our experiment. It can be added as a phenomenological term in Eq. (4.32) by including an additional term $\beta\dot{\Theta}$. Our numerical simulations later will take into account such dissipative term, with $\beta = 5\ 10^{-4}$ rad/s.

Here, in order to mimic a bubble-like behavior, we consider the chain in a circular arrangement. This implies the periodic boundary condition $\Theta_{N+1} = \Theta_1$. In addition to this, the circular configuration incorporates curvature effects, which are not present in the linear chain. We assume an V-shaped coupling (see Fig. 4.7,a), for which coupling strength is given by

$$c^2 = \frac{g d a^2}{4L(L-d)}, \tag{4.33}$$

where d is the distance from the knot to the support, and a the distance between masses [155]. Note that, in this model, the coupling strength can be varied by selecting the position of the knot.

The chain supports different oscillation modes, labeled with an integer index n, corresponding to standing waves with wavenumber k_n. For the circular chain of radius R_0, the relation $k_n = n/R_0$ holds. The relation between driving frequency and mode index (the dispersion relation) can be obtained, for negligible damping and forcing, after linearization and assuming a solution in the form of a harmonic wave, $\exp i(kna - \omega t)$. This results in the relation

$$\omega_n = \sqrt{\frac{g}{L-d}\left[1 - \frac{d}{L}\cos^2\left(\frac{na}{2R_0}\right)\right]}. \tag{4.34}$$

Fig.4.8 shows the dispersion relation Eq.(4.34). The parameters of the ring are: number of pendulums $n = 50$ and the length of each pendulum $L = 103mm$ with a knot located at $d = 30mm$. As the figure shows, the minimum frequency at $f_0 = 3.1Hz$ (In the figure, the frequency has been normalized to Minimum Frequency) and the cut-off frequency at $f_c = 3.7Hz$.

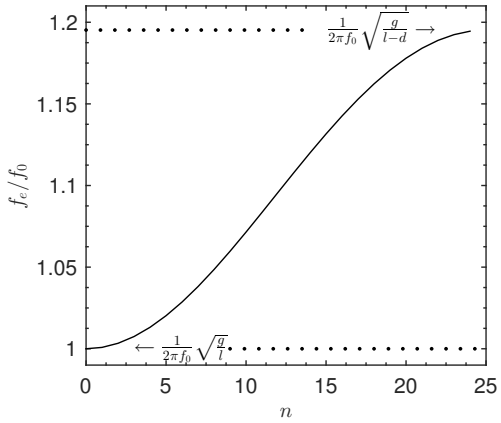

Figure 4.8: Dispersion relation for the coupled pendulum chain.the frequency axis is normalized to the minimum frequency. The minimum frequency at $f_0 = 3.1Hz$ the cut-off frequency at $f_c = 3.7Hz$

As shown in Fig. 4.7,b, which illustrates the chain viewed from the top, the ring of oscillators is equivalent to an equatorial section of a bubble with equilibrium radius R_0,

$$R_i(t) = R_0 + L\sin\Theta_i(t), \tag{4.35}$$

where R_0 is the radius of the ring (equivalent to the equilibrium radius of the bubble). Assuming small angles $\sin\Theta_i \simeq \Theta_i$, the position of each pendulum at a time t can be given by $R_i(t) = R_0 + L\Theta_i(t)$.

4.3.2. CONTINUOUS DESCRIPTION

The bubble surface is a continuum, while the chain of pendula is a discrete system. Therefore, analogies must be searched in the limit where a continuum version of Eq. (4.32) applies. This is the case when we restrict our analysis to long-wavelength modes (low index n), where the mode scale are much larger than the distance between two pendula, $k_n a << 1$, or $na/R_0 << 1$. Considering this limit, the discrete angle coordinates $\Theta_i(t)$ can be replaced by the continuous function $\Theta(x,t)$.

The equation of motion Eq. (4.32) leads to the parametrically driven, small amplitude, sine–Gordon model, that reads

$$\ddot{\Theta} - c^2\Theta_{xx} + (\omega_0^2 + \eta\cos(\omega_e t))\Theta = 0 \tag{4.36}$$

where Θ is a surface deformation related to the bubble radius as $\Theta = (R - R_0)/L$.

Solutions of Eq. (4.36) can be expressed as a superposition of normal modes. For a linear (straight) chain, a proper basis is given by the harmonic functions

$$\Theta(x,t) = \sum_n b_n(t)\cos(k_n x). \tag{4.37}$$

Some solutions of Eq. (4.36) have been discussed for a one-dimensional straight geometry [158].

In the ring geometry considered here, angular coordinates are more suitable to describe the position of a point on the deformed ring, and we use the transformation $x = R\theta$, where $\theta = [0, 2\pi[$ and $R = R_0$ is the equilibrium radius. The Laplacian operator takes the form $\Theta_{xx} = R^{-2}\Theta_{\theta\theta}$. A proper basis for the expansion in this case is

$$\Theta(\theta,t) = \sum_n b_n(t)P_n(\cos\theta), \tag{4.38}$$

where $P_n(\cos\theta)$ is a Legendre polynomial and θ is the angular coordinate.

The equation for the temporal evolution of the mode amplitudes can be obtained by substituting Eq. (4.37) or Eq. (4.38) into Eq. (4.36) and projecting over the different modes (Galerkin projection) using the orthogonality properties of harmonic functions or Legendre polynomials. Independently of the basis chosen for the expansion, the following equation is obtained

$$\ddot{b}_n + \left(\omega_n^2 + \eta\cos(\omega_e t)\right) b_n = 0, \tag{4.39}$$

which is a Mathieu equation, where the parametric excitation amplitude is $\eta = \frac{4\omega_e^2 h_e}{L}$ and the frequency on the n-th mode is given by

$$\omega_n^2 = \omega_0^2 + c^2\frac{n^2}{R_0^2}. \tag{4.40}$$

The same result is obtained from the exact dispersion relation Eq. (4.34) for the discrete system, evaluated in the limit of low index n, where $na/R_0 << 1$.

4.3.3. ANALOGY

In this chapter, the analogy between the ultrasound driven gas bubble and the ring of coupled pendula subjected to a time-dependent acceleration is considered at different levels. One first level is just descriptive, where the mechanical analogue behaves similarly to the microbubble surface under an ultrasound field. The vertical forcing is equivalent to the ultrasound pressure field, in the sense that it excites parametrically the motion, and the chain of pendula play the role of the surface of the bubble, coupling represents surface tension, and so on. In a second level of analogy, we have shown show that in both cases the product

f R_0 can be chosen to be of the same order (the product is fixed for a gas microbubble, given by the Minnaert formula, however in the mechanical analogue the radius of the bubble can be chosen independently of the resonant frequency, which depends on the length of the pendula). So at this level the analogy become quantitative. The ring of pendula in this work, with $R_0 \simeq 0.3$ m, was designed to be excited in the Hz frequency range. The third, and deeper level of analogy is based on the demonstration that the dynamics of both systems is described by the same Mathieu equation, whose coefficients depend on the specific system and can be obtained analytically in simple form. Such coefficients are listed in table 4.1, which is the main result of this work. Once the connections between the parameters in both systems are established, experimental investigation with the macroscopic analogue may result in insight of new phenomena in acoustically driven bubbles.

Table 4.1: Table of analogies between parameters of microbubble and those of the pendula ring.

Parameter	Microbubble	Pendula ring
R_0 [m]	$\simeq 10^{-6}$	$\simeq 0.3$
f_e [s^{-1}]	$\simeq 10^6$	$\simeq 3$
$f_e R_0$ [m s^{-1}]	$\mathcal{O}(1)$	$\mathcal{O}(1)$
ω_n^2 [s^{-2}]	$(n-1)(n+1)(n+2)\frac{\sigma}{\rho R_0^3}$	$\frac{g}{L}+n^2\frac{c}{R_0^2}$
η [s^{-2}]	$\frac{(2n+1)}{2}\omega_e^2\left(\frac{R_\varepsilon}{R_0}\right)$	$4\omega_e^2\left(\frac{h_e}{L}\right)$

4.4. EXPERIMENTS

4.4.1. EXPERIMENTAL SETUP

The setup consists of an aluminum ring, on which pendula of mass $m = 6$ g are fixed with nylon strings forming a "V" shape with the vertical axis as shown in Fig. 4.7,a. The coupling between pendula is obtained by overlapping the strings and fixing them by a knot [155]. The parameter with a stronger influence on the dynamics of the chain is the coupling strength. Here, we focus on a ring with a medium coupling. The ring has a radius $R = 31$ cm, $N = 54$ pendula, pendulum's length is $L = 10$ cm and the distance between the ring and the node is $d = 5$ cm. As Fig. 4.9 shows, the pendula ring lies on the excitation system. The mechanical excitation system consists of a subwoofer loudspeaker driven by an arbitrary waveform generator (Agilent33220A) through an audio amplifier. Thus, the pendula ring is attached to the subwoofer cone and therefore is excited mechanically by a vertical oscillatory force, as shown in Fig. 4.9. The sinusoidal excitation varies from $f_e = 0$ to 5 Hz with amplitudes varying from $A = 0.5$ to 3.5 V_{pp}, corre-

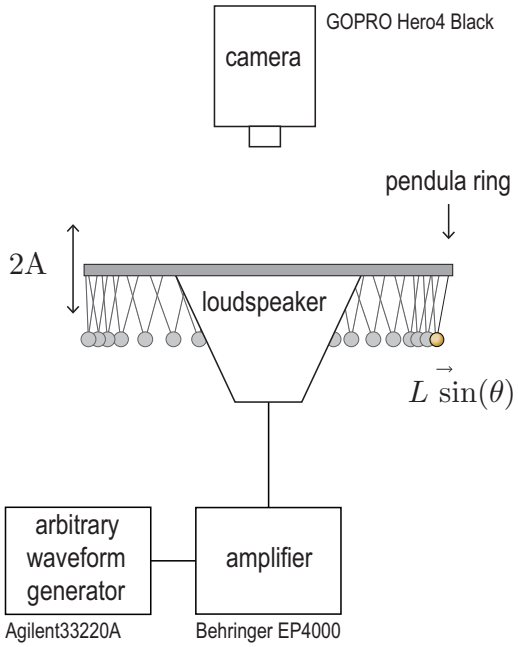

Figure 4.9: Scheme of the experimental setup. The ring of coupled pendula is driven vertically by an sinusoidal force generated by a loudspeaker.

sponding to a vertical displacements ranging from $h_e = 0.5$ mm to 3.5 mm. The pendula are driven near the volumetric resonant frequency and its double to allow the development of surface modes during the mechanical excitation through parametric instability.

The motion of pendula has been recorded from the top with a video camera. The data processing has been performed with the software Image J and the plug-in MJ Track. This plug-in enable to track the motion of each pendulum and thus to determine the distance $R_i(t)$ between the center of the ring and a pendulum at a fixed time t. Applying a spatial fast Fourier transform on $R_i(t)$, the amplitude of each vibration mode of order n can be obtained.

4.4.2. CALIBRATION

Before any process of recording, we have to convert the camera parameters to the real world. The calibration process is done to get all the parameters needed to know the effects of a camera projection. In general the intrinsic parameters are the focal length, image sensor format and the principal point. The focal length is the distance between the center of the image and the main point, the image

sensor format of a digital camera is to determine the angle of view of a particular lens when used with a particular camera and the principal points are the points where the principal planes cross the optical axis [159].

Extrinsic parameters which denote the coordinate system transformations from 3D space coordinates to 3D camera coordinates. Equivalently, the extrinsic parameters define the position of the camera center and the camera's heading in space coordinates.

There are various techniques for camera calibration. They can be classified into two categories: photogrammetric calibration [160, 161] and self-calibration[162, 163]. 1) Photogrammetric calibration. This is done by observing patterns whose geometry in three-dimensional space is known with a good level of accuracy. Calibration standards are typically positioned in two or three orthogonal planes between them. This type of calibration requires an elaborate setup, but its results are efficient. 2) Self-calibration, the method is based on the movement of the camera observing a static scene from traveling and using only the image information. The rigidity of the scene generally imposes restrictions on camera parameters. Three images taken by the same camera with fixed intrinsic parameters are sufficient for both extrinsic and intrinsic parameters [159].

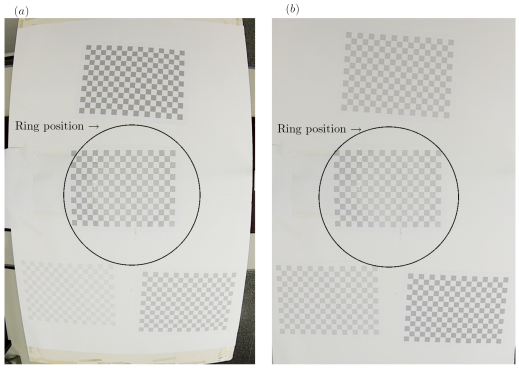

Figure 4.10: The view of the camera during the calibration. Each position of the checkerboard has been recorded in a different video. (a) The captured image with positive radial distortion "Barrel Distortion" (b) Undistorted image after the calibration

The calibration process can generally be divided into two main steps: the first one, is detection of the points of interest in sample images (the corners of checkerboard, in this case) and the second process is estimation of parameters from the detected points (extrinsic and intrinsic parameters of the camera).

CHECKERBOARD DETECTION

We used *Matlab 2015a-MathWorks* in all numerical process especially the calibration toolbox `cameraCalibrator`. This toolbox is used to detect and locate the checkerboard calibration pattern including corner detection with subpixel accuracy. We Estimate all intrinsic and extrinsic parameters including axis skew, calculate radial and tangential lens distortion coefficients, correct the optical distortion. This toolbox also support single camera and stereo calibration.

To start the calibration we have to prepare checkerboard with specific dimensions as shown in Fig.4.10. In our case, the checkerboard is formed by $19x13$ squares each one with length 2 cm. we recorded 50 videos 100fps in different positions Fig. 4.10 for the checkerboard with resolution $1920x1080$. This resolution is enough to track all pendulums (which are very small) without loosing any information.

From `cameraCalibrator` one can load all the calibration images. Notice that at some point in the process are asked about the width of one square of the board and you can choose it in mm or $Pixel$. After processing each image, it will show the overlapping detected corners on the concrete image. If all went well, you should observe all corners; otherwise, it may happen that you have not indicated the end corners with sufficient precision or because there is too much distortion in the image or the number of image is not enough to cover all the area of interest.

Once you extract all corners, now *Matlab* is ready to calibrate the camera. After a series of calculations, the result of the calibration parameters should appear with value of *Focal Length, Distortion, Errors in pixel....etc*. Fig.4.11 shows the corners detection of the checkerboard, the upper row representing the distorted images and the lower part represent the images after calibration.

ERROR ANALYSES

From *Error Analyses*, we obtain a window on which display projection errors and the projection model that you have estimated. Each Image has different error value. The Pixel error calibration information section shown above corresponds to the average of the errors in X and Y displayed in this window. On the other hand, *Matlab* shows you the original calibration images with the detected corners and predicted by the geometric model projection.

4.4.3. BREATHING MODE

We first consider the breathing mode, or the vibration mode of the system with $n = 1$, predicted by the most simple bubble modes. In most applications the bubble is assumed to oscillate in this pattern. In the numerical simulations the

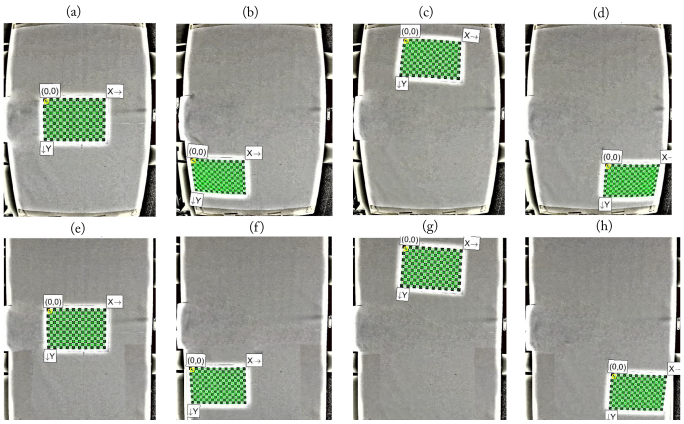

Figure 4.11: Detection of corners of the checkerboard.(a,b,c,d)the images before the calibration process. (e,f,g,h) The images after the calibration process. as you can see the $fish-aye$ has been removed.

breathing mode appears at $f_e/f_0 = 1.08Hz$, and for the experiment at $f_e/f_0 = 1.07$.

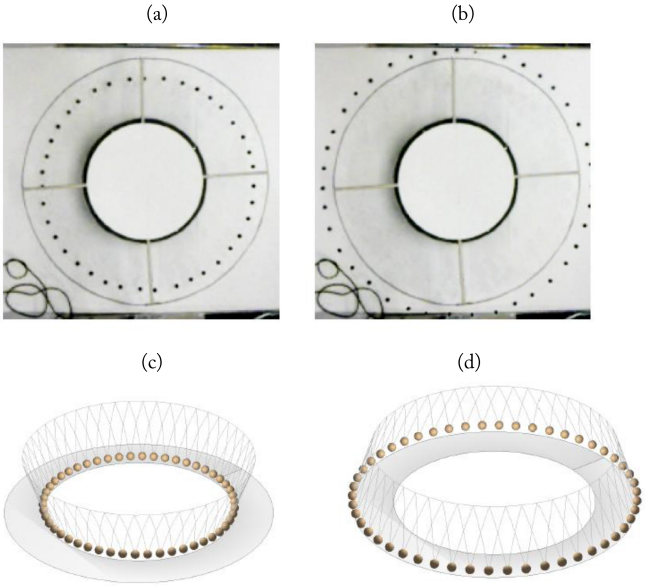

Figure 4.12: (a,b)The experimental results, and numerical simulations (c), (d),results for the breathing mode $n = 1$ of the ring of coupled pendulums

In the next section we report on the main subject of this work, the non-spherical oscillations of the bubble.

4.4.4. SHAPE OSCILLATIONS IN THE MACROBUBBLE

A set of measurements has been carried out for excitation amplitudes between $h_e = 0.5$ and 3.5 mm and frequencies varying from $f_e = 0$ to 5 Hz. Vibration modes have been observed up to $n = 22$, including an unstable volumetric mode for $n = 0$. The mode $n = 1$ corresponding to the displacement of the center of mass has also been observed. An example of the observed patterns is given in Fig. 4.13 for an excitation amplitude $h_e = 2$ mm and frequency $f_e = 3.20$ Hz. Here, the pendula ring shows a mode $n = 3$. A fit to the corresponding Legendre polynomial, shown in continuous line, shows a good agreement.

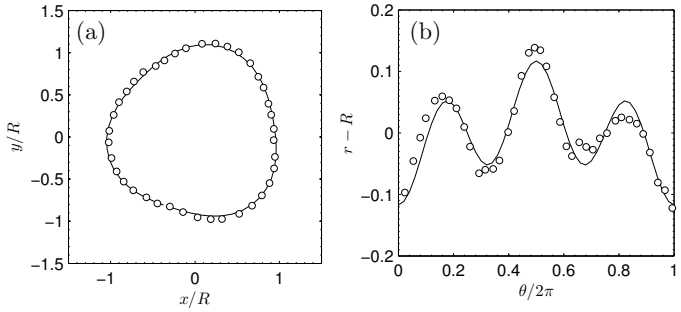

Figure 4.13: Experimental mode $n = 3$ (symbols) and the corresponding fit to a Legendre polynomial $P_3(\cos\theta)$. Two different representations, in cartesian coordinates (a) and in polar coordinates (b).

To compare with the experimental results, Eq. (4.32) has been integrated numerically by an explicit central finite differences scheme, with a temporal step $\Delta t = (2\pi/\omega_0)1000$. A set of solutions were simulated for amplitudes ranging from $h_e = 0$ to 3.5 mm and excitation frequency ranging from $\omega_e = 0.5$ to $3\omega_0$ rad/s. The amplitudes of the vibration modes were evaluated by a spatial Fast Fourier Transform of each numerical solution. A phase diagram showing the domain of existence of vibration modes n for different excitation parameters is presented in Fig. 4.14. The numerical simulation of Eq. (4.32) evidences the existence of different sets of resonances. Due to the damping, there exist a threshold for the excitation of the different modes. The lowest threshold is obtained for the so-called $\frac{p}{q} = 2:1$, (p, q integers) or subharmonic resonance, where the frequency of the excitation is twice the natural frequency of the pendulum. Within each resonance set, each mode has its own instability region, or Arnold tongues, which

are represented in Fig. 4.14 with a different color for each mode. The dark red shaded region corresponds to numerically unstable solutions. Note also the existence of a second set at lower frequencies, with a higher threshold, denoting the 1:1 resonance, that corresponds to modes excited when driving the system at the natural frequency of the pendulum $f_0 = \sqrt{(g/L)} \approx 1.6$ Hz. The symbols in Fig. 4.14 correspond to experimental data. From red to blue, the mode number increases, similarly to the numerical results. No vibration modes are observed at frequencies below $f_e/f_0 = 0.95$, as there are no unstability regions predicted by the theory. From $f_e/f_0 = 0.95$ to 1.90, a first group of vibration modes appears when the excitation amplitude is greater than a threshold. These modes oscillate at a frequency equal to the excitation frequency ($f_{\text{osc}} = f_e$), and correspond to the $\frac{p}{q} = 1:1$ parametric resonance of the system. From $f_e/f_0 = 1.90$ to $f_e/f_0 = 3.17$, a second group of vibration modes oscillating at subharmonics of the excitation frequency ($2f_{\text{osc}} = f_e$) is observed, corresponding to the 2:1 resonance. Therefore, two sets of resonance modes have been observed. Comparing the trend of simulation and experimental data shown in Fig. 4.14, we can conclude that there exists a good agreement.

It is important to note that pure modes exist only in a narrow region. Close to the parametric instability threshold, the Arnold tongues corresponding to each mode n overlap. Thus, most of the modes observed actually correspond to a mixing of neighboring modes, with one mode being clearly dominant. Mode mixing is therefore expected to occur also in ultrasound-driven bubbles; however, such mode mixing has been postulated but not analyzed or observed in such microbubbles. The mechanical analog presented here could be used to explore these complex phenomena.

The numerical simulation of Eq.(4.32) presents in Fig.4.15 which present the pure oscillating mode for $n = 6$ and the spectrum shows that the chain oscillate in same mode we observed. Also the same figure presents the mixed mode state, observe of the slightly higher amplitude which means that the bubble oscillate in a combination of modes $n = 7$ till $n = 14$.

Finally, we note that the maximum excitation has been measured at $f_e = 5$ Hz ($f/f_0 = 3.2$). Above this frequency, measurements cannot be performed due to the setup vulnerability. Oscillations becomes jerky and the coupling between pendula often breaks.

It is interesting to compare our results with the observations done in an experiment with ultrasound-driven microbubbles, shown in Fig. 4.16. There, the variable parameter is not the frequency but the radius of the bubble (which are inversely related as follows from the Minnaert formula). Note the two sets of modes, corresponding to the 1:1 and 2:1 parametric resonances.

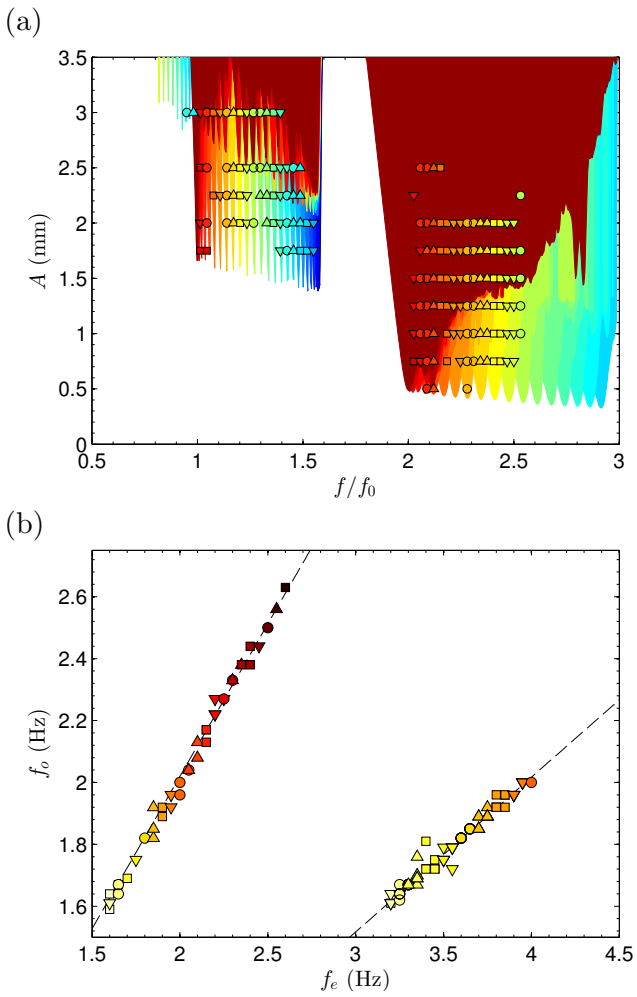

Figure 4.14: (a) Phase diagram showing the appearance of vibration modes for different excitation parameters. The symbols correspond to the experimental data whereas the colored areas are the instability regions obtained numerically. (b) Oscillation frequencies of the pendulum (denoted by f_0) versus the excitation frequency (f_e). On both graphics, each symbol corresponds to a vibration mode.

4.5. CONCLUSIONS

The interaction between a microbubble and an acoustical field has been studied through the use of a macroscopic acousto-mechanical analogy. As for real bubbles, vibration modes and modes mixing have been observed. It is known that, in the case of microbubbles, vibration modes display a strong subharmonic be-

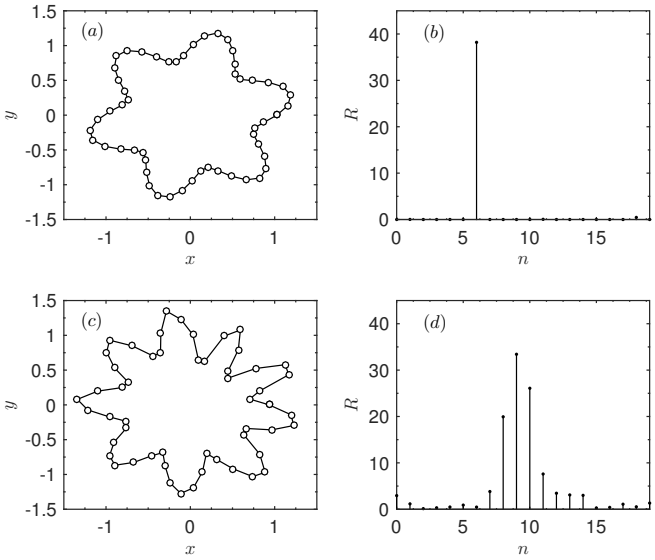

Figure 4.15: numerical simulation for Eq.(4.32) (a)Linear behavior : The radius of the bubble with mode $n = 6$. (b) signal spectrum of (a) where $y - axis$ is the number of modes. (c) Nonlinear behavior: mixed modes. (d) is the spectrum of (c)

havior. Here, with the pendula ring, vibration modes have also been excited in the region where $f_{\text{osc}} = f_e$, corresponding to a $\frac{p}{q} = 1:1$ resonance, p, q integer.

Localized modes like breather have not been discussed here but a previous study on the pendula ring shows the appearance of such modes [164, 165]. One can thus expect to observe these oscillatory behaviors in microbubbles. These results allow to offer new insights in the study of microbubble's dynamics. The analogy between the macroscopic behavior of the pendula ring and the microscopic behavior of a microbubble presented here is valid for low order modes (i.e. in the limit $na/R_0 \ll 1$) and provides important insights for the comprehension of microbubble dynamics. Further studies are underway, particularly an expansion of the analogy to consider encapsulated microbubbles to get information for both imaging and therapeutic applications using contrast microbubbles.

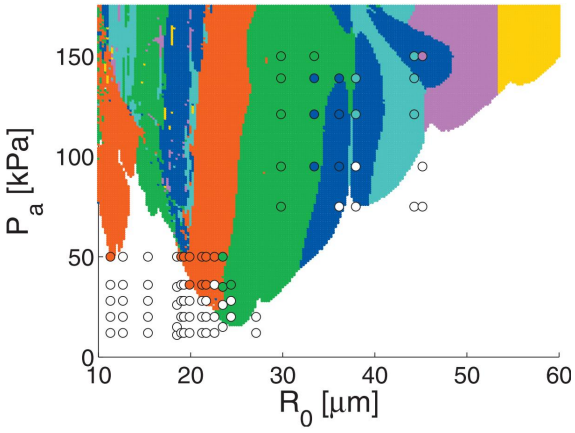

Figure 4.16: Versluis et al [151]. (Color) Phase diagram in R_0 and P_a space for the driving frequency of $f = 130kHz$. Every experimental data point is included as a circle: (white) no shape mode detected, (red) mode 2, (green) mode 3, (blue) mode 4, (turquoise) mode 5, (magenta) mode 6, and (yellow) mode 7. For comparison, also the theoretical result is shown. The color coding indicates the specific mode preference and corresponds to the coding used for the experimental data.

BIBLIOGRAPHY

[1] B. O. Enflo and C. M. Hedberg, *Theory of nonlinear acoustics in fluids*, Vol. 67 (Springer Science & Business Media, 2006).

[2] B. O. Enflo and C. M. Hedberg, *Physical theory of nonlinear acoustics*, Theory of Nonlinear Acoustics in Fluids (2002).

[3] J. T. Cannon and S. Dostrovsky, *The Evolution of Dynamics: Vibration Theory from 1687 to 1742: Vibration Theory from 1687 to 1742*, Vol. 6 (Springer Science & Business Media, 2012).

[4] W. M. Rankine, *On the thermodynamic theory of waves of finite longitudinal disturbance,* Philosophical Transactions of the Royal Society of London (1870).

[5] H. Hugoniot, *Sur la propagation du movement dans les corps et spécialement dans les gaz parfaits,* J. Ecole Polytechnique **58** (1889).

[6] S. K. Chakrabarti, *Standing rankine-hugoniot shocks in the hybrid model flows of the black hole accretion and winds,* The Astrophysical Journal **347**, 365 (1989).

[7] J. M. Burgers, *A mathematical model illustrating the theory of turbulence,* Advances in applied mechanics **1** (1948).

[8] A. Rozanova, *The khokhlov–zabolotskaya–kuznetsov equation,* Comptes Rendus Mathematique **344** (2007).

[9] M. Abramowitz, I. A. Stegun, *et al.*, *Handbook of mathematical functions with formulas, graphs, and mathematical tables,* (1972).

[10] M. F. Hamilton, D. T. Blackstock, *et al.*, *Nonlinear acoustics*, Vol. 427 (Academic press San Diego, 1998).

[11] M. Remoissenet, *Waves called solitons: concepts and experiments* (Springer Science & Business Media, 2013).

[12] R. M. Keolian, *Wave turbulence and soliton dynamics*, Tech. Rep. (DTIC Document, 1992).

[13] M. Molerón, A. Leonard, and C. Daraio, *Solitary waves in a chain of repelling magnets,* Journal of Applied Physics **115**, 184901 (2014).

[14] Y. A. Kosevich, *Nonlinear sinusoidal waves and their superposition in anharmonic lattices,* Physical review letters **71**, 2058 (1993).

[15] M. Peyrard, S. Pnevmatikos, and N. Flytzanis, *Discreteness effects on nontopological kink soliton dynamics in nonlinear lattices,* Physica D: Nonlinear Phenomena **19**, 268 (1986).

[16] A. Savin, Y. Zolotaryuk, and J. Eilbeck, *Moving kinks and nanopterons in the nonlinear klein–gordon lattice,* Physica D: Nonlinear Phenomena **138**, 267 (2000).

[17] S. Pnevmatikos, N. Flytzanis, and M. Remoissenet, *Soliton dynamics of nonlinear diatomic lattices,* Phys. Rev. B **33**, 2308 (1986).

[18] F. Melde, *On the excitation of standing waves on a string,* Ann. Phys. Chem **109**, 193 (1859).

[19] L. Rayleigh, *Xvii. on the maintenance of vibrations by forces of double frequency, and on the propagation of waves through a medium endowed with a periodic structure,* The London, Edinburgh, and Dublin Philosophical Magazine and Journal of Science **24**, 145 (1887).

[20] P. J. Dallos and C. O. Linnell, *Even-order subharmonics in the peripheral auditory system,* The Journal of the Acoustical Society of America **40**, 561 (1966).

[21] P. J. Dallos and C. O. Linnell, *Subharmonic components in cochlear-microphonic potentials,* The Journal of the Acoustical Society of America **40**, 4 (1966).

[22] P. J. Dallos, *On the generation of odd-fractional subharmonics,* The Journal of the Acoustical Society of America **40**, 1381 (1966).

[23] M. Luukkala, *Threshold and oscillation of fractional phonons,* Physics Letters A **25**, 197 (1967).

[24] M. Luukkala, *Fine structure of fractional harmonic phonons,* Physics Letters A **25**, 76 (1967).

[25] D. A. Hutchins, J. Yang, O. Akanji, P. J. Thomas, L. A. Davis, S. Freear, S. Harput, N. Saffari, and P. Gelat, *Ultrasonic propagation in finite-length granular chains,* Ultrasonics **69**, 215 (2016).

[26] C. Kittel, *Introduction to solid state physics. wiley eastern,* (1994).

[27] M. Raizen, J. Gilligan, J. Bergquist, W. Itano, and D. Wineland, *Ionic crystals in a linear paul trap,* Physical Review A **45**, 6493 (1992).

[28] D. Porras, F. Marquardt, J. Von Delft, and J. I. Cirac, *Mesoscopic spin-boson models of trapped ions,* Physical Review A **78**, 010101 (2008).

[29] K. A. Matveev, A. V. Andreev, and M. Pustilnik, *Equilibration of a one-dimensional wigner crystal,* Phys. Rev. Lett. **105**, 046401 (2010).

[30] V. V. Deshpande and M. Bockrath, *The one-dimensional wigner crystal in carbon nanotubes,* Nat. Phys. **4**, 314 (2008).

[31] A. Homann, A. Melzer, S. Peters, and A. Piel, *Determination of the dust screening length by laser-excited lattice waves,* Physical Review E **56**, 7138 (1997).

[32] K. Avinash, P. Zhu, V. Nosenko, and J. Goree, *Nonlinear compressional waves in a two-dimensional yukawa lattice,* Physical Review E **68**, 046402 (2003).

[33] V. Nosenko, K. Avinash, J. Goree, and B. Liu, *Nonlinear interaction of compressional waves in a 2d dusty plasma crystal,* Physical review letters **92**, 085001 (2004).

[34] B. Denardo and S. Putterman, *Theory of nonlinear standing waves in a two-dimensional system of charged particles,* Physical Review B **37**, 3720 (1988).

[35] F. Russell, Y. Zolotaryuk, J. Eilbeck, and T. Dauxois, *Moving breathers in a chain of magnetic pendulums,* Physical Review B **55**, 6304 (1997).

[36] J. F. Archilla, Y. A. Kosevich, N. Jiménez, V. J. Sánchez-Morcillo, and L. M. García-Raffi, *Ultradiscrete kinks with supersonic speed in a layered crystal with realistic potentials,* Physical Review E **91**, 022912 (2015).

[37] V. Sánchez-Morcillo, I. Pérez-Arjona, V. Romero-García, V. Tournat, and V. Gusev, *Second-harmonic generation for dispersive elastic waves in a discrete granular chain,* Physical Review E **88**, 043203 (2013).

[38] J. Frenkel, *Kontorova, t.* J. Phys. USSR **1939**, 1 (1939).

[39] Y. Matsuno, *Exact solutions for the nonlinear klein–gordon and liouville equations in four-dimensional euclidean space,* Journal of mathematical physics **28**, 2317 (1987).

[40] Q. Meng, L. Wu, D. O. Welch, and Y. Zhu, *Lattice vibrations in the frenkel-kontorova model. i. phonon dispersion, number density, and energy,* Physical Review B **91**, 224305 (2015).

[41] F. Frank and J. H. van der Merwe, *One-dimensional dislocations. i. static theory,* in *Proceedings of the Royal Society of London A: Mathematical, Physical and Engineering Sciences*, Vol. 198 (The Royal Society, 1949) pp. 205–216.

[42] M. Chinn and S. C. Fain Jr, *Structural phase transition in epitaxial solid krypton monolayers on graphite,* Physical Review Letters **39**, 146 (1977).

[43] L. M. Floría and J. J. Mazo, *Dissipative dynamics of the frenkel-kontorova model,* Advances in Physics **45**, 505 (1996).

[44] J. Sokoloff, *Sliding charge-density waves in periodic and disordered lattices,* Physical Review B **16**, 3367 (1977).

[45] O. M. Braun and Y. S. Kivshar, *Nonlinear dynamics of the frenkel–kontorova model,* Physics Reports **306**, 1 (1998).

[46] E. Fermi, J. Pasta, and S. Ulam, *Studies of nonlinear problems,* Los Alamos Report LA-1940 **978** (1955).

[47] N. J. Zabusky and M. D. Kruskal, *Interaction of" solitons" in a collisionless plasma and the recurrence of initial states,* Physical review letters **15**, 240 (1965).

[48] D. Bambusi and A. Ponno, *On metastability in fpu,* Communications in mathematical physics **264**, 539 (2006).

[49] G. Zaslavskii, *Stochastic instability of nonlinear oscillations,* Journal of Applied Mechanics and Technical Physics **8**, 8 (1967).

[50] C. Driscoll and T. O'Neil, *Explanation of instabilities observed on a fermi-pasta-ulam lattice,* Physical Review Letters **37**, 69 (1976).

[51] A. Cella, M. Lucchesi, and G. Pasquinelli, *Space–time elements for the shock wave propagation problem,* International Journal for Numerical Methods in Engineering **15**, 1475 (1980).

[52] R. Livi, M. Pettini, S. Ruffo, M. Sparpaglione, and A. Vulpiani, *Equipartition threshold in nonlinear large hamiltonian systems: The fermi-pasta-ulam model,* Physical Review A **31**, 1039 (1985).

[53] T. R. Taha and M. I. Ablowitz, *Analytical and numerical aspects of certain nonlinear evolution equations. ii. numerical, nonlinear schrödinger equation,* Journal of Computational Physics **55**, 203 (1984).

[54] T. P. Weissert, *The genesis of simulation in dynamics: pursuing the Fermi-Pasta-Ulam problem* (Springer Science & Business Media, 2012).

[55] G. Berman and F. Izrailev, *The fermi–pasta–ulam problem: fifty years of progress,* Chaos: An Interdisciplinary Journal of Nonlinear Science **15**, 015104 (2005).

[56] G. Gallavotti, *The Fermi-Pasta-Ulam Problem* (Springer, 2008).

[57] K. Naugolnykh and L. Ostrovsky, *Nonlinear wave processes in acoustics* (Cambridge University Press, 1998).

[58] D. Griffiths, *Introduction to Electrodynamics (3rd ed.)* (Prentice Hall, 2007).

[59] J. M. Camacho and V. Sosa, *Alternative method to calculate the magnetic field of permanent magnets with azimuthal symmetry,* Rev. Mex. Fis. **59**, 8 (2013).

[60] J. H. Cantrell and W. T. Yost, *Acoustic nonlinearity in dispersive solids,* in *Review of Progress in Quantitative Nondestructive Evaluation* (Springer, 1991) pp. 1805–1811.

[61] J. H. Cantrell, *Anharmonic properties of solids from measurements of the stress acoustic constant,* J. Test. Eval. **x**, 223 (1982).

[62] A. Korpel and R. Adler, *Parametric phenomena observed on ultrasonic waves in water,* Applied Physics Letters **7**, 106 (1965).

[63] J. A. Bamberg and B. D. Cook, *Subharmonic generation in an acoustic interferometer,* The Journal of the Acoustical Society of America **41**, 1584 (1967).

[64] L. Adler and M. Breazeale, *Generation of fractional harmonics in a resonant ultrasonic wave system,* The Journal of the Acoustical Society of America **48**, 1077 (1970).

[65] L. Adler, W. T. Yost, and J. H. Cantrell, *Subharmonics, chaos, and beyond,* (2011).

[66] T. B. Benjamin and J. Feir, *The disintegration of wave trains on deep water part 1. theory,* Journal of Fluid Mechanics **27**, 417 (1967).

[67] T. B. Benjamin and K. Hasselmann, *Instability of periodic wavetrains in nonlinear dispersive systems [and discussion],* in *Proceedings of the Royal Society of London A: Mathematical, Physical and Engineering Sciences*, Vol. 299 (The Royal Society, 1967) pp. 59–76.

[68] H. C. Yuen and B. M. Lake, *Instabilities of waves on deep water,* Annual Review of Fluid Mechanics **12**, 303 (1980).

[69] Y. S. Kivshar and M. Peyrard, *Modulational instabilities in discrete lattices,* Physical Review A **46**, 3198 (1992).

[70] Z. Rapti, P. Kevrekidis, A. Smerzi, and A. Bishop, *Parametric and modulational instabilities of the discrete nonlinear schrödinger equation,* Journal of Physics B: Atomic, Molecular and Optical Physics **37**, S257 (2004).

[71] V. E. Zakharov and L. Ostrovsky, *Modulation instability: the beginning,* Physica D: Nonlinear Phenomena **238**, 540 (2009).

[72] D. J. Korteweg and G. De Vries, *Xli. on the change of form of long waves advancing in a rectangular canal, and on a new type of long stationary waves,* The London, Edinburgh, and Dublin Philosophical Magazine and Journal of Science **39**, 422 (1895).

[73] W. Malfliet and W. Hereman, *The tanh method: I. exact solutions of nonlinear evolution and wave equations,* Physica Scripta **54**, 563 (1996).

[74] C. S. Gardner, J. M. Greene, M. D. Kruskal, and R. M. Miura, *Korteweg-devries equation and generalizations. vi. methods for exact solution,* Communications on pure and applied mathematics **27**, 97 (1974).

[75] W. Królikowski and S. A. Holmstrom, *Fusion and birth of spatial solitons upon collision,* Optics letters **22**, 369 (1997).

[76] G. I. Stegeman and M. Segev, *Optical spatial solitons and their interactions: universality and diversity,* Science **286**, 1518 (1999).

[77] J. Drohm, L. Kok, Y. A. Simonov, J. Tjon, and A. Veselov, *Collision and rotation of solitons in three space-time dimensions,* Physics Letters B **101**, 204 (1981).

[78] J. L. Bredas and G. B. Street, *Polarons, bipolarons, and solitons in conducting polymers,* Accounts of Chemical Research **18**, 309 (1985).

[79] A. Sen, *String-string duality conjecture in six dimensions and charged solitonic strings,* Nuclear Physics B **450**, 103 (1995).

[80] Z. H. Musslimani, M. Segev, D. N. Christodoulides, and M. Soljačić, *Composite multihump vector solitons carrying topological charge,* Physical review letters **84**, 1164 (2000).

[81] M. Onoda, Y. Kato, H. Shonaka, and K. Tada, *Artificial muscle using conducting polymers,* Electrical Engineering in Japan **149**, 7 (2004).

[82] A. Hasegawa and Y. Kodama, *Solitons in optical communications*, 7 (Oxford University Press, USA, 1995).

[83] J. P. Gordon and H. A. Haus, *Random walk of coherently amplified solitons in optical fiber transmission,* Optics letters **11**, 665 (1986).

[84] N. Zabusky and C. Galvin, *Shallow-water waves, the korteweg-devries equation and solitons,* Journal of Fluid Mechanics **47**, 811 (1971).

[85] A. Constantin and J. Escher, *Wave breaking for nonlinear nonlocal shallow water equations,* Acta Mathematica **181**, 229 (1998).

[86] M. D. Kruskal and N. J. Zabusky, *Exact invariants for a class of nonlinear wave equations,* Journal of Mathematical Physics **7**, 1256 (1966).

[87] M. A. Porter, N. J. Zabusky, B. Hu, and D. K. Campbell, *Fermi, pasta, ulam and the birth of experimental mathematics a numerical experiment that enrico fermi, john pasta, and stanislaw ulam reported 54 years ago continues to inspire discovery,* American Scientist **97**, 214 (2009).

[88] M. Toda, *Vibration of a chain with nonlinear interaction,* Journal of the Physical Society of Japan **22**, 431 (1967).

[89] N. Zabusky, M. Kruskal, and G. Deem, *Formation, propagation, and interaction of solitons (numerical solutions of differential equations describing wave motion in nonlinear dispersive media),* This film was conceived and produced at the Bell Telephone Laboratories, Whippany, New Jersey, during (1965).

[90] Y. A. Kosevich, R. Khomeriki, and S. Ruffo, *Supersonic discrete kink-solitons and sinusoidal patterns with "magic" wave number in anharmonic lattices,* EPL (Europhysics Letters) **66**, 21 (2004).

[91] O. Braun, Y. S. Kivshar, and I. Zelenskaya, *Kinks in the frenkel-kontorova model with long-range interparticle interactions,* Physical Review B **41**, 7118 (1990).

[92] G. Friesecke and K. Matthies, *Atomic-scale localization of high-energy solitary waves on lattices,* Physica D: Nonlinear Phenomena **171**, 211 (2002).

[93] J. F. Archilla, N. Jimenez, V. J. Sánchez Morcillo, L. García-Raffi, *et al.*, *Moving excitations in cation lattices,* in *Ukrainian Journal of Physics*, Vol. 58 (Department of Physics and Astronomy of the National Academy of Sciences of Ukraine, 2013) pp. 646–656.

[94] S. Takeno, K. Kisoda, and A. Sievers, *Intrinsic localized vibrational modes in anharmonic crystals stationary modes,* Progress of Theoretical Physics Supplement **94**, 242 (1988).

[95] E. Yablonovitch, *Inhibited spontaneous emission in solid-state physics and electronics,* Physical review letters **58** (1987).

[96] V. Romero García, *On the control of propagating acoustic waves in sonic crystals: analytical, numerical and optimization techniques,* (2010).

[97] V. J. Sánchez-Morcillo, I. Pérez-Arjona, V. Romero-García, V. Tournat, and V. Gusev, *Second-harmonic generation for dispersive elastic waves in a discrete granular chain,* Physical Review E **88** (2013).

[98] Y. Yun, G. Miao, P. Zhang, K. Huang, and R. Wei, *Nonlinear acoustic wave propagating in one-dimensional layered system,* Physics Letters A **343** (2005).

[99] D. H. Yong and R. J. LeVeque, *Solitary waves in layered nonlinear media,* SIAM Journal on Applied Mathematics **63** (2003).

[100] B. Liang, B. Yuan, and J.-c. Cheng, *Acoustic diode: rectification of acoustic energy flux in one-dimensional systems,* Physical review letters **103** (2009).

[101] A. M. Kosevich, *The crystal lattice: phonons, solitons, dislocations, superlattices* (John Wiley & Sons, 2006).

[102] K. Naugolnykh and L. Ostrovsky, *Nonlinear wave processes in acoustics* (Cambridge University Press, 1998).

[103] T. Kujawska, A. Nowicki, and P. A. Lewin, *Determination of nonlinear medium parameter b/a using model assisted variable-length measurement approach,* Ultrasonics **51**, 997 (2011).

[104] F. Bloom, *Some remarks on the growth behavior of one-dimensional shock waves in non-linear materials,* International Journal of Non-Linear Mechanics **9**, 147–157 (1974).

[105] X.-L. Wu and E. Ma, *Dislocations in nanocrystalline grains,* Appl. Phys. Lett. Applied Physics Letters **88**, 231911 (2006).

[106] V. Tournat, *Experimental study of nonlinear acoustic effects in unconsolidated granular materials,* AIP Conference Proceedings (2006), 10.1063/1.2210319.

[107] T. Kundu, *Ultrasonic nondestructive evaluation: engineering and biological material characterization* (CRC press, 2003).

[108] X.-f. Gong, Z.-m. Zhu, T. Shi, and J.-h. Huang, *Determination of the acoustic nonlinearity parameter in biological media using fais and itd methods,* The Journal of the Acoustical Society of America **86** (1989).

[109] M. F. Hamilton, D. T. Blackstock, *et al.*, *Nonlinear acoustics*, Vol. 427 (Academic press San Diego, 1998).

[110] A. A. Haigh, B. E. Treeby, and E. C. Mccreath, *Ultrasound simulation on the cell broadband engine using the westervelt equation,* Algorithms and Architectures for Parallel Processing Lecture Notes in Computer Science , 241–252 (2012).

[111] A. Karamalis, W. Wein, and N. Navab, *Fast ultrasound image simulation using the westervelt equation,* Medical Image Computing and Computer-Assisted Intervention – MICCAI 2010 Lecture Notes in Computer Science , 243–250 (2010).

[112] I. M. Hallaj and R. O. Cleveland, *Fdtd simulation of finite-amplitude pressure and temperature fields for biomedical ultrasound,* The Journal of the Acoustical Society of America **105** (1999), 10.1121/1.426776.

[113] J. l. R. d'ALEMBERT, *Reflexions sur la cause generale des vents...* (Chez David, 1747).

[114] A. D. Pierce *et al.*, *Acoustics: an introduction to its physical principles and applications*, Vol. 20 (McGraw-Hill New York, 1981).

[115] L. Rayleigh, *Viii. on the pressure developed in a liquid during the collapse of a spherical cavity,* The London, Edinburgh, and Dublin Philosophical Magazine and Journal of Science **34**, 94 (1917).

[116] M. Minnaert, *Xvi. on musical air-bubbles and the sounds of running water,* The London, Edinburgh, and Dublin Philosophical Magazine and Journal of Science **16**, 235 (1933).

[117] M. Plesset, *On the stability of fluid flows with spherical symmetry,* Journal of Applied Physics **25**, 96 (1954).

[118] E. Neppiras, *Subharmonic and other low-frequency emission from bubbles in sound-irradiated liquids,* The Journal of the Acoustical Society of America **46**, 587 (1969).

[119] A. I. Eller and L. A. Crum, *Instability of the motion of a pulsating bubble in a sound field,* The Journal of the Acoustical Society of America **47**, 762 (1970).

[120] A. Prosperetti, L. A. Crum, and K. W. Commander, *Nonlinear bubble dynamics,* The Journal of the Acoustical Society of America **83**, 502 (1988).

[121] D. F. Gaitan, L. A. Crum, C. C. Church, and R. A. Roy, *Sonoluminescence and bubble dynamics for a single, stable, cavitation bubble,* The Journal of the Acoustical Society of America **91**, 3166 (1992).

[122] M. P. Brenner, D. Lohse, and T. Dupont, *Bubble shape oscillations and the onset of sonoluminescence,* Physical review letters **75**, 954 (1995).

[123] F. Gaitan and G. Holt, *Nonlinear bubble dynamics and light emission in single-bubble sonoluminescence,* The Journal of the Acoustical Society of America **103**, 3046 (1998).

[124] U. H. Augsdörfer, A. K. Evans, and D. P. Oxley, *Thermal noise and the stability of single sonoluminescing bubbles,* Physical Review E **61**, 5278 (2000).

[125] J. Ophir and K. J. Parker, *Contrast agents in diagnostic ultrasound,* Ultrasound in medicine & biology **15**, 319 (1989).

[126] J.-M. Escoffre, A. Novell, A. Zeghimi, and A. Bouakaz, *Ultrasound and microbubbles for in vitro gene delivery,* Drug developpement and delivery **11** (2011).

[127] A. Novell, J.-M. Escoffre, and A. Bouakaz, *Ultrasound contrast imaging in cancer–technical aspects and prospects,* Current Molecular Imaging **2**, 77 (2013).

[128] S. Dos Santos, V. Sánchez-Morcillo, N. Jiménez, J. Chaline, and A. Bouakaz, *Modulational instability and localized modes for ultrasound contrast microbubbles surface oscillations,* in *2011 IEEE International Ultrasonics Symposium* (IEEE, 2011) pp. 648–651.

[129] S. Dos Santos, V. Sánchez-Morcillo, N. Jiménez, A.-P. Abellard, and A. Bouakaz, *Modulational instability of microbubbles surface modes,* in *INTERNATIONAL CONGRESS ON ULTRASONICS: Gdańsk 2011*, Vol. 1433 (AIP Publishing, 2012) pp. 311–314.

[130] R. Gramiak and P. M. Shah, *Echocardiography of the aortic root,* Investigative Radiology **3**, 356–366 (1968).

[131] H. Shekhar, J. J. Rychak, and M. M. Doyley, *Modifying the size distribution of microbubble contrast agents for high-frequency subharmonic imaging,* Med. Phys. Medical Physics **40**, 082903 (2013).

[132] E. Quaia, *Classification and safety of microbubble-based contrast agents,* Medical Radiology Contrast Media in Ultrasonography , 3–14.

[133] *microbubble imaging techniques,* Encyclopedia of Diagnostic Imaging , 1138–1138.

[134] K. Park, *Microbubble ultrasound-guided targeted delivery to tumors,* Journal of Controlled Release **157**, 167 (2012).

[135] J. Stassen, *In vitro and in vivo models to investigate clot lysis and thrombolysis,* New Therapeutic Agents In Thrombosis And Thrombolysis, Revised And Expanded (2002), 10.1201/9780203909317.ch40.

[136] B. E. Oeffinger and M. A. Wheatley, *Development and characterization of a nano-scale contrast agent,* Ultrasonics **42**, 343–347 (2004).

[137] F. E. Fox, *Gas bubbles with organic skin as cavitation nuclei,* The Journal of the Acoustical Society of America J. Acoust. Soc. Am. **26**, 984 (1954).

[138] N. D. Jong and L. Hoff, *Ultrasound scattering properties of albunex microspheres,* Ultrasonics **31**, 175–181 (1993).

[139] L. Hoff, P. C. Sontum, and J. M. Hovem, *Oscillations of polymeric microbubbles: Effect of the encapsulating shell,* The Journal of the Acoustical Society of America **107**, 2272 (2000).

[140] M. Haran, *A viscoelastic model of the interaction of ultrasound pulses with biological tissue,* Ultrasonic Imaging **6**, 240 (1984).

[141] P. Frinking and N. D. Jong, *Modeling of ultrasound contrast agents,* 1997 IEEE Ultrasonics Symposium Proceedings. An International Symposium (Cat. No.97CH36118) 10.1109/ultsym.1997.663302.

[142] B. E. Noltingk and E. A. Neppiras, *Cavitation produced by ultrasonics,* Proceedings of the Physical Society. Section B Proc. Phys. Soc. B **63**, 674–685 (1950).

[143] A. Papanastasiou, L. Scriven, and C. Macosko, *Bubble growth and collapse in viscoelastic liquids analyzed,* Journal of Non-Newtonian Fluid Mechanics **16**, 53–75 (1984).

[144] C. C. Church, *The effects of an elastic solid surface layer on the radial pulsations of gas bubbles,* The Journal of the Acoustical Society of America **97**, 1510 (1995).

[145] D. Chatterjee and K. Sarkar, *A newtonian rheological model for the interface of microbubble contrast agents,* Ultrasound in medicine & biology **29**, 1749 (2003).

[146] P. Marmottant, S. van der Meer, M. Emmer, M. Versluis, N. de Jong, S. Hilgenfeldt, and D. Lohse, *A model for large amplitude oscillations of coated bubbles accounting for buckling and rupture,* The Journal of the Acoustical Society of America **118**, 3499 (2005).

[147] M. Plesset, *On the stability of fluid flows with spherical symmetry,* Journal of Applied Physics **25**, 96 (1954).

[148] P. L. Marston and S. G. Goosby, *Ultrasonically stimulated low-frequency oscillation and breakup of immiscible liquid drops: Photographs,* Physics of Fluids (1958-1988) **28**, 1233 (1985).

[149] T. Lundgren and N. Mansour, *Oscillations of drops in zero gravity with weak viscous effects,* Journal of Fluid Mechanics **194**, 479 (1988).

[150] O. A. Basaran, *Nonlinear oscillations of viscous liquid drops,* Journal of Fluid Mechanics **241**, 169 (1992).

[151] M. Versluis, D. E. Goertz, P. Palanchon, I. L. Heitman, S. M. van der Meer, B. Dollet, N. De Jong, and D. Lohse, *Microbubble shape oscillations excited through ultrasonic parametric driving,* Physical Review E **82**, 026321 (2010).

[152] T. Leighton, *The acoustic bubble* (Academic press, 2012).

[153] L. Ruby, *Applications of the mathieu equation,* American Journal of Physics **64**, 39 (1996).

[154] O. M. Braun and Y. Kivshar, *The Frenkel-Kontorova model: concepts, methods, and applications* (Springer Science & Business Media, 2013).

[155] B. Denardo, B. Galvin, A. Greenfield, A. Larraza, S. Putterman, and W. Wright, *Observations of localized structures in nonlinear lattices: Domain walls and kinks,* Physical review letters **68**, 1730 (1992).

[156] W.-z. Chen, *Experimental observation of solitons in a 1d nonlinear lattice,* Physical Review B **49**, 15063 (1994).

[157] R. B. Thakur, L. English, and A. Sievers, *Driven intrinsic localized modes in a coupled pendulum array,* Journal of Physics D: Applied Physics **41**, 015503 (2007).

[158] D. Armbruster, M. George, and I. Oprea, *Parametrically forced pattern formation,* Chaos: An Interdisciplinary Journal of Nonlinear Science **11**, 52 (2001).

[159] Z. Zhang, *Camera parameters (intrinsic, extrinsic),* Computer Vision , 81–85 (2014).

[160] W. Wester-Ebbinghaus, *Simultaneous calibration of a photogrammetric stereopair,* The Photogrammetric Record **12**, 519–523 (2006).

[161] J. Patterson, *Calibration of photogrammetric cameras,* Photogrammetria **34**, 69–78 (1978).

[162] R. Tang and D. Fritsch, *Correlation analysis of camera self-calibration in close range photogrammetry,* The Photogrammetric Record Photogram Rec **28**, 86–95 (2013).

[163] T. O. Crompton, *Self calibration,* The Photogrammetric Record **11**, 125–125 (2006).

[164] V. Sánchez-Morcillo, N. Jiménez, N. González, S. Dos Santos, A. Bouakaz, and J. Chaline, *Modeling acoustically driven microbubbles by macroscopic discrete-mechanical analogues,* Modelling in science education and learning **6**, 75 (2013).

[165] V. Sánchez-Morcillo, N. Jiménez, J. Chaline, A. Bouakaz, and S. Dos Santos, *Spatio-temporal dynamics in a ring of coupled pendula: analogy with bubbles,* in *Localized Excitations in Nonlinear Complex Systems* (Springer, 2014) pp. 251–262.

Appendices

A

List of Publications

- A. Mehrem, N. Jiménez, L. Salmerón, X. García-Andrés, L. García-Raffi, R. Picó, V. J. Sánchez-Morcillo, *Nonlinear dispersive waves in repulsive lattices*, is submitted.

- A. Mehrem , L. Salmerón, N. Jiménez, V. J. Sánchez-Morcillo, R. Picó, Luis García-Raffi, Juan F. R. Archilla, and Yuriy A. Kosevich. *Kinks in a lattice of repelling particles: Experimental study with a chain of coupled pendulums*, is submitted in Mathematical Theory and Computational Methods in Nonlinear Systems.

- N. Jiménez, A. Mehrem, R. Picó, L. M. García-Raffi, and V. J. Sánchez-Morcillo (2016). *Nonlinear propagation and control of acoustic waves in phononic superlattices.* Comptes Rendus Physique, 17(5), 543-554.

- J. Chaline, N. Jiménez, A. Mehrem, A. Bouakaz, S. Dos Santos, V. J. Sánchez-Morcillo, (2015). *Macroscopic acousto-mechanical analogy of a microbubble.* The Journal of the Acoustical Society of America, 138(6), 3600-3606.

- N. Jiménez, V. J. Sánchez-Morcillo, A. Mehrem, El-M. Hamham, R. Picó, L. M. García-Raffi, (2015). *Propagation of intense acoustic waves in sonic crystals.* In Physics Procedia (Vol. 70, pp. 271-274).

B

List of Conferences

- Ahmed Mehrem, El. Mokhtar Hamham, N. Jiménez, Alejandro Cebrecos, Rubén Picó, V. Sánchez-Morcillo · Lluís M García-Raffi, *Nonlinear acoustic waves in periodic media*, 7th Forum Acusticum, Krakow; 09/2014.

- A. Mehrem, N. Jiménez, L. Salmerón, X. García-Andrés, Ll. García-Raffi, R. Picó, V. J. Sánchez-Morcillo, *Nonlinear waves in a Discrete Magnetic Lattice*, 3rd International Conference on Phononic Crystals/Metamaterials, Phonon Transport and and Phonon Coupling (Phononics 2015), Paris; 07/2015.

- V J Sánchez-Morcillo, N. Jiménez, A. Mehrem, R. Picó, Ll. García-Raffi, V. Romero-García, V. Tournat, *Nonlinear waves in periodic media from lattices to superlattices and phononic crystals*. 3rd International Conference on Phononic Crystals/Metamaterials, Phonon Transport and and Phonon Coupling (Phononics 2015), Paris; 07/2015.

- Ahmed Mehrem, N. Jiménez, Víctor Sánchez Morcillo, *Theoretical study of Microbubbles dynamics under the action of an ultrasonic field*, I Encuentro de Estudiantes de Doctorado, Universidad Politécnica de Valencia, Valencia, Spain 7/2013.

- V. J. Sanchez-Morcillo, N. Jimenez, A. Mehrem, EL. Hamham, L. Garcia-Raffi, R. Pico *Propagation of Intense Acoustic Waves in Sonic Crystals.* International Congress on Ultrasonics (ICU 2015), Metz; 05/2015.

- Víctor Sánchez-Morcillo, Noe Jiménez, A. Mehrem, Rubén Picó, Lluís M. García-Raffi: Nonlinear waves in phononic lattices and superlattices ASME 2015 International Mechanical Engineering Congress Exposition, Houston, Texas,11/2015.

- Noé Jiménez, Ahmed Mehrem, Rubén Picó, Lluís M. García-Raffi, Víctor J. Sánchez-Morcillo, *Nonlinear propagation and control of acoustic waves in phononic superlattices*, Comptes Rendus Physique, Volume 17, Issue 5, May 2016, Pages 543-554, ISSN 1631-0705.

- A. Mehrem, V. J. Sánchez-Morcillo, N. Jiménez, L. J. Salmerón-Contreras, X. Garcia-Andres, R. Picó, L. M. García-Raffi, *Second harmonic propagation in Coupled Oscillators.* EuroRegio, Porto, Portugal; 06/2016.

- A. Mehrem, Noe Jiménez, Víctor Sánchez-Morcillo, Lluís M. García-Raffi, Rubén Picó, Luis J. Salmerón Contreras: *Second harmonic generation in a chain of magnetic pendulums.* NoLineal 2016, Sevilla, Spain; 06/2016.

- L. J. Salmerón-Contreras, L. M. García-Raffi, N. Jiménez, Ahmed Mehrem, R. Picó, Rubén, V. J. Sánchez-Morcillo,(2016). *Sonificación de fenómenos físicos: El ejemplo del péndulo.* V Jornadas de Modelización Matemática. Valencia, Spain.

- A. Mehrem, R. Picó, V. J. Sánchez-Morcillo, L. M. García-Raffi, L. J. Salmerón-Contreras, N. Jiménez, K. Staliunas: *Solitary waves in nonlinear phononic crystals*, EuroRegio, Porto, Portugal; 06/2016.

- L. J. Salmerón-Contreras, L. M. García-Raffi, N. Jiménez, Ahmed Mehrem, R. Picó, Rubén, V. J. Sánchez-Morcillo, Kestutis Staliunas (2016). *Acoustic gap solitons in layered media.* International conference on nonlinear mathematics and physics, NoLineal 2016 . Sevilla, Spain; 06/2016.

- A. Mehrem, V. J. Sánchez-Morcillo, N. Jiménez, L. J. Salmerón-Contreras, X. García-Andres, R. Picó, L. M. García-Raffi, *Simple models for the understanding of nonlinear dynamics*, La Jornada de Modelizacion Matemática V 2016, Valencia, Spain.

- L. J. Salmerón-Contreras, L. M. García-Raffi, Ahmed Mehrem, R. Picó, V. J. Sánchez-Morcillo, N. Jiménez, K. Staliunas *Gap Soliton in Acoustic Layered Media*, EuroRegio, Porto, Portugal; 06/2016.

LIST OF FIGURES

Cover images:

- Pends. (c)Ahmed Mehrem, CC BY-NC 2.0.
- Phase diagram (c)Kevin Dooley, CC BY 2.0.